

DESIGN OF FRETTING RIG AND THIN CONTACT DISPLACEMENT SENSOR FOR FRETTING EXPERIMENTS

Thesis

submitted in partial fulfillment of the requirements for the degree of

DOCTOR OF PHILOSOPHY

by

RAJA PANDI R.
(155118 AM15F07)



**DEPARTMENT OF WATER RESOURCES AND OCEAN ENGINEERING
NATIONAL INSTITUTE OF TECHNOLOGY KARNATAKA
SURATHKAL, MANGALORE - 575 025, INDIA**

AUGUST, 2022

DESIGN OF FRETTING RIG AND THIN CONTACT DISPLACEMENT SENSOR FOR FRETTING EXPERIMENTS

Thesis
submitted in partial fulfillment of the requirements for the degree of
DOCTOR OF PHILOSOPHY

by

RAJA PANDI R.
(155118 AM15F07)

Under the guidance of

Dr. VADIVUCHEZHIAN KALIVEERAN
Assistant Professor



**DEPARTMENT OF WATER RESOURCES AND OCEAN ENGINEERING
NATIONAL INSTITUTE OF TECHNOLOGY KARNATAKA
SURATHKAL, MANGALORE - 575 025, INDIA**

AUGUST, 2022

DECLARATION

I hereby declare that the Ph.D. Thesis entitled “**DESIGN OF FRETTING RIG AND THIN CONTACT DISPLACEMENT SENSOR FOR FRETTING EXPERIMENTS**” which is being submitted to **National Institute of Technology Karnataka, Surathkal**, for the partial fulfillment of the requirement for the award of degree of **Doctor of Philosophy** in the **Department of Water Resources and Ocean Engineering** is a bonafide report of the work carried out by me. The material contained in this Ph.D. Thesis has not been submitted to any university or Institution for the award of any degree.



.....
RAJA PANDI R. (155118 AM15F07)


Department of Water Resources and Ocean Engineering
National Institute of Technology Karnataka, Surathkal

Place: NITK, SURATHKAL.

Date: 12 - 10 - 2021

CERTIFICATE

This is to certify that the Ph.D. Thesis entitled “**DESIGN OF FRETTING RIG AND THIN CONTACT DISPLACEMENT SENSOR FOR FRETTING EXPERIMENTS**” submitted by **RAJA PANDI R. (155118 AM15F07)**, as the record of the work carried out by him, is accepted as the Ph.D. Thesis submission in partial fulfillment of the requirements for the award of the degree of **Doctor of Philosophy** in the **Department of Water Resources and Ocean Engineering, National Institute of Technology Karnataka, Surathkal**, is a bonafide work carried out by him under my supervision and guidance.

 13-10-2021

.....
Dr. VADIVUCHEZHIAN KALIVEERAN

Assistant Professor

Department of Water Resources and Ocean Engineering

National Institute of Technology Karnataka, Surathkal

 13/10/2021

.....
Chairman - DRPC

Department of Water Resources and Ocean Engineering

National Institute of Technology Karnataka, Surathkal

Chairman (DRPC)
Dept. of Water Resources & Ocean Engineering

ACKNOWLEDGEMENT

First of all, I would like to thank **Dr. K. Vadivuchezhian** for giving me the opportunity to carry out this PhD research, and for his constant enthusiasm and useful guidance throughout these years. I wish to express my gratitude to him for sharing his broad expertise with me and many other technical aspects of my work. Without his precious help, these years would have surely been even more challenging. I am also grateful to **VDK sir's family members** for their love and support towards me on these research journey. Thank you!

I am also thankful to **Prof. G. S. Dwarakish, Prof. Amai Mahesha** and **Prof. Amba Shetty** former Heads of the Department and **Prof. B.M. Dodamani**, present Head of the Department of Water Resources and Ocean Engineering, NITK, Surathkal for permitting me to carry out my research work and to make use of institutional infrastructure facilities.

I am grateful to Research Progress Appraisal Committee members, **Prof. M.K. Nagaraj, Dr. Jeyaraman, Prof. S.M. Murigendrappa** and **Dr. K. Subrahmanya** for their thoughtful comments on my work and the stimulating discussions we had during my research seminars. I sincerely acknowledge the help and support of **Dr. S.C. Kattimani, Dr. Srikanth Bontha** and **Dr. M.R. Ramesh** during my initial phase of research work.

At the workplace, I've found many people who were inspiring me, supporting me and guiding me not only in research and in my life hurdles also. My Annaya(s), **Dr. Ramachandra Rao** and **Dr. Amogh bhai**, who were and are keep sharing time whenever I needed. **Dr. Suman mam**, an elder sister to me who prayed for me and shares thoughts as well as food. **Dr. Murali sir**, who helped me and supported me in my research phase and even now. **Kumaran**, my machi, who helped me in many ways and offering a food many a times and because of him only I've been by-passed the critical phase ever faced in my life. **Dr. Vijay**, my machi, who supports me and keep on giving me a straight forward ideas though I couldn't able to follow everything he said. The time spares with them are never fade away from my memory and it holds a special place in my heart till my last breath. **Palani sir**, who helped me a lot to fabricate

materials and components and to conduct experiments along with the support from **Srinivas, Murugan, Raveesh** and other colleagues. I sincerely acknowledge and convey my heartfelt thanks to the invariable help rendered from all above and other research scholars (**Dr. Diwan, Dr. Vivek, Dr. Ajuy, Dr. Karthik, Dr. Jeykesh, Dr. Sylus, Dr. Prakatheesh, Senthil Anna** and **Dr. Vipin**) of our own department and other departments.

I sincerely acknowledge the help and support of **Balu Anna, Prathima Mam, Seetharam sir, Jagadish Sir, Anil Anna, Anand Anna, Padmanaban Anna, Gopal Anna** and **all other non-teaching staff** of Department of Water Resources and Ocean Engineering, NITK, Surathkal, in completing the work. A very special gratitude to everyone in the Administrative block and Accounts section for their cooperation. I am also grateful to the operators, fabrication specialists and machine suppliers from Chennai who gave me a support to conduct my experiments.

Finally, I would like to express my deepest gratitude to my family: **M. Rajendran, R. Pandiammal, R. Rajalakshmi** and **K. Palpandi** for their endless support and encouragement during my life, which is too much to describe by any languages. Thank you all. This thesis is for my beloved family.

Thanks for all your encouragement!

Raja Pandi R.

ABSTRACT

The present work mainly focuses on understanding the fretting phenomenon and its effects on life of the components/assemblies. To accomplish this, the suitable fretting setup which comprises of proper fretting rig/fixture and an instrument/technique to measure relative contact slip between the tightly contacted pair is needed.

The design and fabrication of fretting rig begins with One-Dimensional (1-D) and Three-Dimensional (3-D) finite element analysis on proposed model of fretting rig. From the analysis results, the fretting rig model which produces 50% Load transfer Ratio (LTR) for the given load is selected for the fabrication alongwith with the consideration of machine bed dimensions and difficulties arised when mounting the rig on the machine bed. To ensure this condition, initially eleven cases of simple one-dimensional (1-D) fretting rig models have been designed and Finite Element (FE) analysis of these models was carried out. Afterwards four more different fretting rig models have been designed and analyzed with the inclusion of machine constraints and its results are also presented here. Among these models, the finite element model with optimum LTR was selected to conduct fretting experiments and the detailed three-dimensional (3-D) finite element study of the selected model has been performed and its results were validated. Following this, the selected fretting rig was fabricated and tested. These tests revealed that the fabricated fretting rig failed to maintain constant normal load during fretting experiments. So, the necessary modifications have been made in the fabricated fretting rig to conduct fretting experiments by applying constant normal load on the specimen. The fretting rig thus designed would be used for conducting fretting experiments.

Also, this work proposes a new thin curved sensor/strip to measure the relative slip between pad and specimen under fretting condition. Since the relative contact displacement is an important parameter to categorize the fretting process, the measurement of contact displacement between pad and specimen is necessary. Because of high yield strength and the ability to return to its initial position even with notable deflection, the spring steel have chosen to fabricate the thin curved strip. Before the fabrication, the detailed Finite Element Analysis (FEA) of the thin curved sensor was

carried out. The strip consists of different shapes (rectangular, circular and elliptical) of slots and the number of slots in each strip is varied from 2 to 6. The Strain Energy Approach (SEA) has been used to calculate the displacement for the curved strip and it was compared, verified and validated with its FEA and Experimental results. From FEA study of thin curved strip with slots, four configurations were chosen to measure micro level displacement between pad and specimen under fretting experiments. The study reveals that the increasing number and size of holes presented in the curved strip indicate that the increased in displacement and von-Mises stress values which offers the higher flexibility to the strip. The reduction in area and minimum thickness of the curved strip could be the reason for the decrease in the stiffness of the curved strip. This study explores the use of new simple and novel instrument/sensor to capture the micro level relative displacement between the pad and specimen under fretting condition.

Keywords: Fretting rig, Relative slip measurement, Thin Curved Strip/Sensor, Load Transfer Ratio, Finite Element Analysis.

TABLE OF CONTENTS

ABSTRACT	i
TABLE OF CONTENTS	iii
LIST OF FIGURES	v
LIST OF TABLES	viii
NOMENCLATURE	ix
CHAPTER 1	
INTRODUCTION AND LITERATURE SURVEY	1
1.1 INTRODUCTION	1
1.2 MOTIVATION	1
1.3 LITERATURE REVIEW	2
1.3.1 Contact Mechanics	2
1.3.2 Friction and wear	7
1.3.3 Fatigue	9
1.3.4 Fretting	10
1.4 RESEARCH GAPS	18
1.5 OBJECTIVES AND OVERVIEW OF THESIS	19
1.6 STRUCTURE OF THE THESIS	19
CHAPTER 2	
DESIGN AND FABRICATION OF FRETTING RIG	21
2.1 INTRODUCTION	21
2.2 DESIGN OF FRETTING RIG	30
2.2.1 Development of suitable fretting rig	30
2.2.2 Description of proposed fretting rig structure	30
2.2.3 Finite element analysis of fretting rig	32
CHAPTER 3	
DESIGN AND FABRICATION OF DISPLACEMENT SENSOR	39

3.1	INTRODUCTION	39
3.2	METHODS AND MATERIALS	41
3.2.1	Strain Energy Approach (SEA)	42
3.2.2	Finite Element Analysis (FEA)	48
3.2.3	Experimental details	51
CHAPTER 4		
RESULTS AND DISCUSSIONS		55
4.1	FRETTING RIG RESULTS AND DISCUSSIONS	55
4.1.1	Experimental study of the fretting rig	60
4.2	THIN DISPLACEMENT SENSOR RESULTS AND DISCUSSIONS	64
4.2.1	SEA Results	64
4.2.2	FEA Results	64
4.2.3	Experimental Validation	75
4.3	FRETTING EXPERIMENTS USING FABRICATED FRETTING RIG AND THIN DISPLACEMENT SENSOR	76
CHAPTER 5		
CONCLUSIONS		81
5.1	CONCLUSIONS FROM FRETTING RIG DESIGN	81
5.2	CONCLUSIONS FROM THIN DISPLACEMENT SENSOR DESIGN	82
5.3	CONCLUSIONS FROM FRETTING EXPERIMENTS	82
5.4	LIMITATIONS OF THE STUDY	83
5.5	SCOPE FOR FUTURE WORK	83
REFERENCES		85
PUBLICATIONS BASED ON PRESENT RESEARCH WORK		97
CURRICULUM VITAE		99

LIST OF FIGURES

Figure 1.1	Types of contacts	4
Figure 1.2	Example for incomplete contact - Roller bearing	5
Figure 1.3	Schematic view of a dovetail joint	5
Figure 1.4	Flanged joint - Example for receding contact	6
Figure 1.5	Connecting rod - Example for common edge contact	7
Figure 1.6	Schematic of general relative motions of fretting contacts (a) tangential fretting, (b) radial fretting, (c) rotational fretting and (d) torsional fretting	12
Figure 1.7	Schematic of fretting test rig	14
Figure 1.8	Failure locations of the blade (at point C') and disk (at point C)	17
Figure 1.9	a) Normal and shear stresses in cylindrical and nominally flat contacts, b) coefficient of friction in nominally flat contact	18
Figure 2.1	Fretting fatigue experimental setup of turbine blade and disk	22
Figure 2.2	Failed turbine blade and disk	22
Figure 2.3	Bridge type rotary four-point bending test	23
Figure 2.4	Schematic representation of the floating bridge used in fretting tests	25
Figure 2.5	Fretting apparatus using cantilever bridge	26
Figure 2.6	a) Perfectly aligned specimen and pad. Misalignment by pad rotation Θ b) around x1 axis or c) around x2 axis	26
Figure 2.7	a) Schematic and b) Picture of Bramhall test rig	28
Figure 2.8	Fretting test rig used by Nowell & Hills (1990) (left) and Szolwinski & Farris (1998) (right)	28
Figure 2.9	Schematic of loading system to conduct a) full sliding and b) fretting tests	32
Figure 2.10	Free body diagram of specimen in a) full sliding and b) fretting tests	32
Figure 2.11	Type-1 fretting rig model cases used for 1-D finite element analysis	33
Figure 2.12	a) Case-3, b) Case-4, model of type-2 fretting rig used for 1-D	35

	FEA	
Figure 2.13	a) Case-5, b) Case-6, model of type-2 fretting rig used for 1-D FEA	36
Figure 2.14	a) Case-7, b) Case-8, model of type-2 fretting rig used for 1-D FEA	36
Figure 2.15	a) Case-9, b) Case-10, c) Case-11, model of type-2 fretting rig used for 1-D FEA	37
Figure 3.1	Illustration of the dependence of wear coefficient with displacement amplitude in fretting concerning the slip regime	39
Figure 3.2	Free body diagram of considered curved section	42
Figure 3.3	Normal stress distribution along cross-section in curved members	44
Figure 3.4	Thin curved strip with loads and boundary conditions	45
Figure 3.5	a) Thin curved sensor without slot; b) Schematic view of a curved beam with neutral axis shift from the centroidal axis (magnified view)	47
Figure 3.6	Implications of slot dimensions	48
Figure 3.7	3-D model of a thin curved strip with rectangular slots	49
Figure 3.8	3-D model of a thin curved strip with circular slots	50
Figure 3.9	3-D model of a thin curved strip with elliptical slots	50
Figure 3.10	a) Schematic representation of thin curved strip and its arrangement; b) Closer view of thin curved strip and its arrangement during experiments	51
Figure 3.11	Thin strip holder arrangement in specimen and pad	51
Figure 3.12	Experimental setup	53
Figure 4.1	Schematic fretting rig model used for 1-D FEA after considering machine bed dimensions	56
Figure 4.2	1-D model of actual fretting rig	57
Figure 4.3	a) 3-D model and b) meshed model of actual fretting rig	59
Figure 4.4	Fabricated fretting rig	60
Figure 4.5	a) 3-D model and b) meshed model of modified fretting rig	61
Figure 4.6	Modified fretting rig	62

Figure 4.7	Mesh Convergence study undertaken to select the element size and no of elements	65
Figure 4.8	von Mises stress results of Strip_2_Rec_45deg_1_0.25 model	67
Figure 4.9	von Mises stress results of Strip_2_Rec_45deg_1_0.5 model	68
Figure 4.10	von Mises stress results of Strip_2_Rec_45deg_2_0.25 model	68
Figure 4.11	von Mises stress results of Strip_2_Rec_45deg_2_0.5 model	69
Figure 4.12	von Mises stress results of Strip_4_Rec_45deg_2_0.25 model	69
Figure 4.13	von Mises stress results of Strip_4_Rec_4_2_0.25 model	69
Figure 4.14	von Mises stress results of Strip_6_Rec_2_2_0.25 model	70
Figure 4.15	von Mises stress results of Strip_6_Rec_4_2_0.25 model	70
Figure 4.16	von Mises stress results of Strip_4_Circ_1 model	70
Figure 4.17	von Mises stress results of Strip_4_Circ_3 model	71
Figure 4.18	von Mises stress results of Strip_6_Circ_1 model	71
Figure 4.19	von Mises stress results of Strip_6_Circ_3 model	71
Figure 4.20	von Mises stress results of Strip_4_Ellip_2_1 model	72
Figure 4.21	von Mises stress results of Strip_4_Ellip_4_1 model	72
Figure 4.22	von Mises stress results of Strip_4_Ellip_2_3 model	72
Figure 4.23	von Mises stress results of Strip_4_Ellip_4_3 model	73
Figure 4.24	von Mises stress results of Strip_6_Ellip_2_1 model	73
Figure 4.25	von Mises stress results of Strip_6_Ellip_4_1 model	73
Figure 4.26	von Mises stress results of Strip_6_Ellip_2_3 model	74
Figure 4.27	von Mises stress results of Strip_6_Ellip_4_3 model	74
Figure 4.28	Schematic of specimen and cylindrical pad	76
Figure 4.29	Fabricated Dog-bone specimen and cylindrical pad	77
Figure 4.30	Fretting experiment result- Q/P ratio vs No. of cycles	78

LIST OF TABLES

Table 2.1	Material Properties of elements used	34
Table 2.2	Elements Used for 1-D FEA	35
Table 3.1	Slot dimensions considered for Finite Element Analysis	48
Table 4.1	LTR values of different cases	55
Table 4.2	Load transfer ratios were obtained for different rig dimensions	58
Table 4.3	LTR values for four different cases of fretting rig 1-D FEA	59
Table 4.4	Finite Element Analysis results of the thin strip with slots	66
Table 4.5	Chemical composition of Al 6061-T6 alloy (%)	77
Table 4.6	Fretting experiment results	78

NOMENCLATURE

A	Area, mm ²
a	Half-length of contact, mm
dl	Deformed Length of the considered layer, mm
e	Eccentricity, mm
E	Young's modulus, N/mm ²
l	Initial length of the considered layer, mm
M_b	Applied moment, N/mm
N	Number of Slots
P	Applied load, N
$p(x)$	Normal traction
$q(x)$	Shear or Tangential traction
r_c	Radius of centroidal axis, mm
r_n	Radius of neutral axis, mm
U	Strain energy
v, δ_{\max}	Vertical deflection at free end, mm
v_1, δ_{mid}	Vertical deflection at middle portion, mm
y	The distance between neutral axis and outer layer, mm

Greek symbols

ξ	Strain
σ	Stress, N/mm ²

Superscripts & Subscripts

i	real number, 1, 2, n.
-----	----------------------------

CHAPTER 1

INTRODUCTION AND LITERATURE SURVEY

1.1 INTRODUCTION

Essentially, friction involves all the acts at the point of contact of solid bodies. Friction, is necessary when people have to walk, is not needed when the machine elements are subjected to their intended operation. So, friction's importance is depending on where it gets to be involved. Necessarily friction studies are very important since they are helpful to enhance the machine elements' lifespan and reliability of the machines.

This thesis aims to understand the friction distribution between the incomplete contacts when they are subjected to fretting where different parameters/factors have been used. To accomplish this, a suitable fretting rig and an instrument that helps to capture the relative slip between pad and specimen are needed.

This chapter gives the motivation behind the chosen work, detailed literature review and review of half-space theory. Finally, it provides an objective of work and an overview of the consecutive research chapters.

1.2 MOTIVATION

In the present scenario, researchers are working on fretting of plane contacts, fretting fatigue, fretting wear and fretting life of components. Improvement in the fretting life of the components is dependent on the understanding of the fretting process, which includes fretting wear and fretting fatigue, stress distribution at surface and sub-surface levels, the effect of fretting parameters and the process of strengthening the component materials and their surfaces. Analysis of contacting bodies at the contact interface is essential to estimate the contact stresses, to improve the life of components and to suggest remedial measures. There is a limited number of studies available to understand the effect of parameters on fretting and stress analysis of fretted contacts. Incomplete contact problems are found in dovetail joints of jet engines, gas turbines, riveted joints, roller bearings, threaded pipe connections in oil and gas pipelines, nub/valley

connection of pressure armour and several other engineering applications. When these components experienced service loads, surface damages in the form of crack initiation and propagation, deterioration of surface, etc., may occur due to higher stresses underneath the contact interface. The present work mainly focuses on understanding the variation of friction coefficient, at the contact interface which facilitates the estimation of contact tractions developed at the contact interface due to fretting. The study also focuses on the effect of tribological parameters on obtaining shear traction and fretting.

1.3 LITERATURE REVIEW

This section outlines the survey of selective literature on contact mechanics, friction and wear, fatigue and fretting and its types are discussed.

1.3.1 Contact Mechanics

Contact mechanics is a wide field and indispensable sector of solid mechanics. In transferring forces to the deformable body, the contacts play an important role. Hence the studies regarding contacts and tractions developed between contacts are essential to manufacturing reliable assembly of machine parts. When the contact interface is involving tangential loads, three possible conditions are occurring at the contact interface. They are;

1. Particles haven't moved tangentially in contact interface i.e. fully stuck condition.
2. A condition at which all the particles of one body are moving relative to the adjacent body particles i.e. fully slip condition.
3. A condition at which only some particles of one body are moving relative to the other body and remaining particles are stick together i.e. Partial slip condition.

Due to the existence of the above-said conditions, different types of failures occur between the contact interfaces. The type of failure could be wear failure or fatigue failure or a combination of both and these will be explained later.

In a general way, contacts could be separated into two categories namely conformal and non-conformal contacts. A conformal contact is, defined as the contacts with a

finite contact extent in the absence of external forces, one where the curvatures of two bodies have the same direction. The outer contact formed by the bearing and ring is an example of conformal contact which is shown in Figure 1.1. A non-conformal contact is a contact with a tiny contact area when no external forces are applied. Here the contact area is very small and incomparable with the actual dimensions of the contacting bodies and the effect of faraway regions of the contact area can be omitted. These arrangements can be treated as half-spaces or half-planes which aids to simplify the problem definition and getting analytical solutions.

If the contact dimensions are very small and are incomparable with those of contacting bodies' dimensions, it is evident that the faraway regions of contact are not having any well-founded influence on the contact. Hence, each body can be considered as a semi-infinite elastic solid which was limited by a plane surface, also named as an elastic half-plane. It helps us to use the elasticity theory formulated for half-spaces in contact mechanics.

The use of half-planes in mechanics was initiated by the study of Flamant in 1892. He found the solution for unknown displacements and stress values caused by the point load and then this can be integrated to find the displacement and stress value as a result of applied distributed load. This solution has been used reversely where the applied traction is not known and the produced displacement value is known.

When two cylinders are in contact (Hertzian contact) with the normal load, the length of the contact (2a) and the normal traction, $p(x)$, can be found analytically by using Hertz solutions. In the same way, the analogous solutions for the shallow wedge (Sneddon, 1951) and nominally flat contacts (Ciavarella, 1998) can be found. On many occasions, several numerical schemes have been used to solve the integral equation.

Once the effect of normal loads on contacts has been resolved, it is natural to start studying the effects of shear loads on contacts. A partial slip problem where the applied tangential loads are not sufficient to cause sliding was addressed first by Cattaneo in 1938. It was re-examined by Mindlin in 1949. For a Hertzian contact, Cattaneo and Mindlin's studies were claimed that the corrective traction was scaled and similar to that produced by the sliding contacts. Ciavarella (1998) and Jäger (1998) later

confirmed that the above-mentioned similarity arguments would be applied to all the contact profiles. The Ciavarella-Jäger theorem has not been applied to the problems where the tangential traction is produced by applied bulk loads and it is suited and applied in the case of tangential load only. The studies conducted by Nowell and Hills (1987), Ciavarella and Macina (2003) and Vázquez et al. (2013) have used the corrective traction for the sliding contacts. Their studies ensure that the tangential traction in the slip regime is correct but needs corrective terms to identify the correct strain in the stick regime.

Different categories of contacts have been put down as one of four types (or some of them are paired together) as depicted in Figure 1.1.

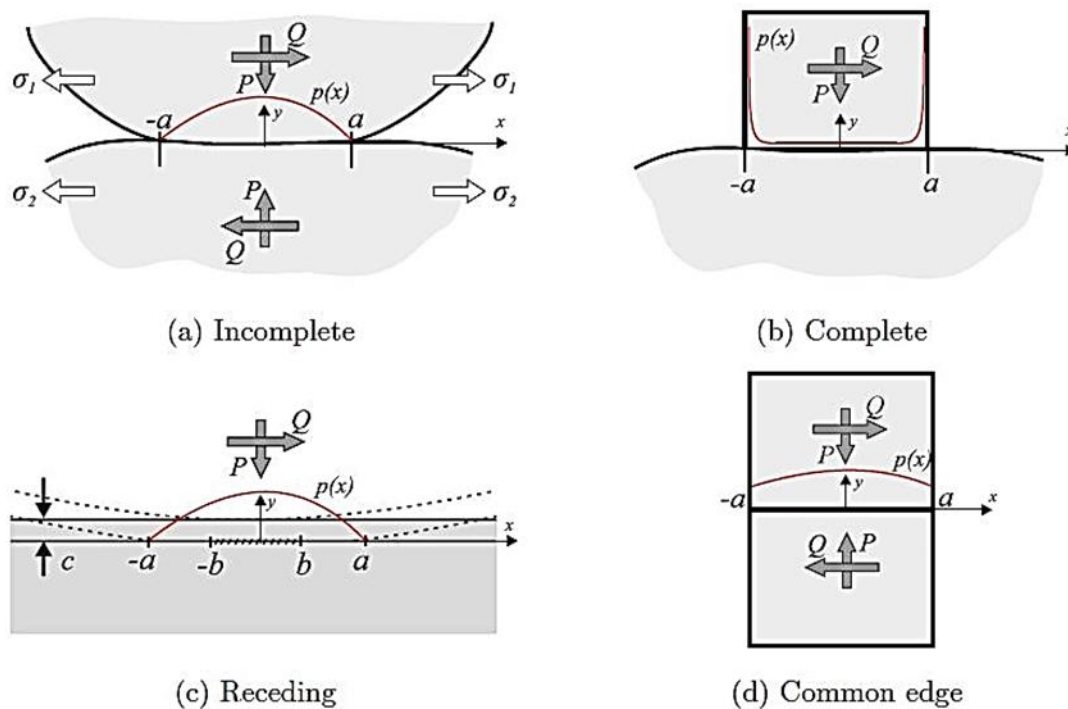


Figure 1.1: Types of contacts (R. Ramesh, 2018)

A schematic diagram of incomplete contact with its pressure profile is shown in Figure 1.1: a. In incomplete contact problems, the contact patch is getting bigger when the applied normal load is increasing. The pressure distribution is maximum p at the middle and tends to zero as it approaching the edge of contact. In this thesis, only in-complete non-conformal contacts have been interpreted with the state that each contact body can

be considered as a half-plane (e.g., the inner contact in the roller bearing in Figure 1.2: a). An advantage of this kind of contact problem is it can be isolated while solving without considering the geometry which is remote from the contact area. The other examples regarding this class of contact problems are railway wheel and rail and a shallow groove ball bearing.



Figure 1.2: Example for incomplete contact - Roller bearing (Ahn et al., 2008)

A schematic view of a dovetail joint together with the applied loads is depicted in Figure 1.3. It can be considered as an example of an incomplete contact.

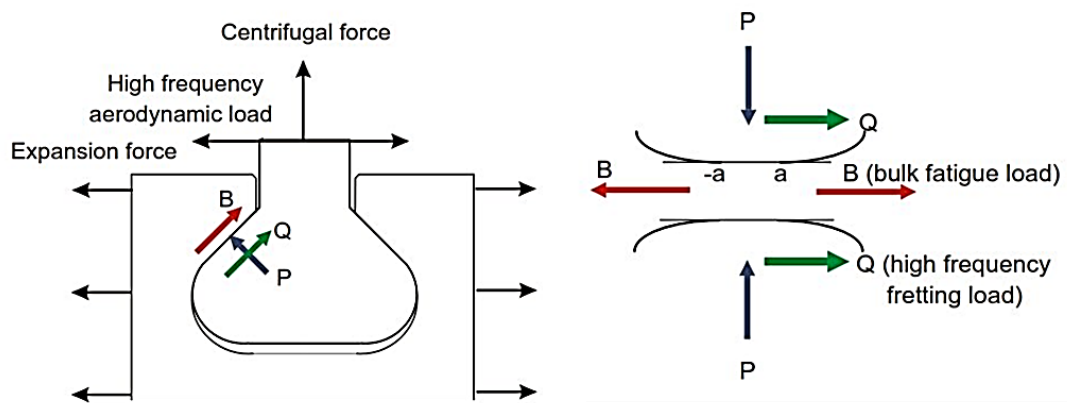


Figure 1.3: Schematic view of a dovetail joint (J.A. Araujo & D. Nowell, 2009)

An elastic square block of side $2a$ is pressed against an elastically similar half-space shown in Figure 1.1: b can be treated as the simplest possible example for complete contact. This contact problem is deceptively simple but it cannot be solved using analytical way, can be solved by employing some numerical techniques such as the

boundary element method or finite element method. The singularities presented in both normal and tangential traction at the contact edges causes complication for numerical techniques.

In complete contacts, the contact length/area is never dependent on the changes in applied normal load, unlike incomplete contacts. In an incomplete contact, the elastically similar contacts even with different radii produce an equal amount of lateral displacement. So there is no generation of tangential traction under the contact interface due to the normal load. But incomplete contact, the traction-free surfaces should be formed on the sides of the contact which helps to arrest the sideways movement. This resistance is in the form of frictional force and is governed by the friction coefficient. Hills and Dini (2004) describe the level of coefficient of friction $\mu > 0.543$ as the condition to secure that there is no particle movement in outwards.

The first identification and analysis of receding contacts started around the early 1970s. Receding contacts are defined as the contacts wherein the contact size decreases on the application of forces as depicted in Figure 1.1: c. Receding contacts is merely seen in bolted joints of the flanged joint shown in Figure 1.4. Hills et al. (2017) have shown that the similarities between incomplete and receding contacts in their work.



Figure 1.4: Flanged joint - Example for receding contact

Figure 1.1: d shows the schematic view of common edge contacts. The contact area is called common edge contact when it is defined by both bodies simultaneously and shares the edges of both solids. In common edge contacts, the pressure distribution is finite value all along the contact interface unlike the above said contacts. In engineering, it is very hard to make perfect alignment between common edge contacts and hence the

practical suitability is limited. An engineering example for these common edge contacts is connecting rod which is shown in Figure 1.5. With the concept of misalignment, generally, the common edge contacts have been considered as complete contacts near the edge. Therefore the analysis of common edge contacts has been done with the factor of misalignment and the contact edges might be considered as complete contacts.



Figure 1.5: Connecting rod - Example for common edge contact

1.3.2 Friction and wear

Frictional contacts between enormous solids exist in nature and also in many engineering applications. Frictional sliding of feet on land results in movement; frictional sliding of land along fault lines results in earthquakes; tribo-electrical contacts of clouds emerge as lightning. Frictional sliding importance in engineering applications can be understood from the examples which include wheel and rail contact, turbine blade joints, motor drives, machine tool and workpiece systems, bolt and rivet connections in assembly, the interaction of bow and string in a violin and brake systems. Friction is the main cause of wear failures and surface deterioration. Losses due to friction are accountable for losses up to 1.6 % of the Gross Domestic Product (GDP) of developed countries (Mang et al., 2011). On the contrary, friction is essential for a walk, accelerate, run, slow down or stop the movement. Many string instruments used friction to generate sound. Also, frictional contacts act as a shock absorber and damping system for harsh vibrations in the assembly of machine structures, turbine-blade joints and

electric motor drives. Friction is a crucial and very complex phenomenon to be considered in machine design and analysis.

Friction is defined as the resistive force existing between two bodies in contact with each other when these two bodies experience relative movement. The frictional laws were established in the 17th century by Amontons. He studied and postulated that static friction is necessary to originate sliding between solids. In the 18th century, Coulomb has taken this study further and found results with the inclusion of kinetic friction. Both Amontons and Coulomb have claimed that friction begins with the interlocking of surface protrusions (asperities) and depressions (initial roughness of surface). There are three classical friction laws which are stated as follows (Terres et al., 2012):

1. Frictional force is in direct proportion to the applied normal load.
2. Frictional force isn't dependent on the apparent contact area.
3. Frictional force isn't dependent on the sliding velocity.

From the first law, the relationship between normal load F_n and frictional (tangential) force F_t is defined as follows:

$$F_n = \mu \cdot F_t \quad (1)$$

Where, μ is the friction coefficient between the surfaces. The generated tangential force is acting in a parallel direction to the sliding surface and its direction is always against the sliding motion. When the sliding occurred between the sliding surfaces due to tangential force, then the fact to be claimed is the shear traction (q) is equal to the friction coefficient times of normal pressure (p) which is stated as follows:

$$q = \mu \cdot p \quad (2)$$

By considering the above, it is obvious that the friction coefficient is limited by the values of shear traction and normal load. Under the contacts, if some points are sticking together, the above said condition does not prevail. Therefore, the condition at which this locally stuck region exists is $q > \mu \cdot p$. Stresses at contact and sub-surface stresses are getting affected by shear traction (Hills & Nowell, 1994).

Wear is the deteriorating process by which the contact surfaces are getting damaged and it leads to the component or assembly failure. Many important parameters affect the wear, namely, normal load, the geometry of the contact, contact area, sliding distance and sliding velocity. Wear mechanisms can be classified as adhesive wear, abrasive wear, erosive wear, surface fatigue, corrosion and fretting wear. Fretting wear is associated with adhesive, abrasive and corrosive wear mechanisms. Friction is the important parameter to infuse wear under the contact surfaces and both are interrelated (Hutchings IM (1992) and Bhushan B (2013)).

1.3.3 Fatigue

Components in a machine are used to perform their intended functions for a long time despite it is performed under complex, two or multiaxial loading conditions. When a component is performing its function under cyclic loading, the fatigue failure may arise even with the minimum stress value than its yield value. In fatigue failure, a crack is always existing which is due to the manufacturing process by which the component was made or the applied loading conditions. Fatigue failure follows stages like crack nucleation on the surfaces where the higher stress concentration is there followed by crack propagation due to applied cyclic stresses thus leads to the catastrophic failure at final. The process of fatigue crack growth can be classified as short crack regimes, where the crack size is in micrometre scale and long crack regimes where the crack length is in millimetre level. The crack growth rate is higher in short crack regimes than in long crack regimes (Schivje, J. (2009), Socie DF. & Marquis GB. (1999), Suresh S. (1998)).

Depending on the number of loading cycles undergone ahead of fracture, the fatigue consists of two regimes namely low cycle regime and high cycle regime. If fracture occurred in the components before 1000 loading cycles then it is called low cycle fatigue. Due to the inclusion of plastic deformation in each cycle, the strain-life approach has been used in low cycle fatigue regime. In contrast, the loading cycle is between 1000 to 10⁵ cycles in the high cycle fatigue where the stress-life approach is used to determine the fatigue limit of the component. If the plasticity effect is small, the stress-life approach can be used successfully for low cycle fatigue regime (Socie

DF. & Marquis GB. (1999)). The total fatigue life of the component is determined by the sum of crack nucleation time and crack propagation time (Schivje, J. (2009), Suresh S. (1998)).

1.3.4 Fretting

When two rough surfaces experiencing relative motion results in several tribological problems. Among those tribological problems, Fretting is one kind. Fretting is a failure phenomenon that occurs between two mechanically fastened/clamped parts when these parts are subjected to a micro-level (or even smaller) relative slip between contact interfaces due to external cyclic forces and moments.

The works of literature regarding fretting failures and their mechanisms will be given below along with its historical background.

Firstly, the fretting occurrence was found and reported by Eden et al in 1911. They have interpreted iron oxide as the fretting debris between contact areas of the specimen and grips. The systematic way of study of fretting was done by Tomlinson in 1927 and he called that the fretting resulted from molecular attrition. Later his findings got discounted. Further observation was done by Tomlinson in 1939 which led to the outcome of fretting as a purely mechanical process assisted with micro slip. The result of the fretting process was influencing the fatigue strength of the material was found by Warlow-Davies in 1941. In 1953, McDowell found that the fretting affects and decrease the fatigue strength of the material by 2-5 times or more. Godfrey et al in 1950, 1953, 1954, 1956 were attempted to found the fretting mechanisms and early stages involved in it and they claimed that adhesion and fine particles (subsequently it got broken and oxidized) were found in contacts and the cyclic motion was not essential for the fretting process. Wright (1952a, 1952b) believed that oxygen was the main factor to cause fretting damage. Feng and Rightmire (1952, 1953, 1955, 1956) was found four stages in fretting and hypothesized as the initial stage, transition period, declining stage and steady-state stage. They quoted that the fretting process included that splitting the particles, successional oxidation and abrasion. Waterhouse (1955) hypothesized that fretting was combined with adhesion, the breakage in welds and metal transfer.

Halliday and Hirst were the first researchers who found that the slip amplitude influences the fretting process in 1956.

In the 1960s and early 1970s, Nishioka et al. (1968, 1969a, 1969b, 1969c, 1969d, 1972) used cylindrical pads against steel specimens in their experiments to explore the factors involved in fretting fatigue. Their findings were significant and includes the occurrence of crack initiation near the contact edge where the stress values are high, high friction coefficient values in the experiments, the little effect of mean stress value in crack initiation and the occurrence of micro-level slip zones near both contact edges when the applied shear load was applied which is less than that necessary to produce sliding. Also, they quoted that the fretting fatigue life-span of the material was influenced little by its hardness.

The damage threshold for the fretting process was used by Waterhouse (1972), Hoepfner and Goss (1974) and Endo and Goto (1976). To find any detrimental effect of material's fatigue strength, a definite amount of fretting damage was essential [Hoepfner and Goss (1974)]. Through the experiments, Endo and Goto (1976) suggested that the initial propagation of fretting fatigue cracks is dependent on fretting conditions and the initial crack propagation process was much faster than plain fatigue cracks. Alic and Kantimathi (1979) found that after the initiation of cracks due to fretting conditions, the fretting does not influence the propagation of these fretting cracks. Experiments have been conducted by Bramhall in 1973 and later by Nowell in 1988 showed that the presence of critical contact length within which the contacts last longer till the end of experiments and at the same time the larger contacts encounter identical stress which is distributed spatially.

Till now, the historical background of fretting was explained with relevant literature. Since 1980, more researchers have started to understand better about fretting by conducting experiments, using analytical techniques and numerical techniques.

The design of fretting experimental setups mainly depends on the type of application that is going to be simulated. Generally, the relative motions of the fretting surface are tangential, radial, rotational and torsional fretting (Zhu M.H. and Zhou Z.R., 2011). The present fretting fixture will be designed to simulate the tangential fretting motion with

cylinder on flat contact configuration. The general fretting motion configurations are shown in Figure 1.6.

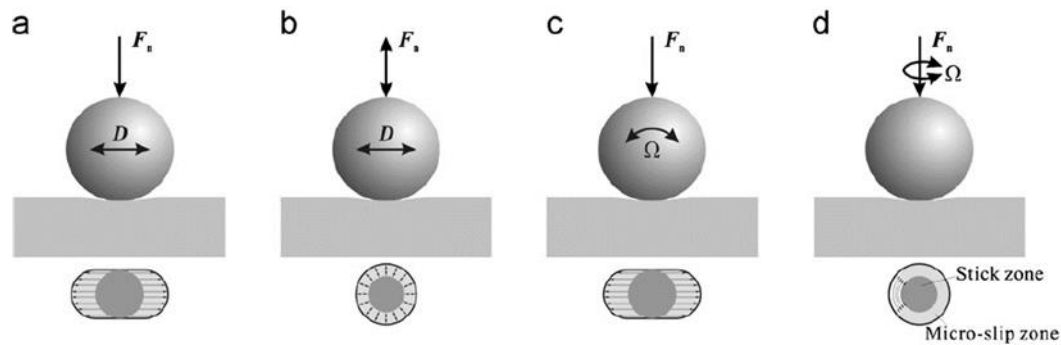


Figure 1.6: Schematic of general relative motions of fretting contacts (a) tangential fretting, (b) radial fretting, (c) rotational fretting and (d) torsional fretting (Zhu M.H. & Zhou Z.R. (2011))

J. A. Pape & R. W. Neu (1999) conducted fretting fatigue tests with two different contact configurations namely cylinder on flat and flat on flat. The authors observed that the crack initiation and propagation happened earlier in the cylinder on flat configuration than in flat due to the occurrence of larger slip regions and high shear and normal tractions at the contact interface. The fretting rig designed and fabricated by B. D. Leonard et al. (2012) was used to conduct fretting tests with various configurations like ‘crossed cylinder’, ‘ball on flat’ and ‘flat on flat’ configurations. This was developed using a magnetostrictive linear actuator which can generate peak to peak displacement amplitude of 250 μm with a frequency of 0 Hz to 1000 Hz. The fretting displacement amplitudes were measured by using a capacitive position sensor. This setup had a provision to apply the normal load to the specimen using dead weights.

A new, cheaper Rotating Bending Fretting Fatigue (RBFF) test apparatus was designed and fabricated by E. Zalenzhad et al. (2014) and it was used to perform both the fretting fatigue and the plain fatigue tests on Al7075-T6 alloy specimens. The Dog-Bone specimens were used for the tests and the fretting pad was attached to the middle portion of the specimen. The contact pressure was applied to fretting pads with the help of the proving ring which was loaded with 100 MPa load. The fretting pads were made up of stainless steel of grade 410 material and it has a bottom width of 2 mm and a span length

of 7 mm. An adjusting screw was used to apply a normal load to the specimen and the same was measured by using the Wheatstone bridge circuit. Four strain gauges were attached to the proving ring and fretting pads to measure both the normal load and the tangential load with the help of the Wheatstone bridge circuit. The constant load tensile tests were conducted on the specimens, before the RBFF tests by INSTRON tensile test apparatus. During the test, the friction force between the fretting pad and specimen was measured by using strain gauges which were attached at bottom of the fretting pad. The friction coefficient value was obtained by dividing the friction force at the fretting pad foot by contact load at the same foot. An inverter was used to vary the frequency ranges, up to 50 Hz. Due to the rotation of the specimen along with the fretting pad during the RBFF tests, the rotating strain gauge data were converted to stationary outlets by using an electrical slip ring. Finally, they have validated their RBFF test machine results with the results obtained from the Shimadzu fatigue test machine and they found that their results have errors in the range of 2.78 % to 8.22 %. A. A. Walvekar et al. (2014) studied the fretting fatigue behaviour of AISI 4140 steel specimens against Ti-6Al-4V cylinders by introducing cylinders on flat configuration between them. Single clamp type of fretting fatigue test was carried out using a fretting rig with the following experimental configurations: normal force was 11 kN, the frequency was 5 Hz, bulk stress varied from 100 to 600 MPa and stress ratio (R) was -1. The difference between the axial loads obtained from the load cells attached to the bottom grip and the upper grip is twice the tangential load (FT) transmitted between the pads and specimen ($F_b - F_u = 2*FT$). The normal load application system used in this study is attached to the main columns of the experimental setup which creates a compliance effect. So the normal load application method used by these authors is not effective. The proposed fretting fixture will be mounted on the machine bed to avoid the problems involved in the fretting fixture used by Walvekar A. A. et al. (2014) and to ensure effective transfer of normal load to the test specimen. The first stage of the present research proposal involves the design and fabrication of fretting fixtures, which is based on the fretting fixture designed by Farris et al., 2003 (Figure 1.7).

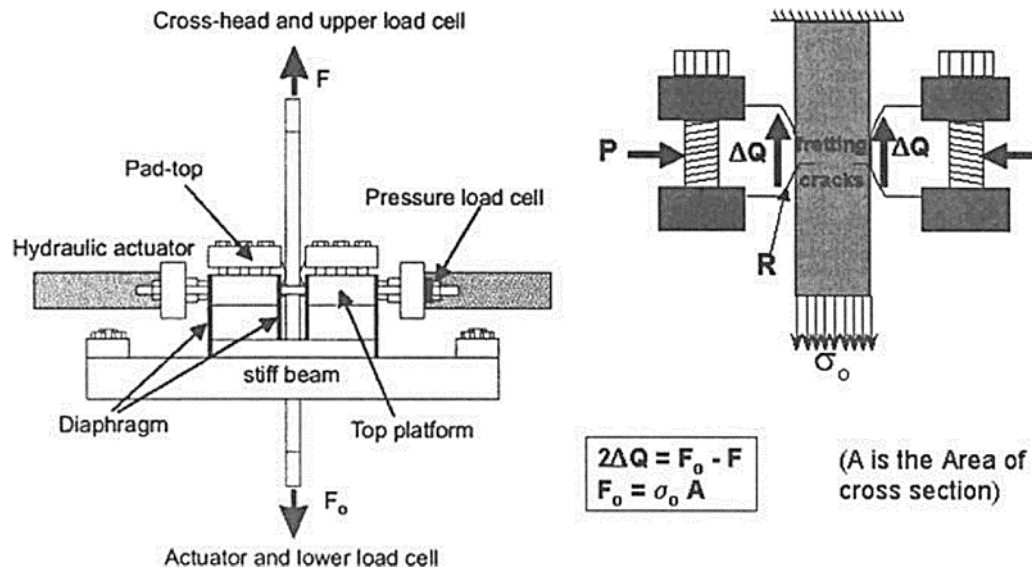


Figure 1.7: Schematic of fretting test rig (Farris et al., 2003)

The study regarding friction and its evaluation between materials is described hereafter. Godfrey et al. (1953) conducted friction studies on the contacts of copper/steel, copper/copper and copper/glass. In their study, they claimed that the coefficient of friction (COF) values was increased to 1.5 for the initial few cycles and then it decreased and stabilized the value of 0.6 within 100 load cycles. The same scenario of peaking at initial and gradual decrease and stabilization to the particular value after few cycles on COF was observed by Pape JA & New RW (2007), Rybiak et al. (2010) and Asai et al. (2013) for quenched and tempered steel, stainless steel and 12% Cr steel material respectively. The initial increase in COF value to 1.7 was found by Leidich et al. (2013) while doing their fretting experiments on tempered steel against chromium alloy steel. However, the increase in COF for the initial few cycles and stabilizes between the value of 0.6 and 1.0 were observed without striking the peak value by Naidu NKR & Raman SGS (2005), Ding et al. (2009) and Kubiak et al. (2011). From their experiments, the notable remark is the materials and test conditions can change the COF values and stabilization times. For instance, the decreased value of COF value from 0.8 to 0.5 was observed when the ambient temperature was having raise from 25 °C to 200 °C by Pearson et al. (2013). They found these changes in their fretting experiments on high strength alloy steel. Mohrbacher et al. in (1995), conducted fretting tests between bearing steel and hardened high-speed steel with TiN coating, found that

the COF value was close to unity when the relative humidity (RH) was 10 % and COF was adequately low when the RH value as high as 80 %.

An analysis involving fretting loops has given the view towards frictional force as it isn't necessary to keep a constant value during the gross sliding in the fretting experiment. A lot of researches (Degat et al. (1997), Fouvry et al. (2004), Rybiak et al. (2010), Mulvihill et al. (2011), Hirsch MR & Neu RW (2011) and Lavella M & Botto D (2011)) have claimed that the frictional force is increased gradually when the fretting displacements approach its utmost positions. For these frictional conditions, the calculation of COF is done by using Equation 3 and the mean COF is related with frictional energy dissipation (E_d), Normal load (P) and sliding amplitude (u_a) (Fouvry et al. (2004), Rybiak et al. (2010) and Lavella M & Botto D (2011)).

$$COF_{mean} = \frac{E_d}{4.P.u_a} \quad (3)$$

The above-said condition is so-called Non-Coulomb friction which has explained by mechanical interlocking along tangential direction since it is classified by the scale of interlocking namely as macroscopic and microscopic interlocking. Macroscopic interlocking has occurred when the pad surface has ploughed a trench on the specimen surface under fretting. It happened, because of the specimen's plastic deformation (Fouvry et al. (2004)) or wear (Rybiak et al. (2010) and Lavella M & Botto D (2011)), with the dependency of type of contact and load types and its magnitudes. Microscopic interlocking was explained, by Mulvihill et al in (2011), as the non-Coulomb frictional phenomenon was originated from interlocked protrusions along with tangential directions and depressions under the contact interface. They also noted that this microscopic interlocking is not dependent on the geometry of the specimen, the effect of fretting scar along the tangential direction on total frictional force with the assumption of these interactions led to an inclined sliding state.

The uncommon value of stabilized COF as 0.05 was reported after a gradual decrease from 0.7 in the fretting experiments (on mild steel contact) conducted by Halliday et al. (1956). This very low value of COF was observed because of the to and fro rolling motion of wear debris in the contact interface and thus results in rolling friction instead

of sliding. Additionally, the velocity accommodation scheme was influenced the COF value and wear rate in the fretting process. It was acknowledged by Mohrbacher et al. in (1995). The effect of variation in contact length on COF was observed by Merhej R & Fouvry S. (2009). In their study, they used sphere on flat contact condition of steel-steel material and they found that the reduction of COF value from 0.8 to 0.5 was observed when the contact radius is increased from 0.122 mm to 0.754 mm. They claimed that the contact radius has a strong influence on COF and it was explained using velocity accommodation mechanism through entrapped debris particles.

Analysis of contact stresses, in components where fretting occurs, is important due to high-stress gradients at the contact interfaces. These high stresses at the contact interface lead to crack formation, crack propagation and finally the failure of the component. The blade-disk attachment of the gas turbine is one of the examples where the fretting phenomenon occurs. The general failure locations in blade and disk arrangement due to fretting are given in Figure 1.8 (Sinclair G. B. et al., 2002). In the present study, the contact tractions will be estimated from an experimentally measured average coefficient of friction and the loads applied at the contact interface. Detailed contact traction profiles would be estimated thoroughly for the cylinder on flat contacts of Al6061 T6 alloy.

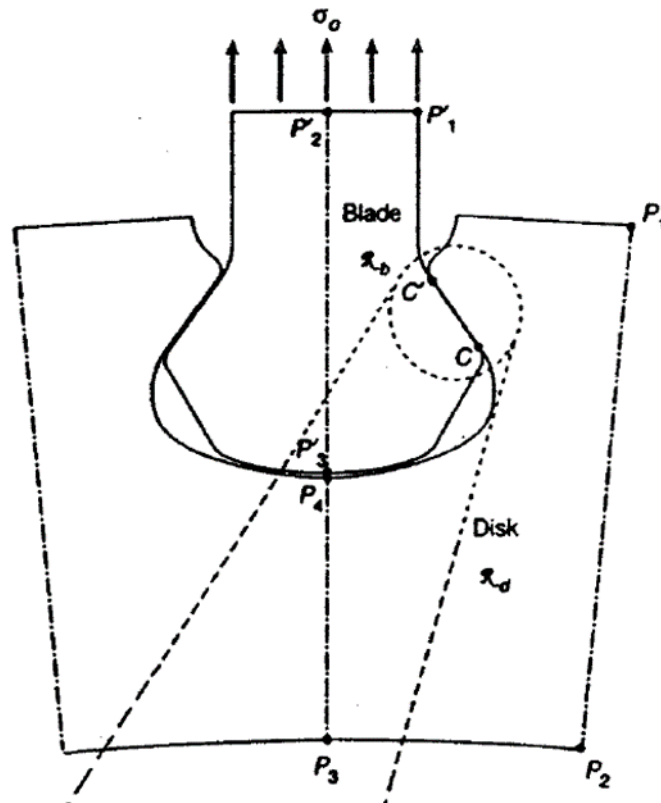


Figure 1.8: Failure locations of the blade (at point C') and disk (at point C) (Sinclair G. B. et al., 2002)

McVeigh P. A. & Farris T. N. (1997) analysed the fretting stresses using finite element methods and calculated the normal and tangential stress distributions using ABAQUS. Analysis was done without considering the bulk load effect and results were compared with the Mindlin theory. The analysed normal stresses showed good agreement with the Mindlin solution while the shear stresses were not in good agreement. Sinclair G. B. et al., (2002) analyzed the contacts of dovetail blade disk arrangement using finite element analysis. Finite element analysis was carried out using ANSYS software. PLANE 42 element and CONTAC 48 element were considered for the two-dimensional analysis of the contact model. Convergence study was done with the help of coarse, medium and fine mesh elements for both global and local contact areas. Murthy H. and Vadivuchezhian K. (2017) estimated the friction in partial flip contacts by considering the basic assumption that the friction coefficient is a function of sliding distance. The authors achieved a good agreement between estimated and experimental results. The authors explained the profile of normal stresses and shear stresses for both cylindrical

and nominally flat contacts (Figure 1.9: a). The coefficient of friction of nominally flat contact with 3 mm radius curved edges is presented in Figure 1.9: b and this coefficient of friction is used for estimation of shear stresses at contact.

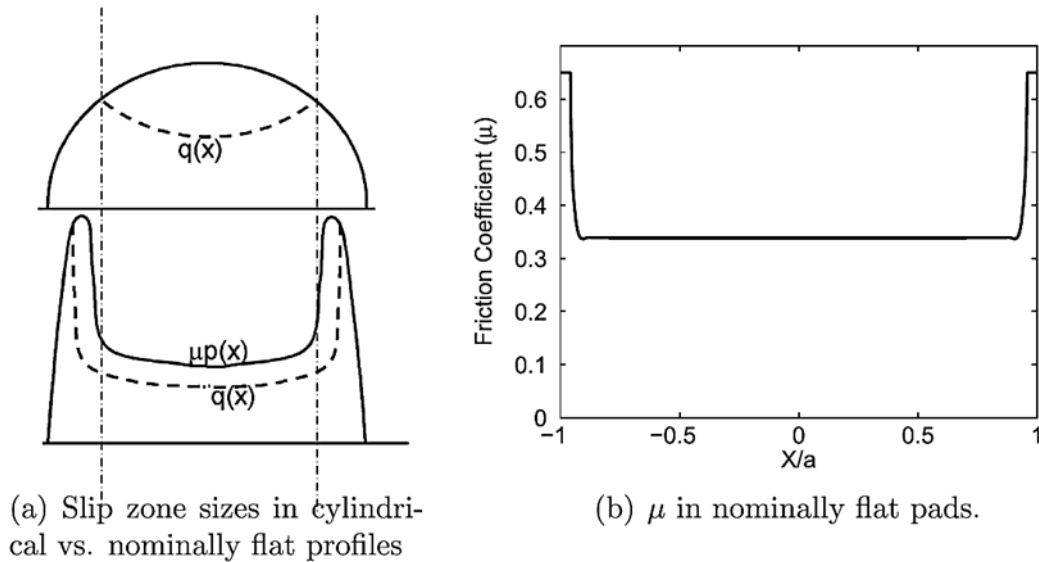


Figure 1.9: a) Normal and shear stresses in cylindrical and nominally flat contacts, b) coefficient of friction in nominally flat contact (Murthy H. & Vadivuchezhian K., 2017)

1.4 RESEARCH GAPS

- A critical review of the literature reveals that many experimental setups were used for fretting studies but many of those experimental facilities need recalibration and many load measuring devices. The proposed fretting fixture uses a simple mechanics-based approach to capture loadings and this doesn't need any recalibration.
- Many researchers conducted experiments with a sphere on flat contacts. The proposed set-up will be used to accommodate both the cylinder on flat and the nominally flat on flat contact configurations.
- Shear traction profiles along the contact length will be obtained from the experimentally observed average coefficient of friction of components subjected to fretting. So, to estimate the stresses at the contact interface the shear traction profiles are important.

1.5 OBJECTIVES AND OVERVIEW OF THESIS

The objectives of the study are as follows:

- To design and fabricate the fretting fixture using a mechanics-based approach and FEM based approach.
- To measure the relative slip between the pad and specimen, using a thin curved displacement sensor, under fretting conditions.
- To design a thin curved strip to measure the contact displacements using a mechanics-based approach and FEM based approach.
- To conduct the fretting experiments using a fabricated fretting rig and fabricated thin curved strips.

1.6 STRUCTURE OF THE THESIS

In **Chapter 1**, an introduction to the importance of friction is provided. This chapter elaborates the motivation for the present study, literature review on contact mechanics, literature review on the coefficient of friction between the contact interfaces, literature review on the surface deterioration of metallic contacts, literature review on fatigue and in-depth literature review on fretting. Finally, it provides the research gap and objectives for this study.

In **Chapter 2**, a little more review on literature is made of available fretting rigs and fixtures focusing on its arrangements, instrumentation, operations and damage characterization before introducing our customized fretting rig.

In **Chapter 3**, a design involved in a new thin curved displacement sensor used for fretting experiments is explained. The details of an adopted Strain Energy Approach (SAE), Finite Element Analysis (FEA) and Experimental methods of various types of thin curved sensors are presented.

Chapter 4 describes the results of SEA and FEA studies of the fretting rig and thin curved displacement sensor. Then, the hurdles which were encountered in the fabrication of the fretting rig and thin curved sensor are presented along with the

solution to overcome those complications. Then, the experimental results obtained using the fabricated fretting rig and thin displacement sensor are given.

In **Chapter 5**, the conclusions are drawn from this study, limitations of the present study and scope for future work are presented followed by references and publications.

CHAPTER 2

DESIGN AND FABRICATION OF FRETTING RIG

2.1 INTRODUCTION

The sole purpose of experiments is to verify the results of theoretical models and they allow us to calculate stress, strain and displacement data for a specific contact type and dimension. One more challenging purpose is to investigate the evolution of damage in terms of friction, surface deterioration i.e., wear and crack nucleation and its propagation. Friction evolution can be obtained using some well-known theories (e.g. Coulomb friction theory), but in practice, friction and wear could be possibly affected by other parameters such as contact type, roughness, loads, boundary conditions, frequency, material type, sliding speed, etc. In a general way, Hills and Nowell in 1994 explained three different types of tests that can be carried out particularly for fretting fatigue tests.

1. *Experiments based on simulating real engineering fretting problems.* The motive behind these tests is to reproduce the contact conditions, occurring in practical applications, in laboratories as close as possible either on full-scale or medium-scale. After conducting experiments, the results can be directly transferred to the real engineering problem without any changes. The most important experiments were conducted by Ruiz et al. (1984) in this regard by developing a medium-scale test model in which they simulated the contact conditions between the turbine blade and its disk. Later, the same kind of contact type was implemented by Nowell et al. (2006) in their experiments. Their experimental setup and failure model of turbine blade against its disk is shown in Figure 2.1 and Figure 2.2 respectively. However, attention is needed on size effects and machining imperfections which was claimed by Hills & Nowell (1994) for these types of experiments. The size effect is the effect implemented due to the dimensional reductions of tested samples than the prototype's dimensions. For example, due to these dimensional reductions, the smaller contact patch could be formed than actual and it leads to different slip amplitudes which may affect the stresses and strains. Necessarily the concentration should lay on machining imperfections also

since minor machining mismatch could cause different contact patches and it produces a difference in the distribution of contact stresses particularly if it's a complete contact.

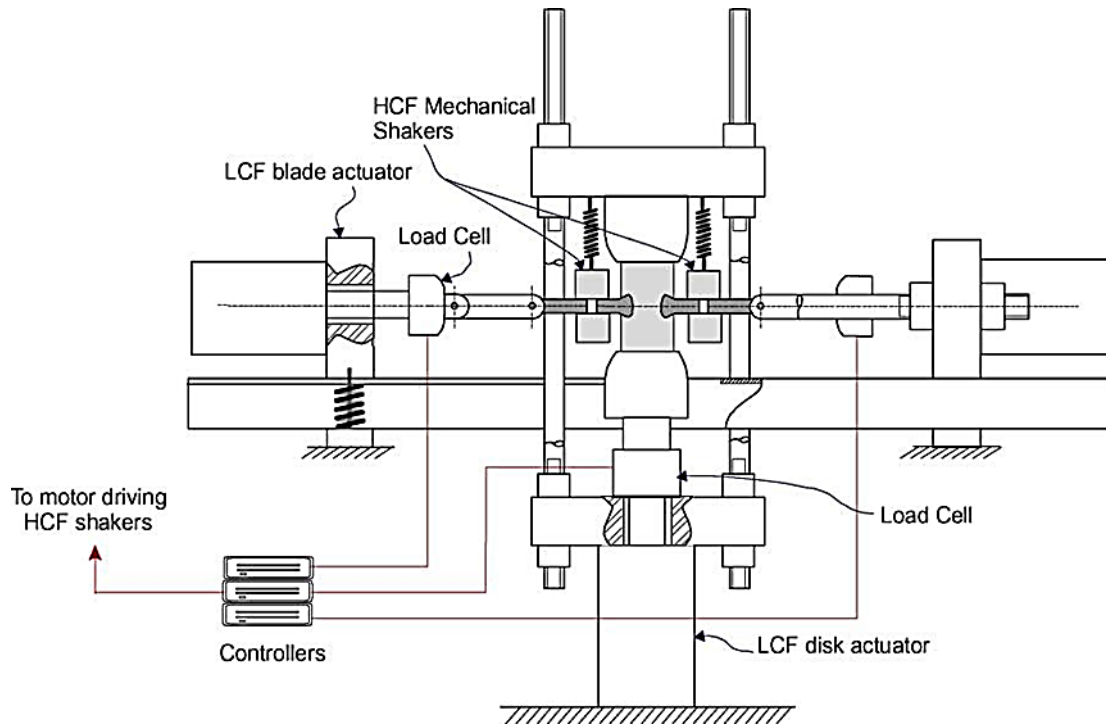


Figure 2.1: Fretting fatigue experimental setup of turbine blade and disk (Nowell et al., 2006)



Figure 2.2: Failed turbine blade and disk (Nowell et al., 2006)

2. Material ranking tests. The main motive of these kinds of an experiment is to do the comparative study on different materials or different surface treatment methods. Usually, the simplified model of contacts can be selected and attention is to be paid to experimental procedures and testing conditions than contact details.

Anyhow, the repetition of the selected contact model is allowed from one test to another. An example of this type of test is a method explained by Hills & Nowell (1994) to adopt a rotary bending test, to understand the behaviour of railway axles shown in Figure 2.3, proposed firstly by Wöhler. The specimens were clamped using bridge pads which has a flat surface on feet with the help of a proving ring. The setup was made in the way that the proving ring can float without any constraints over the specimen and rotate together with the specimen while doing experiments. Due to the circular cross-section of the specimen and the specimen's rotation, the tensile and compressive load was acting simultaneously on the specimen. As already said, the contact condition is simple here and the speed of the test is high which avoids inertial effects in the tests. The focus should be paid to balancing the fretting pads when the specimen is in rotation.

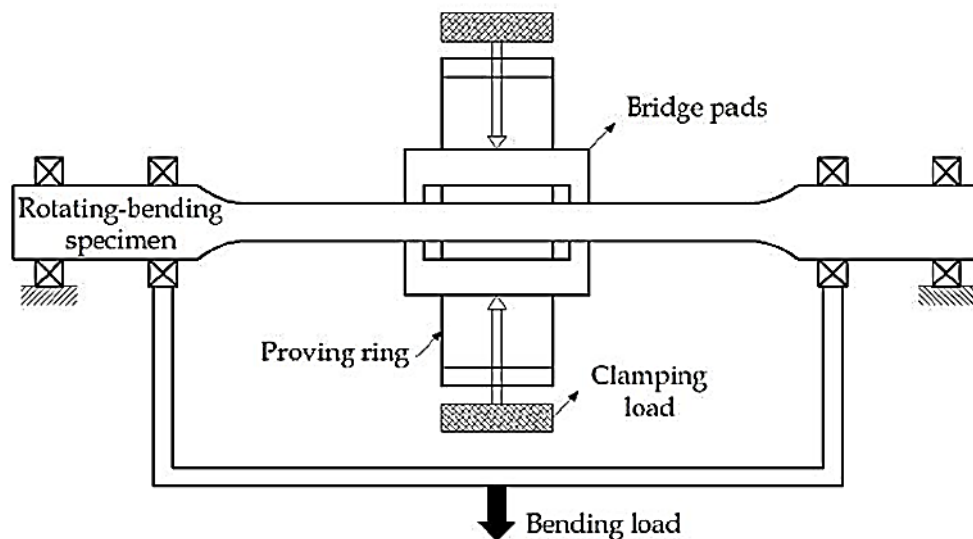


Figure 2.3: Bridge type rotary four-point bending test (Hills & Nowell, 1994)

3. Idealised fretting experiments. The objective of these types of tests is to develop suitable experimental data that gives the support to understand the mechanisms involved in the fretting process. The contact type must be well defined and aids to determine the outcomes like stress, strain, displacement and relative slip, etc.

analytically. The knowledge developed from this test is in a more generic way and true for other contact types, conditions and even for real problems.

Except for the second type of test, the other two test types accommodate the common purpose of understanding the fretting behaviour of real engineering problems by providing experimental results. Though the first type is straightforward, all the real conditions cannot be implemented in laboratory environments and it is very expensive to try. However, the third type does not give direct insight into the contact but provides a basic tool for understanding the fretting behaviour. So, hereafter the details of configurations used in the fretting experiments by various researchers and their findings will be given.

The evolution in the idealized fretting experiment configurations will be given in detail. Generally, fretting tests would be conducted under partial slip or full/gross slip regime conditions. It needs a micron level (or even smaller) of displacement at the contact interface in a well-controlled manner. Usually, these slip conditions are prevailing around 50 μm . In practice, it is very difficult to achieve and maintain this small magnitude of displacement in experiments using external actuators or cams or any other linkage mechanisms (Hills & Nowell (1994)). To achieve this small tangential displacement, other methods have to exploit such as using specimen compliance while performing fretting tests. One of the famous methods have used is keeping a floating bridge as a pad and due to which multiple contacts can be made in the experiments. In this kind of experiment, the system compliance can be controlled either by the bridge pad or specimen. Typically, the bridge pad feet are flat by which the complete contact can be made between pad and specimen. The schematic representation of the floating bridge used for inducing relative slip are shown in Figure 2.4.

The two bridges were attached to the tensile specimen with the help of a proving ring. The normal load used to be given through screw tightening methods via the proving ring. The cyclic load can be applied to the specimen by a mechanical actuator. The compliance of the proving ring can be combined along with the compliance of the specimen and bridge to produce desired tangential displacement during experiments. However, the slip regimes under the contact conditions between all the feet and specimen should be identical if the surface finish and cleanliness of the specimen and

bridge feet were the same. But in reality, different sliding regimes were existing under each contact condition.

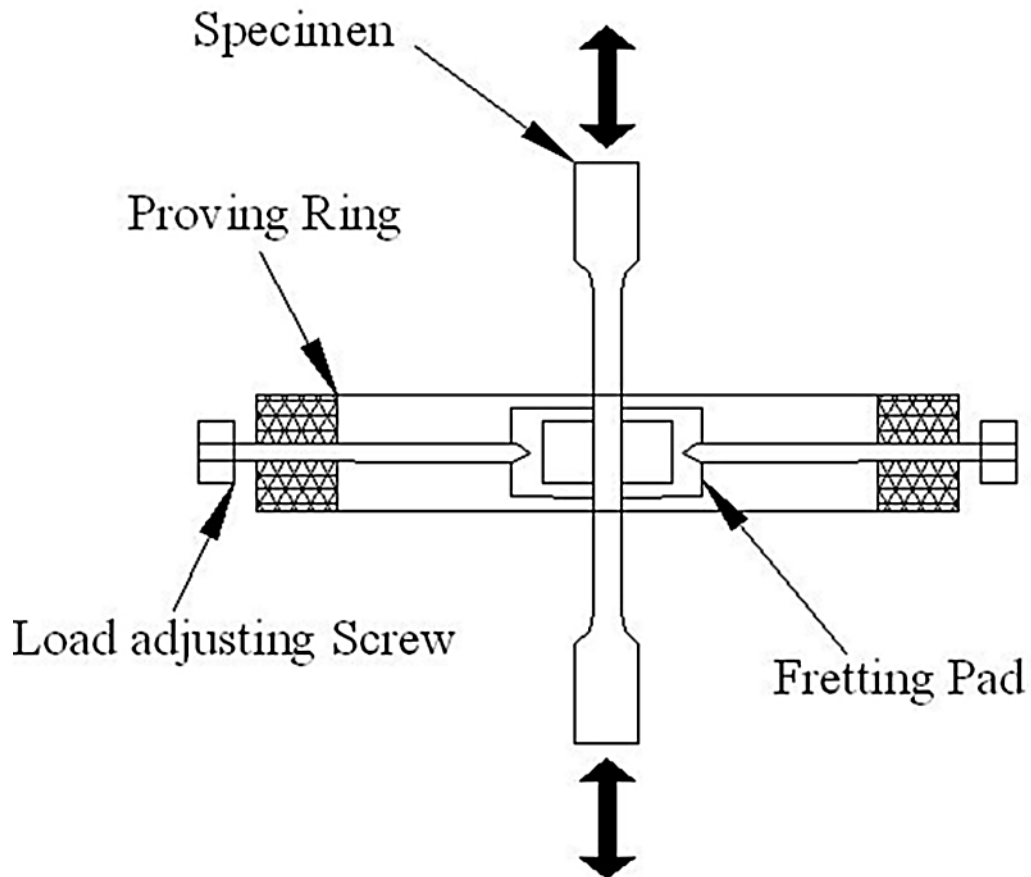


Figure 2.4: Schematic representation of the floating bridge used in fretting tests (Zhang & Liu, 2011)

To avoid the formation of different slip regimes at each contact pair, an alternative was used by proposing a bridge in which the movement is on one side of the bridge and another end is fixed as rigid (Figure 2.5). When the contact pair is made with complete contact then getting the stress results at contacts would be cumbersome. The major worries lie in stress singularity at contact edges, machining defects and the occurrence of bending in bridges. Intuitively a minor machine imperfection or a little change in the positioning of the pad would lead the way of affecting not only local contact pressure but also affect the overall contact conditions. The way to overcome this is to convert the complete contact into incomplete contact and this change was introduced by Nishioka & Hirakawa in 1969. They have used cylindrical configurations instead of flat as shown in Figure 2.5.

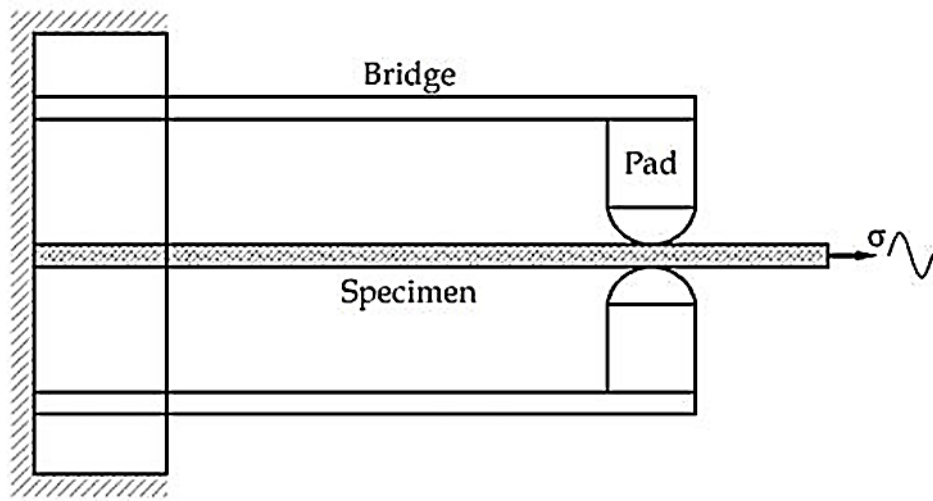


Figure 2.5: Fretting apparatus using cantilever bridge

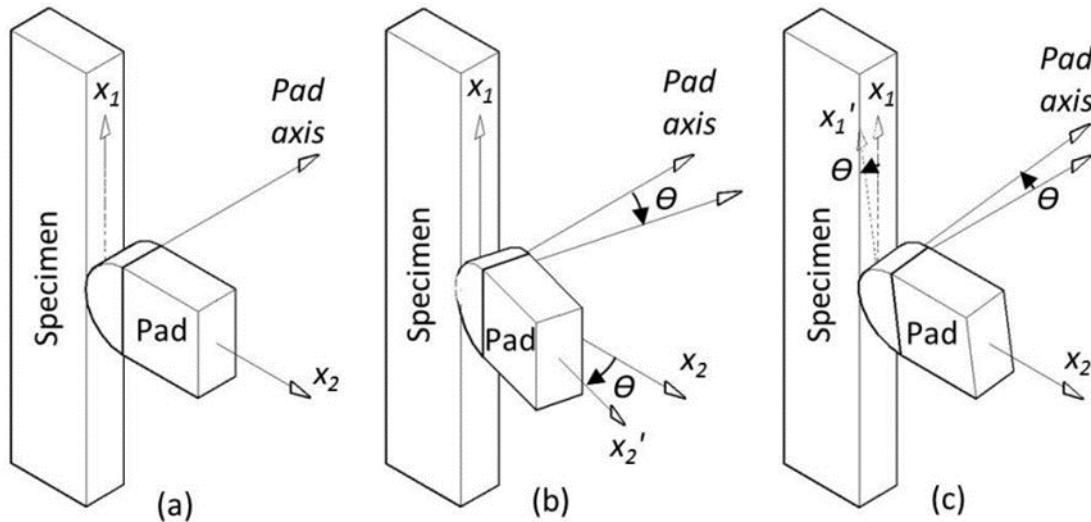


Figure 2.6: a) Perfectly aligned specimen and pad. Misalignment by pad rotation Θ b) around x_1 axis or c) around x_2 axis (Vaduchezhian et al., 2011)

This contact configuration formed by a cylindrical pad allows a closed-form solution in contact stress calculations not only in fretting cases and in fatigue also. As discussed earlier, the edge effect and alignment of pads are playing the main role, it needs to be addressed properly. Theoretically, the edge effect is not arising in contacts when the dimensions of the cylinders are infinite. Since the infinite value in dimensions is not existing and the stress intensity zones might be present at the edges. These edge effects can be neutralized or minimized by the use of identical width specimens and pad in contacts. An alignment of the pad on the specimen needs to be carefully dealt with since any tilt or rotation of the pad is causing a disturbance in tractions (Figure 2.6). Even

though the tilt in the pad axis on the specimen does not affect the pressure distributions but it makes the loss in applied normal force. The study regarding misalignment of pads and proper and improper contacts can be found in Vaduchezhian et al. (2011). The axisymmetric contact (spherical face) on the specimen is not brought any misalignment but it makes a more complex state of stress condition. Complete analysis regarding this contact configuration can be found in Hills & Nowell (1994). Experimental works regarding this contact can be found in Kuno et al. (1989) and Navarro et al. (2008).

The little modification in the form of adjusting the spring stiffness of the cantilever beam instead of keeping it fixed was made in the process of evolution of fretting test rigs. This kind of test rig can be found in Bramhall (1973), Nowell & Hills (1990) and Szolwinski & Farris (1998) and schematic view and the picture of their system are shown in Figure 2.7: a, Figure 2.7: b and Figure 2.8. The advantage of using this test rig in fretting tests are providing no unwanted phase shift between cyclic and shear forces and being inexpensive. Sufficient bulk load has to be applied on the specimen to produce the required amount of tangential force irrespective of the spring stiffness value. It should not be used in experiments where plain fretting occurs. The condition of keeping constant fatigue load during the fretting experiment is called plain fretting. The fretting rig with a single actuator was originated for the tests with bridge-type pads have been used where the process of inducing micro-level tangential displacement using an external actuator is cumbersome. The availability of a better method to control the production of displacement leads to perform the fretting experiments with two external actuators which were done by Fellows et al. in 1997. The main cause for this invention was to give a try to separate crack nucleation and crack propagation times in their study. Since the separate external actuator was used to produce tangential displacement, the fretting rig has the advantage to produce the real-time scenario of the fretting problems in the lab environment by varying the waveform, frequency and amplitudes. However, well-controlled experimental facilities have to be made to be able to manage two actuators.

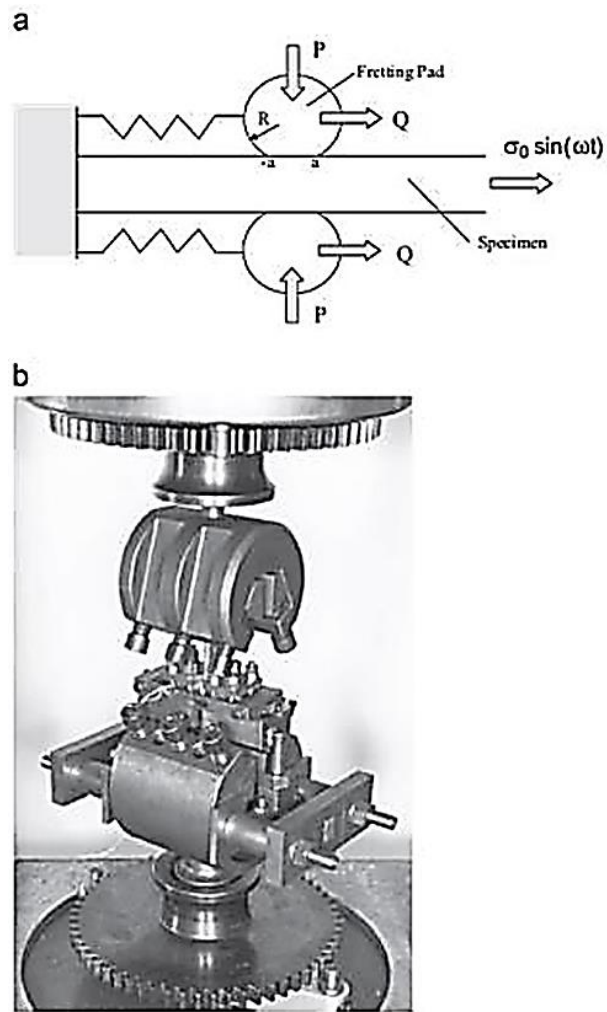


Figure 2.7: a) Schematic and b) Picture of Bramhall test rig (Hills & Nowell, 2014)

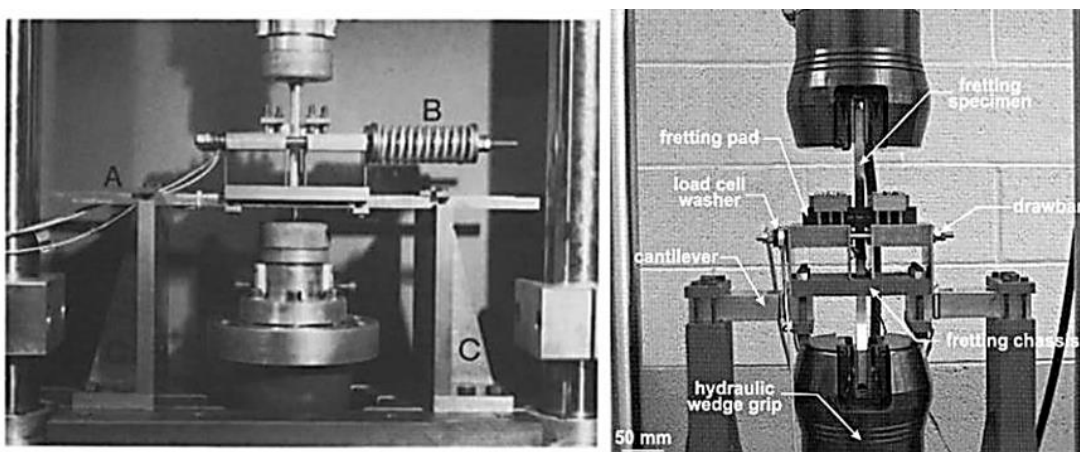


Figure 2.8: Fretting test rig used by Nowell & Hills (1990) (left) and Szolwinski & Farris (1998) (right)

Meriaux et al. in 2010 have used a fretting rig with two collinear actuators in their fretting fatigue experiments. In addition to the two actuators, they have equipped the rig with potential drop and acoustic emission systems which were used to monitor the crack nucleation and its propagation. In 2014, Hills & Nowell have used an advanced rig with three actuators to control the fatigue load, tangential load and normal load individually.

Since the 1980s onwards, various researchers have implemented special setups and rigs to conduct fretting and friction experiments. A short brief study regarding the usage and findings of fretting experiments with various rigs is given hereafter. Bridge type pads along with ring type load cells were used, in their fretting experiments, by Wharton and Waterhouse (1980), Swalla and Neu (2001) and Naidu and Raman (2005). Ouyung et al in 1993 and Goto and Ashida in 1999 have used proved ring setup for their fretting experiments. A troublesome setup, which has six load cells in which two have been used to measure normal loads and four have been used to measure tangential load, was used by Wittowsky et al. in 1999. Pape and Neu (1999) popularized a new fretting setup which has flat on flat contact on one side and cylinder on flat contact on another side. This was achieved by using bridge type fretting pads in their fretting experiments. They have used the proving ring concept to measure tangential loads indirectly by taking readings from pasted strain gauges below the fretting pads. Due to the calibration time accounted for the proving ring for each experiment, this fretting setup is laborious to use. Though the fretting failure study is very crucial for the aerospace field particularly dovetail joints of a jet engine (Figure 2.2), a dovetail fixture was used by Conner and Nicholas (2006) and Golden et al. (2008) in their fretting experiments. This particular fixture can be useful to apply both normal and shear loads. By using this setup in their fretting experiments, they found that both normal and shear loads vary simultaneously as a counter of applied bulk load on the specimen. A new fretting setup was designed, fabricated and used in experiments by Arora et al. in 2007. This setup, which was attached to the specimen with the help of bolt and nut arrangement, has the advantage to measure tangential load directly by the load cells which was attached to the pad holders of this setup. The difficulty was arising when mounting the fixture on the specimen. The dual actuator setup was used by Lee et al. (2007) in which one was used to giving the movement to the specimen and another one was used to give tangential

load between pad and specimen. Instead of using a separate actuator to create a tangential load, the better way to produce a low amplitude of motion between pad and specimen and necessary shear load is to use the specimen compliance and the bulk load which is applied to the specimen (Hills and Nowell (1994)). Farris et al. (2003b) and Golden et al. (2008) have used a bridge-type fretting setup in their experiments in which they have utilized the compliance of specimen or bridge or both to produce shear load between pad and specimen. In their setups, the generated tangential load is a reactional force to the applied bulk load on the specimen. Additional modifications have been done on these rigs by Murthy et al. (2006) and used for their high-temperature study. Since the setup was implemented and used by Farris et al. (2003b) has the advantage to minimize the setup time by measuring the tangential load directly, it is chosen as a base for our fretting study with necessary modification.

2.2 DESIGN OF FRETTING RIG

2.2.1 Development of suitable fretting rig

The development of a suitable fretting rig is based on a standard fretting fatigue rig used by some researchers (Farris et al., 2003). While designing, emphasis has to be given to minimizing the setup time for the conduct of experiments. This rig does not need recalibration during every experiment unlike rigs developed by the researchers (Ouyang et al., 1993; Goto and Ashida, 1999, etc.). Two load cells are being attached on threaded rods by which the normal loads are given on the specimen. The top and bottom load cells between the specimen grips is helpful to measure the applied bulk load and transferred load onto the support grip. The difference between these two values gives the tangential load directly.

2.2.2 Description of proposed fretting rig structure

The schematic representation of the proposed fretting rig, which can be used for both reciprocating/full sliding and fretting tests, is shown in Figure 2.9. The specimen is clamped at the upper grip. Pads, one on either side of the specimen, are clamped onto the specimen through pad holder blocks. Pad holder block is made of two parts that can be bolted together. The two parts have grooves in the centre to accommodate the pads.

The pad is placed in the grooves in the top and bottom portion of the pad holder block. The two halves of the pad holder are then bolted together with standard bolts. Each pad holder block is connected to the chassis by a set of thin plates (diaphragms) (Figure 2.9). Normal load (P) is applied to the contact interface with the help of two threaded rods passing through free holes in the pad holder. It is applied by tightening the nuts against the pad holder and the load is measured by a load washer embedded between the pad holder and the nut. The sum of the loads applied from the two rods gives the overall normal load (P) applied. The rods are located symmetrically on either side of the pad. To eliminate out of the plane moment at the contact, the loads on both the rods must be identical. Since the pad holders are connected to the rigid platform with thin plates which act as membranes (diaphragms), most of the load is applied to the pad holder block in the horizontal direction (i.e., normal/transverse load on the set of plates) is transmitted to the pad-specimen interface. This is because the resistance offered by a membrane to transverse loads is negligible. At the same time, these four diaphragms provide very good stiffness in the vertical direction (i.e., to in-plane loading), due to which tangential or frictional load (Q) is generated at the specimen-pad interface. This fixture can be used for fretting tests as well as reciprocating sliding friction tests. A free body diagram for both full sliding and fretting tests is depicted in Figure 2.10. For fretting or fretting fatigue tests, both the ends of the specimen could be clamped. When a load (F_o) is applied to the top end of the specimen through the hydraulic actuator, it is transferred to the chassis through the contact between the specimen and pad ($Q + Q$). This is referred to as tangential load or frictional load in this work. The amplitude given at the actuator will be decided by the axial stiffness of the specimen (from the contact interface to the lower gripping portion) and the stiffness of the diaphragms.

To bring this proposed rig into practice, the 1-D and 3-D Finite Element Analysis (FEA) was performed using ANSYS Software followed by the fabrication of this fretting rig could be completed. Then, the fretting experiments will be conducted and the details are given hereafter.

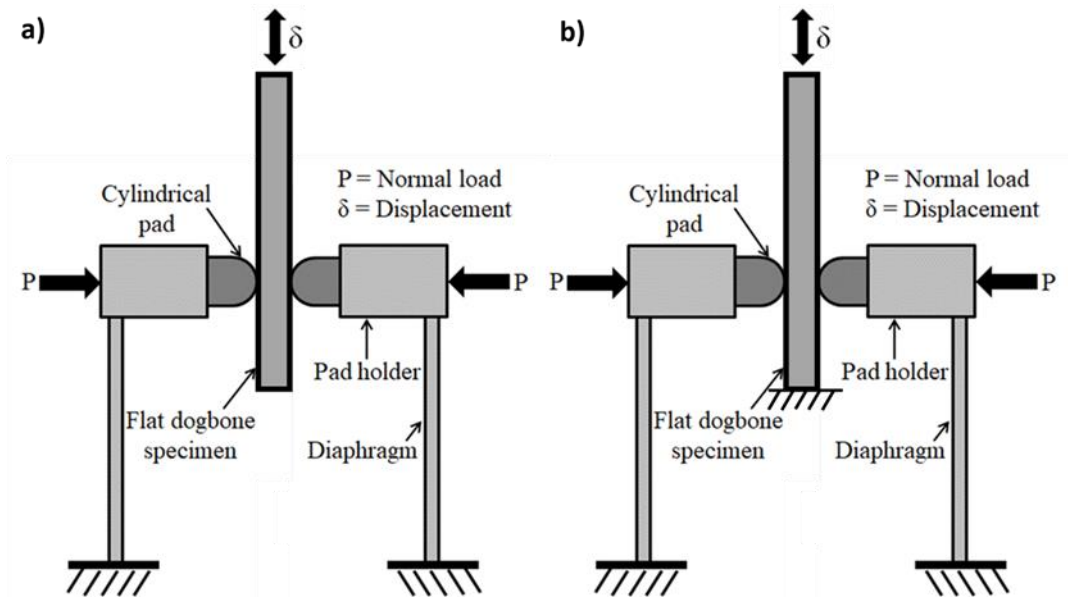


Figure 2.9: Schematic of loading system to conduct a) full sliding and b) fretting tests

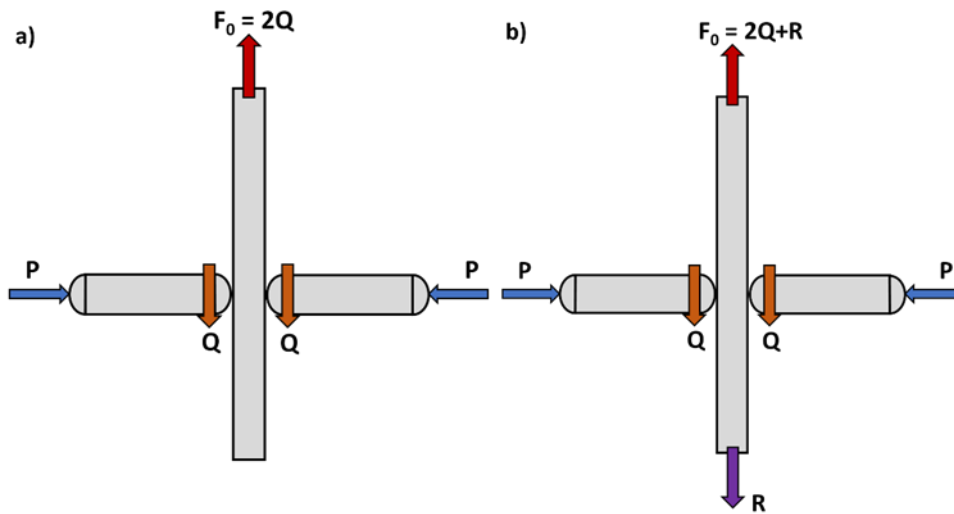


Figure 2.10: Free body diagram of specimen in a) full sliding and b) fretting tests

2.2.3. Finite element analysis of fretting rig

Fretting experiments were conducted with cyclic loads involving a suitable stress ratio ('R' ratio). To decide the 'R' ratio, we need to understand the load transfer ratio (LTR). LTR is the ratio between the load transferred to the top of the specimen and the load applied to the bottom of the specimen. LTR needs to be the least value which is approximately close to 50 % to conduct fretting experiments and this value had taken

from the Dovetail joint analysis of aero-engines (Farris et al. (2003)). To ensure the above condition, eleven cases of simple one-dimensional (1-D) fretting rig models have been grouped into two types:

- Without a vertical beam
- With a vertical beam

The main difference, between the type-1 and type-2 fretting rig models, is in the provision of the vertical beam between the bottom column supports and horizontal beam-2. By considering three and one vertical column supports, the type-1 fretting rig model has been divided into two cases. According to the variation in the length of the vertical beam, the type-2 model is classified into nine cases. In both 1-D and 3-D FE analyses, the specimen and pads are considered as Aluminium alloy material.

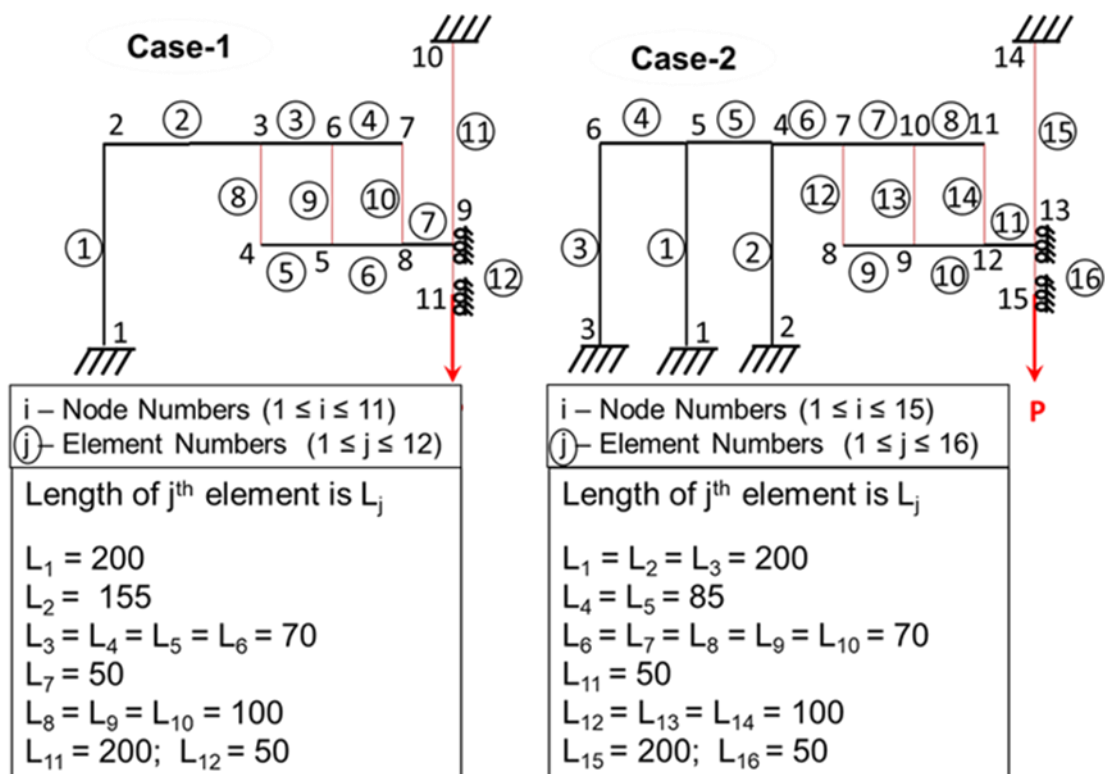


Figure 2.11. Type-1 fretting rig model cases used for 1-D finite element analysis

These eleven cases have been designed and finite element (FE) analysis of these models will be carried out. The schematic representation of these two types of 1-D finite

element fretting rig model with dimensions is depicted in Figure 2.11, Figure 2.12, Figure 2.13, Figure 2.14 and Figure 2.15.

1-D finite element analysis was performed using ANSYS software. BEAM188 and LINK180 elements are used for the analysis. The BEAM188 is a 2-node linear element having six degrees of freedom (DOF) (3 translations along the three perpendicular axes (u, v and w) and 3 rotations about the three perpendicular axes at each node (θ_x , θ_y and θ_z). LINK180 is an element that has 3 DOF (3 translations along the three perpendicular axes) at each node (u, v and w). For 1-D FEA, thin diaphragms (considered as spring elements) and specimen (considered that having only deformation along the loading direction) are modelled with LINK180 element and remaining portions of the rig structure are modelled with BEAM188 element. The node numbers 1, 2, 3 and 15 are restrained in all three directions. Specimen length is considered as 240 mm for the analysis without the consideration of curved portion and gripping portion lengths. Element numbers 16 and 17 are specimen which connects the nodes 14-15 and 14-16. In an attempt to reduce the time of the analysis, the fretting rig analysis has been carried out with only one side of the rig with the consideration of rig is symmetric concerning specimen axis. Node numbers 14 and 16 are restrained with symmetrical boundary conditions along X-direction. The normal load (P) applied at node number 16 is 1 N.

Material properties used for 1-D FE analysis are tabulated in Table 2.1. The element number, component name and its corresponding element used in 1-D FE analysis is shown in Table 2.2.

Table 2.1: Material Properties of elements used

Element Number	Young's modulus(E) in GPa	Poisson' s ratio (ν)
1 to 12	210	0.27
13 to 17	70	0.30

Table 2.2: Elements Used for 1-D FEA

Element No.	Component Name	Elements Used
1,2,3	Vertical column support	Beam188
4,5	Horizontal beam-1	Beam188
6	Vertical Beam	Beam188
7	Horizontal beam-2	Beam188
8,9,10,11	Horizontal beam-3	Beam188
12	Pad	Beam188
13,14,15	Thin diaphragm	Link180
16,17	Specimen	Link180

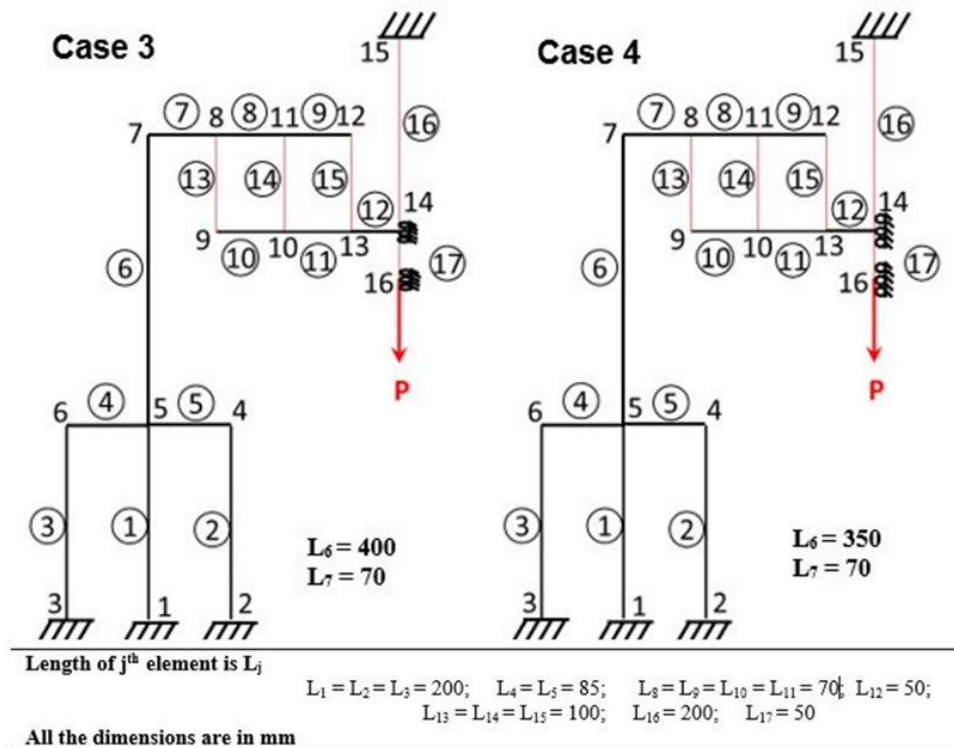


Figure 2.12: a) Case-3, b) Case-4, model of type-2 fretting rig used for 1-D FEA

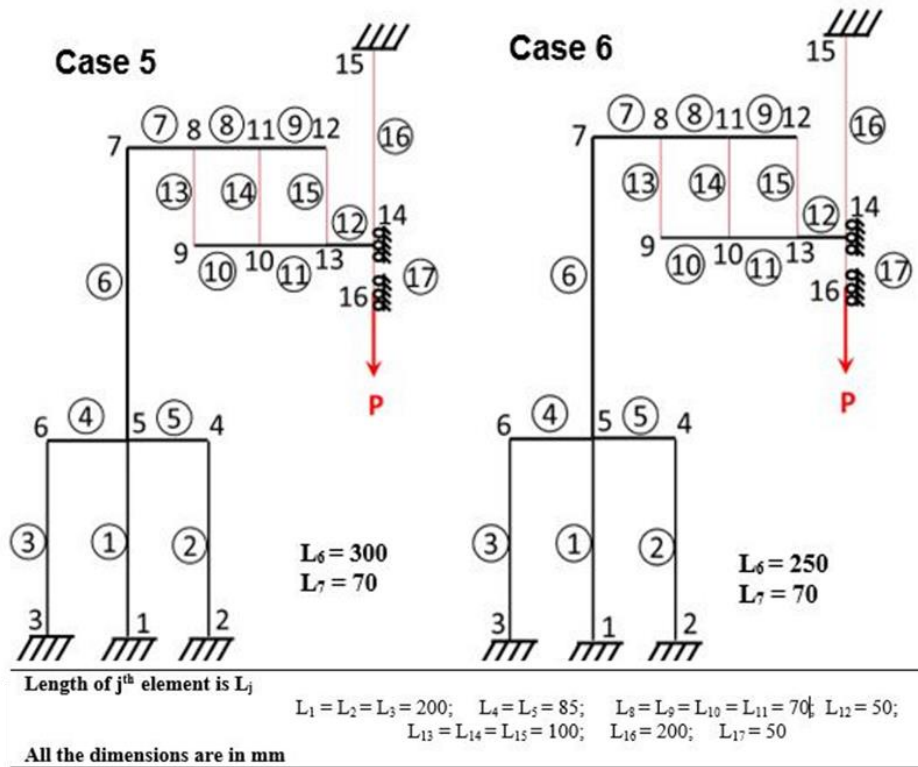


Figure 2.13: a) Case-5, b) Case-6, model of type-2 fretting rig used for 1-D FEA

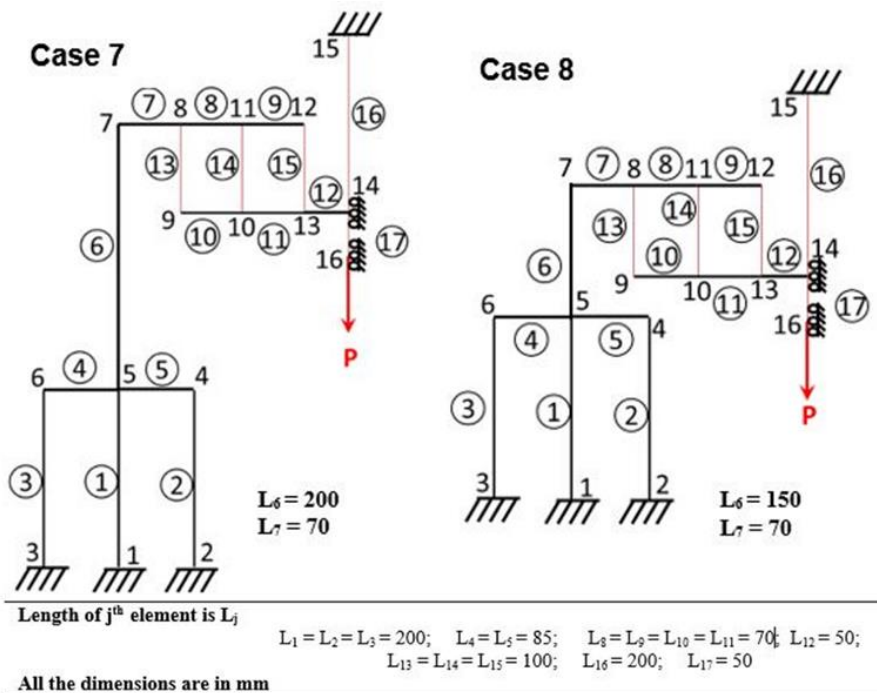
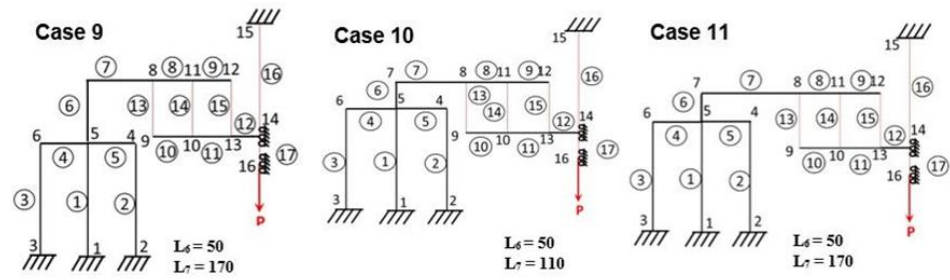


Figure 2.14: a) Case-7, b) Case-8, model of type-2 fretting rig used for 1-D FEA



Length of j^{th} element is L_j

$$L_1 = L_2 = L_3 = 200; \quad L_4 = L_5 = 85; \quad L_8 = L_9 = L_{10} = L_{11} = 70; \quad L_{12} = 50;$$

$$L_{13} = L_{14} = L_{15} = 100; \quad L_{16} = 200; \quad L_{17} = 50$$

All the dimensions are in mm

Figure 2.15: a) Case-9, b) Case-10, c) Case-11, model of type-2 fretting rig used for 1-D FEA

DESIGN AND FABRICATION OF DISPLACEMENT SENSOR

3.1 INTRODUCTION

J.A. Collins in 1965 has introduced the damage factor concept for the fretting fatigue process and grouped the parameters into eight categories. More than 50 parameters that are influencing the fretting process have been identified (J.M. Dobromirski, 1992). Among these parameters, the primary parameters which affect the fretting are coefficient of friction, normal force, shear traction and slip amplitude. Tangential slip under the contact interface has been affected by the normal force, tractive force and coefficient of friction, though all are interdependent (D.A. Hills, 1994). There have been various studies that showed the use of slip amplitude length as an identification parameter to describe the partial slip and gross slip changes during the fretting process. An increase in slip amplitude length has been considered to increase the fretting wear damage (Figure 3.1). However, slip amplitude has a strong influence on the fretting fatigue damage also (O. Vingsbo and S. Söderberg (1988) and S. Fouvry et al. (1996)). In fretting fatigue, the crack initiation and crack propagation time are affected by various factors (contact stresses, frequency, environmental conditions, etc.) including slip amplitude.

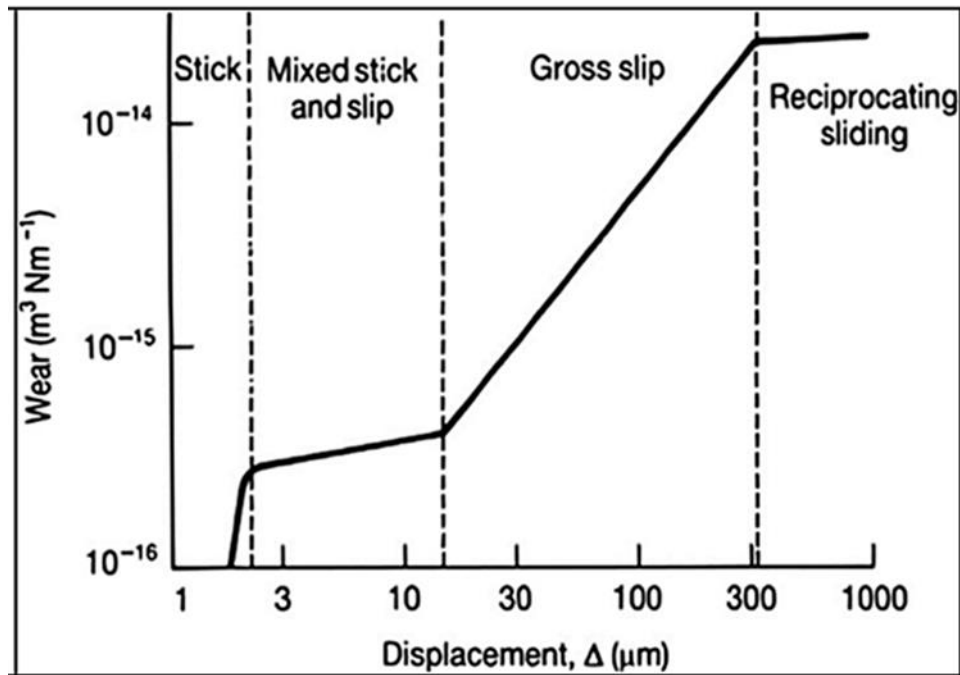


Figure 3.1: Illustration of the dependence of wear coefficient with displacement amplitude in fretting concerning the slip regime (O. Vingsbo and S. Söderberg, 1988)

Identification of slip amplitude is necessary with regards to wear analysis and also used in fretting fatigue criterion directly (C. Ruiz et al., 1984). The deteriorating effect of fretting wear due to the increase in slip amplitude was explained by G.M. Spink in 1990. O. Vingsbo and S. Söderberg (1988) have reported the effect of slip amplitude on the fretting fatigue life of materials. Measurement of relative slip between pad and specimen is necessary for completing the functional requirement to identify the changes of fretting regimes. Slip amplitude measurement at the contact interface under fretting, is a tedious and important job to characterize the fretting process, which was carried out by many researchers. In fretting, measurement of slip amplitude has been done either by using devices such as Eddy current non-contact transducers (H.H. Farrahi, and G. Maeder, 1992), extensometers (H. Lee et al, 2007), Linear Variable Differential Transformers (LVDTs) (A. A. Walvekar et al., 2014), laser displacement sensor (J. Ferrero et al., 2004) and Capacitance position sensor (L.H. Favrow et al. (2000) and K. Vadivuchezhian et al. (2011)) or by adopting Digital Image Correlation (DIC) (J. Juoksukangas et al., 2017) method. Using the above-mentioned devices/techniques/methods, other than DIC, to measure slip amplitude, involve the

following difficulties: usually slip amplitude is at micron level or even less than micron level and it is hard to measure at the contact interface by adopting the above-mentioned devices, the possibility of error occurrence in the slip measurement due to the inclusion of compliance effect of measuring device and test device and difficulties involved in the installation of measuring device at the contact interface (A. Ramalho, and J.P. Celis (2003) and J. De Pauw et al. (2014)). So, there is a need for the development of a simple and precise apparatus to measure contact slip and make an apparatus into a widely usable one.

The present study proposes a new strip and sensor arrangement to estimate the relative slip between pad and specimen under fretting conditions. To accomplish this a numerical and analytical study of the proposed thin curved strip with the strain gauge, usually termed here as “sensor”, were performed. The validation of displacement value obtained from both analytical approach and numerical approach has been done by conducting experiments with the thin curved sensor.

3.2 METHODS AND MATERIALS

The present study involves the design of a thin-walled curved sensor to measure the relative displacement between the pad and the specimen during fretting experiments. As stated earlier, usually the relative displacement is in micron or even less in scale, hence the displacement sensor should merely be stretchable when the load is applied and also be able to retract back to its original position when the applied load is removed. The relative displacement is a function of axial load applied to the specimen, tangential force at the contact and compliance of machine and pad supports. A thin flat strip hasn't been considered due to the applied load on the specimen would be acting in the lateral direction of the strip. So, a thin curved strip has been selected, with and without slots on it, for the analysis. The design process of the thin curved sensor was done by adopting the following two approaches; the Strain Energy Approach (SEA) and Finite Element Analysis (FEA).

3.2.1 Strain Energy Approach (SEA)

As part of the preliminary design process, a thin curved strip without a slot has to be modelled and it is used for finite element study. The thin curved strip without slot is shown in Figure 3.2a). Before doing the finite element analysis, the Strain Energy (SE) approach was used to find the maximum deflection, the deflection at the middle of the strip and maximum stress of the thin curved strip and the formulae have been given in equations (1), (2) and (3). The formulae have been derived from the strain energy approach and pure bending equation.

In the design process of any curved member, a basic understanding of the difference that exists between a straight beam and a curved beam is necessary. The main difference is locating the neutral axis of the beam concerning the centroidal axis. In straight beams, both the axis coincides whereas, in curved members, the neutral axis is slightly shifted towards the centre of curvature of the member (S. Timoshenko, 1955). The distance between the centroidal axis and neutral axis is known as eccentricity 'e'. The normal stress distribution across sections is linear and its value at the centroidal axis is zero for straight beams. However, the normal stress variation across cross-sections is hyperbolic in curved beams. The following assumptions are considered for any design involved in curved members. The assumptions are,

- The material of the beam is perfectly homogeneous [i.e., same material throughout] and isotropic [i.e., equal elastic properties in all directions].
- The cross-section has symmetry concerning the plane axis along the length of the beam.
- The material of the beam obeys Hooke's law.
- The transverse sections which are plane before bending remain plane after bending also.
- Each layer of the beam is free to expand or contract and it never depends on the layer above or below it.
- Young's modulus (E) is same for the material both under tension and compression.
- The radial strain produced, when the load is applied, is negligible.

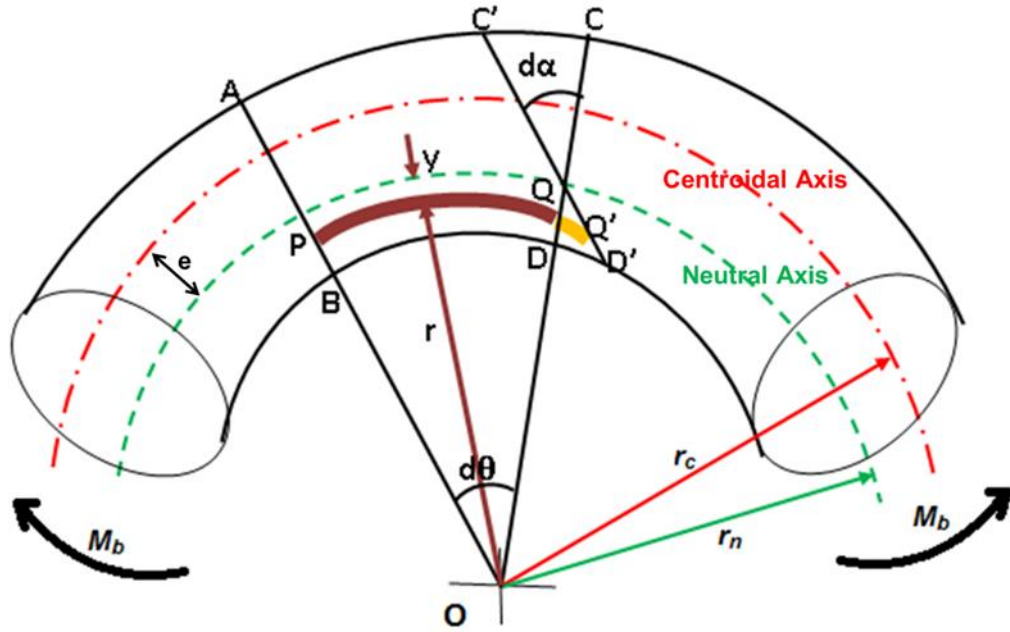


Figure 3.2: Free body diagram of considered curved section

Deformed length of the considered layer is, $dl = y * d\alpha$

Initial length of the considered layer is, $l = r * d\theta$

So, Strain (ξ) in that layer is,

$$\xi = \frac{dl}{l} = \frac{y * d\alpha}{r * d\theta} = \frac{y * d\alpha}{(r_n - y) * d\theta} \quad (1) \quad (\text{Since, } r = r_n - y)$$

By Hooke's law,

Stress (σ) = Young's Modulus (E) X Strain (ξ)

$$\sigma = \frac{E * y * d\alpha}{(r_n - y) * d\theta} \quad (2)$$

By applying 2 static equilibrium equations, we can find the value of $d\alpha/d\theta$. They are,

1. The summation of force distribution along the cross-section is zero.

$$\iint (\sigma \cdot dA) = 0 \quad (3)$$

2. Applied moment is equal to the internal resisting moment.

$$\iint (\sigma \cdot y \cdot dA) = M_b \quad (4)$$

By substituting (2) in (3), we get,

$$\iint \frac{E \cdot y \cdot d\alpha}{(r_n - y) \cdot d\theta} dA = 0$$

$$\iint \frac{y}{(r_n - y)} dA = 0 \quad (5) \quad \left(\text{Since } \frac{E \cdot d\alpha}{d\theta} \neq 0\right)$$

From (4),

$$\iint \frac{E \cdot y \cdot d\alpha}{(r_n - y) \cdot d\theta} y \cdot dA = M_b \quad \rightarrow \quad \iint \frac{E \cdot d\alpha (y^2 - r_n \cdot y + r_n \cdot y)}{(r_n - y) \cdot d\theta} dA = M_b$$

$$\frac{E \cdot d\alpha}{d\theta} \left[- \iint \frac{y \cdot (r_n - y)}{(r_n - y)} dA + r_n \iint \frac{y}{(r_n - y)} dA \right] = M_b$$

In the above equation, the second integral is zero (Ref. Eqn. (5)). So,

$$\frac{E \cdot d\alpha}{d\theta} \left[- \iint y \cdot dA \right] = M_b \quad \rightarrow \quad \frac{E \cdot d\alpha}{d\theta} \left[-(-eA) \right] = M_b$$

$$\frac{d\alpha}{d\theta} = \frac{M_b}{E \cdot A \cdot e} \quad (6)$$

By substituting Eqn. (6) in Eqn. (2), we get,

$$\sigma = \frac{M_b \cdot y}{(r_n - y) \cdot A \cdot e} \quad (7)$$

From Eqn. (7), we know that the value of e and r_n are required to find the stress. By using Eqn. (5), the derivation for the radius of the neutral layer (r_n) is obtained.

$$\iint \frac{(y-r_n+r_n)}{(r_n-y)} dA=0 \quad \rightarrow \quad -A + \iint \frac{r_n}{(r_n-y)} dA=0$$

$$r_n = \frac{A}{\iint \frac{dA}{(r_n-y)}} = \frac{A}{\iint \frac{dA}{r}} \quad (8)$$

By using the above equation, we can calculate the neutral layer radius (r_n) and eccentricity (e) is the distance between the centroid layer and neutral layer and it can be calculated by Eqn. (9).

$$e = r_c - r_n \quad (9)$$

From Eqn. (7), we can conclude that the stress distribution is hyperbolic fashion and it is shown in Figure 3.3 along with the stress equation.

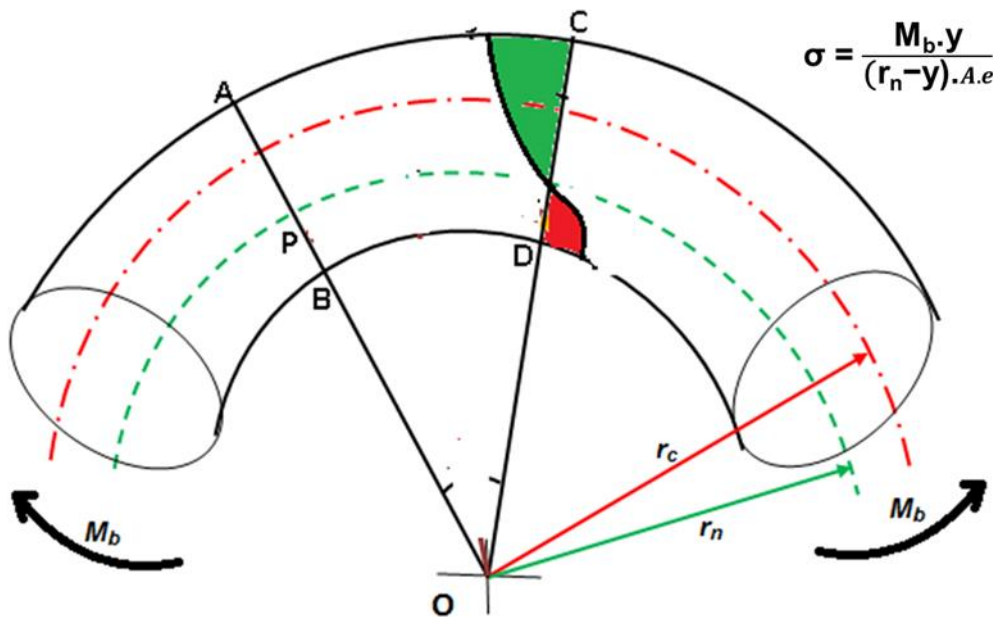


Figure 3.3: Normal stress distribution along cross-section in curved members

The deflection produced by the applied load (P) in the curved beams is to be found by using Castigliano's theorem. Castigliano's first theorem states that "the partial derivative of the strain energy (U) of the structure for any particular force (P_i) gives the

displacement (u_i) of the point of application of that force in the direction of its line of action". In equation form it can be stated as follows:

$$\frac{\partial U}{\partial P_i} = u_i ; i = 1, 2, 3, \dots, n \quad (10)$$

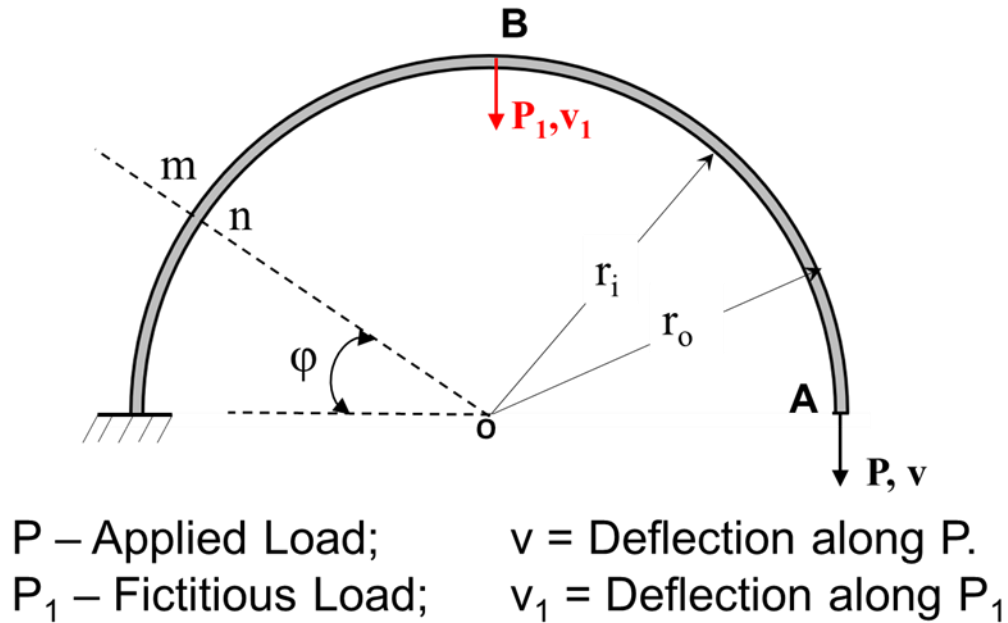


Figure 3.4: Thin curved strip with loads and boundary conditions

The proposed model of a thin curved strip (Figure 3.4) is going to be modelled for only 180° to maintain the symmetry in material, dimensions and loading conditions. Here, one end is fixed for analysis and the load (P) is applied on the other end. The midpoint deflection of the curved strip is more important for the analysis. Since the fictitious load (P_1) is considered to be applied at the midpoint by which the deflections (v & v_1) along loading direction can be calculated using Castigliano's first theorem and it will be explained hereafter.

Generally, the strain energy stored in the body due to the applied load is calculated using equation 11. Here the moment created by the applied load is dominant and it is only considered for the analysis.

Strain energy stored in the body due to the applied load (P) is,

$$U = \int_0^s \frac{M^2}{2EI} ds \quad (11)$$

The moment (M) due to the applied load (P) concerning the section m-n is,

$$M = -[P.R.(1 + \cos \varphi) + P_1.R.\cos \varphi] \quad (12)$$

$$ds = R.d\varphi \quad (13)$$

By applying Castigliano's theorem and by substituting Eqn. (12) and (13) in Eqn. (11), we get,

The maximum deflection (v or δ_{\max}) at the free end along the direction of applied load (P),

$$v = \delta_{\max} = \frac{\partial U}{\partial P} = \int_0^{\pi} \frac{M}{EI} \frac{\partial M}{\partial P} R.d\varphi$$

$$v = \delta_{\max} = \frac{3\pi}{2} \frac{PR^3}{EI} \quad (14) \text{ and}$$

The midpoint deflection (v_1 or δ_{mid}) at the midpoint of the curved strip along the direction of fictitious load (P_1),

$$v_1 = \delta_{\text{mid}} = \frac{\partial U}{\partial P_1} = \int_0^{\pi} \frac{M}{EI} \frac{\partial M}{\partial P_1} R.d\varphi$$

$$v_1 = \delta_{\text{mid}} = \frac{\pi}{2} \frac{PR^3}{EI} \quad (15)$$

Where P is applied normal load in N, r is the mean radius of the thin curved strip in mm, E is the elastic modulus of the strip material in N/mm², I is the moment of inertia of strip in mm⁴ and M is maximum moment acting on the strip in Nmm. For the curved sections, the neutral layer axis is not coinciding with the centroidal axis of the section. So, the distance between the neutral axis and the outer layer is referred to as y in mm (Figure 3.5:b). Since, the consideration of the rectangular curved section for the thin strip, the radius of the neutral axis (r_n) is calculated by using Eqn. (16).

The radius of the neutral axis,

$$r_n = \frac{A}{\int \frac{dA}{r}} = \frac{b \cdot h}{b \cdot \ln\left(\frac{r_o}{r_i}\right)} = \frac{h}{\ln\left(\frac{r_o}{r_i}\right)} \quad (16)$$

Where r_o is an outer radius, r_i is an inner radius, b and h are the width and height of the thin curved strip respectively and their unit is mm.

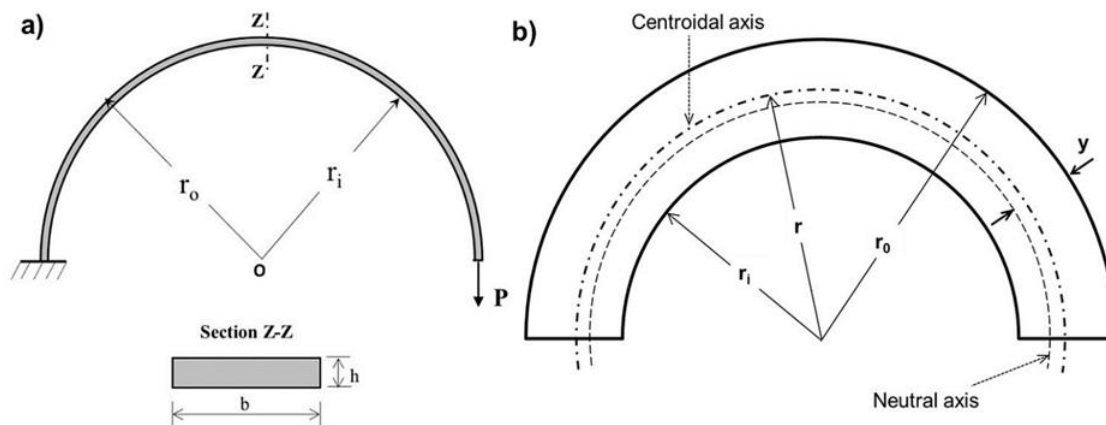


Figure 3.5: a) Thin curved sensor without slot; b) Schematic view of a curved beam with neutral axis shift from the centroidal axis (magnified view)

3.2.2 Finite Element Analysis (FEA)

The FEA has been performed using ANSYS with SOLID185 element for the solid model and SHELL181 element for the surface model. SOLID185 element has eight nodes and each node has three translational degrees of freedom (u , v and w). SHELL181 is a four-node element and it has six degrees of freedom at each node (three translations (u , v and w) along three axes (X , Y and Z) and three rotations (θ_x , θ_y and θ_z) about the three axes).

The thin slotted strip can capture the least possible displacement values and possess a lower stiffness value and higher flexibility than the strip without a slot for the same applied load. So, the thin slotted curved strip has been considered as a simplified suitable arrangement to measure small displacement at the contact interface under fretting conditions.

Finite element analysis of thin curved strip with different slots have been done with various dimensional modifications involved in the thin strip with different slot types, slot size, number of slots, fillet radius of slot and the width of the thin strip and their details are as follows:

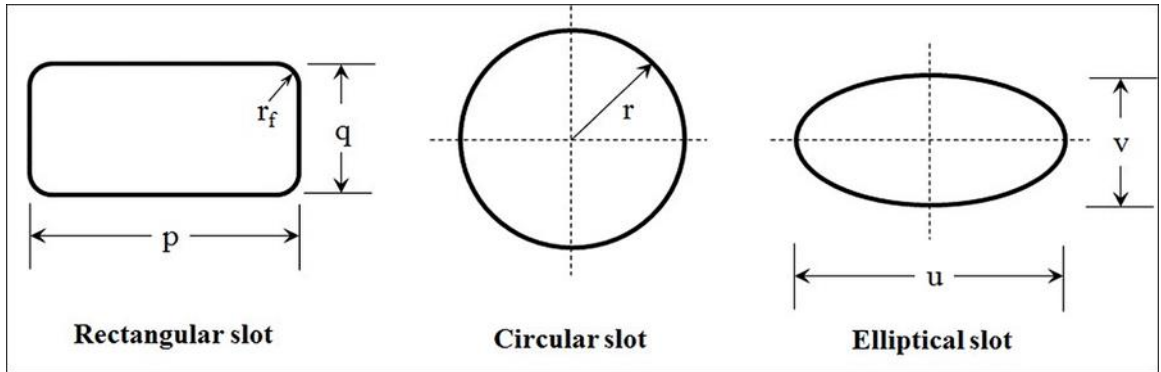


Figure 3.6: Implications of slot dimensions

The thin strip with rectangular slots, circular slots and elliptical slots were considered for the Finite Element study. The number of slots and their dimensions is different for each case and the number of slots varies from two to six. The geometric symmetry conditions, loading conditions and boundary conditions are the same as thin strips without slots and it has been maintained for all the cases of the thin strip with the slot. The dimensional implications of the different slots are depicted in Figure 3.6.

Table 3.1: Slot dimensions considered for Finite Element Analysis

S. No.	Type	Number of Slots/Holes (N)	Dimensions considered (mm)	Name of a thin strip
1	Rectangular slot	N = 2	$\theta_s = 45^\circ$; $q = 1, 2$; $r_f = 0.25, 0.5$	Strip_N_Rec_ θ_s _q_ r_f
		N = 4, 6	$p = 2, 4$; $q = 2$; $r_f = 0.25, 0.5$	Strip_N_Rec_p_q_ r_f
2	Circular slot	N = 4, 6	Radius (r) = 1, 3	Strip_N_Circ_r
3	Elliptical slot	N = 4, 6	$u = 2, 4$ $v = 1, 3$	Strip_N_Ellip_u_v

The dimensions considered for the slots and the name for each case of the thin strip are given in Table 3.1. Instead, the value of width (p), the slot angle (θ_s) has been mentioned in Table 3.1 for the thin strip with two rectangular slots. In the rectangular slot thin strips, r_f refers to fillet radius. The thin curved strip with various types of slots i.e. Rectangular, Circular and Elliptical are shown in Figure 3.7, 3.8 and 3.9 respectively.

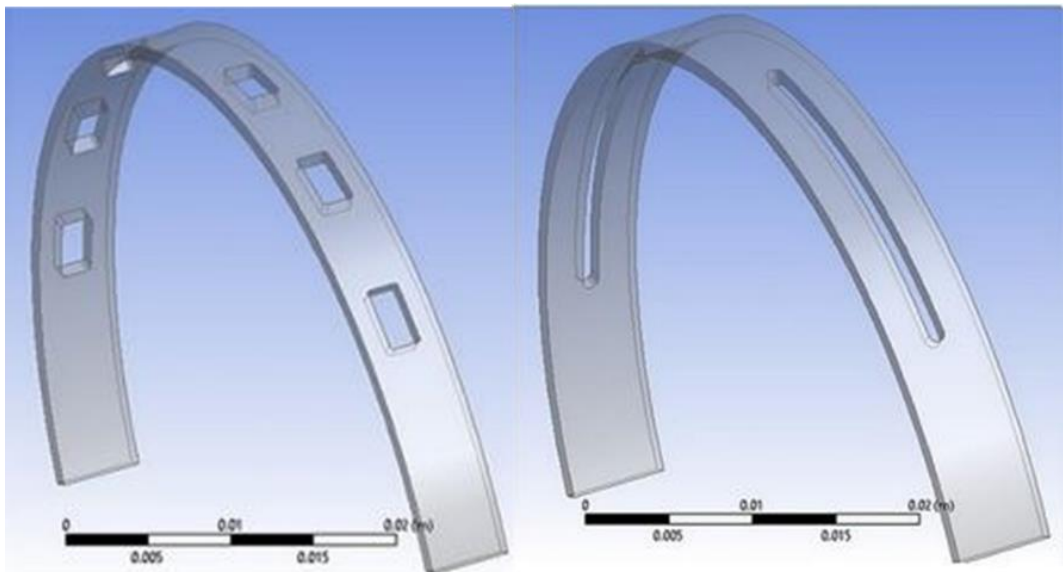


Figure 3.7: 3-D model of a thin curved strip with rectangular slots

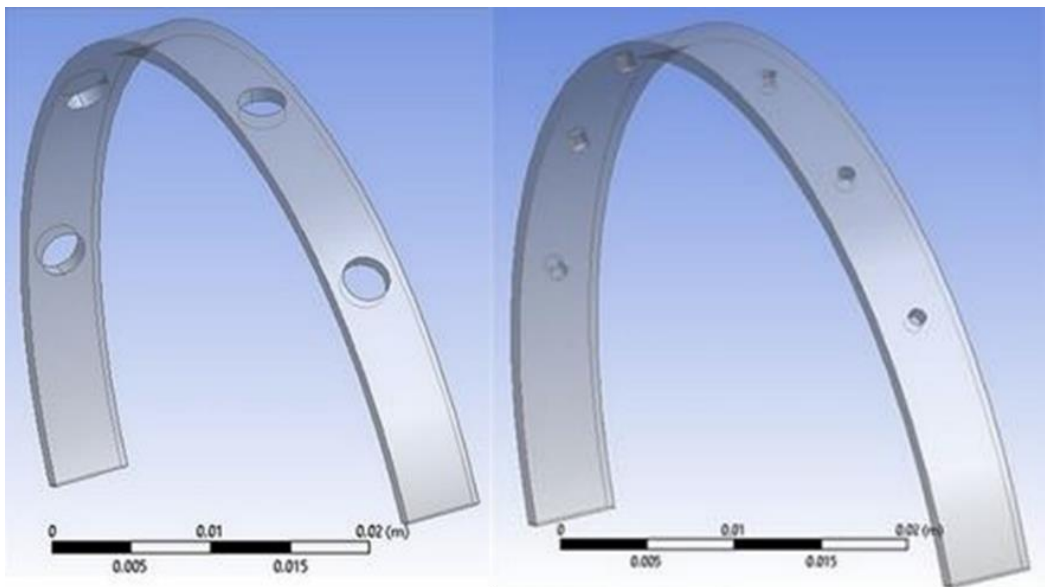


Figure 3.8: 3-D model of a thin curved strip with circular slots

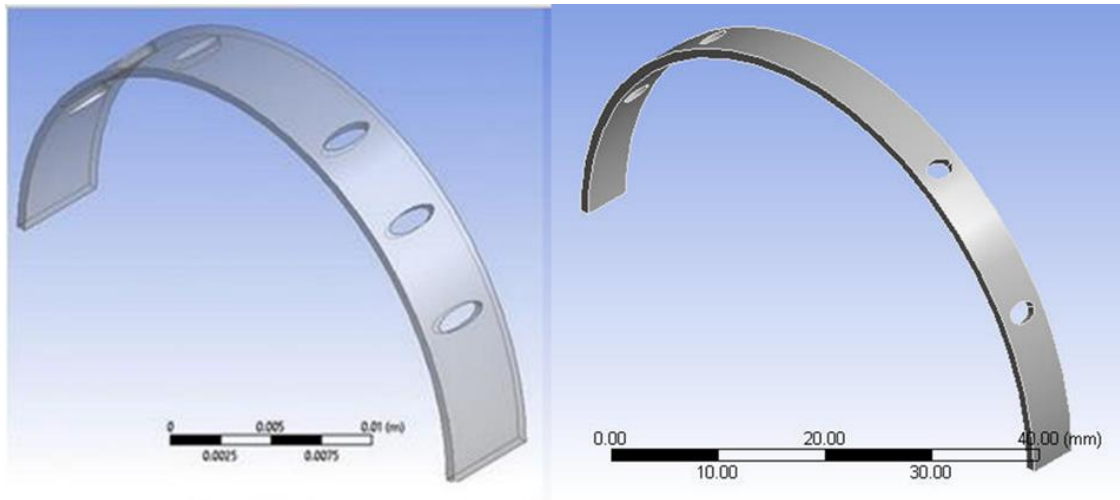


Figure 3.9: 3-D model of a thin curved strip with elliptical slots

3.2.3 Experimental details

A thin strip of possible minimum thickness is to be proposed for the experimental study. In an experiment, there was a rift in the stiffness values at the contact position of the specimen due to the applied normal load (K. Vadivuchezhian et al., 2011). These split in stiffness values resulted in decreasing the applied bulk load and it leads to minimum relative slip at the contact position. The material has chosen to fabricate the thin strip is EN32 material since it has good elastic and ductile properties and also it is readily available. To ensure the curvature throughout the experiments, the thin strip was heat treated. Strain gauges were pasted on both the inner and outer surface of the curved strip at the middle portion along the curved surface to record the strain values (Figure 3.10:a). The curved portion of the strip was extended to a length up to 15 mm to hold the strip during the experiments (Figure 3.10:b). Initially, the thin sensor is connected with the strip holder using two screws on both sides of the strip. Before using adhesives on the surfaces, all the surfaces were well polished and cleaned using acetone solution. One end of the strip along with its holder was fixed on the pad, another strip holder was pasted on the specimen using Araldite adhesive. To ensure a permanent fix of strip holders at both ends, nearly 1 mm thick adhesive has been used to paste the thin strip holder onto the pad and specimen. Here the bondage between the pad and strip holder

confirms the fixed end and the bondage between specimen and strip holder ensures that it is the end where the load is transmitted.

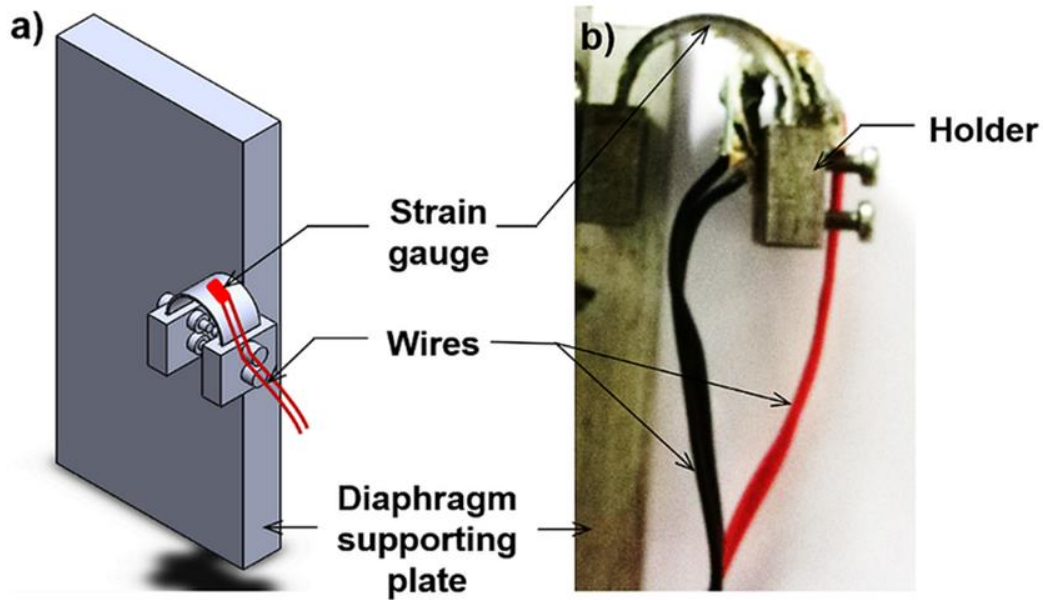


Figure 3.10: a) Schematic representation of thin curved strip and its arrangement; b) Closer view of thin curved strip and its arrangement during experiments

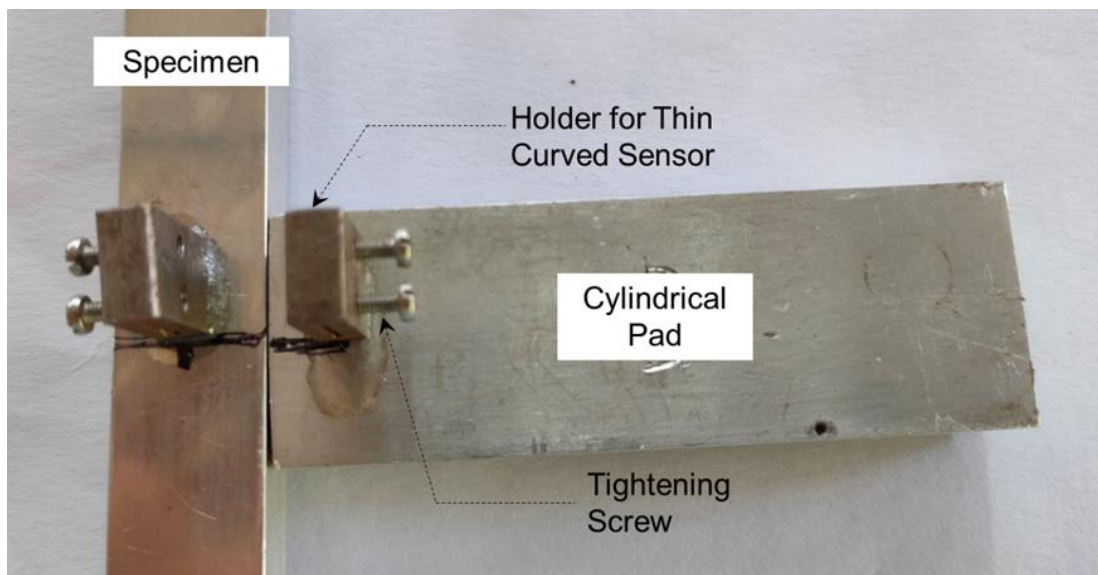


Figure 3.11: Thin strip holder arrangement in specimen and pad

The symmetry conditions of load transmissions were checked by getting the strain values from the strain gauges which are pasted at the centre of vertical plates. The

vertical column is having two slots through which the threaded rods were inserted and the normal load is applied using nut arrangements on both sides.

The Universal Testing Machine (UTM) with the capacity of 5 Ton has been used for this curved sensor experiment. The machine has a stationery upper jaw and movable lower jaw, between them the specimen is placed. The experiment has been started with the applied load of 2 kg and further, it went in the increment of 2 kg till 50 kg. To hold and keep the pads on either side of the specimen and applying the normal load through these pads onto the specimen, a separate rig was made and attached to the machine (Figure 3.11 and Figure 3.12). A rig consists of two vertical plates and two separate pad holders along with two threaded rods. While doing experiments, a constant normal load was applied on both the side of the specimen through pad using attached threaded rods manually. Load cells are used to measure the applied normal loads. All the experiments were performed in ambient air conditions.

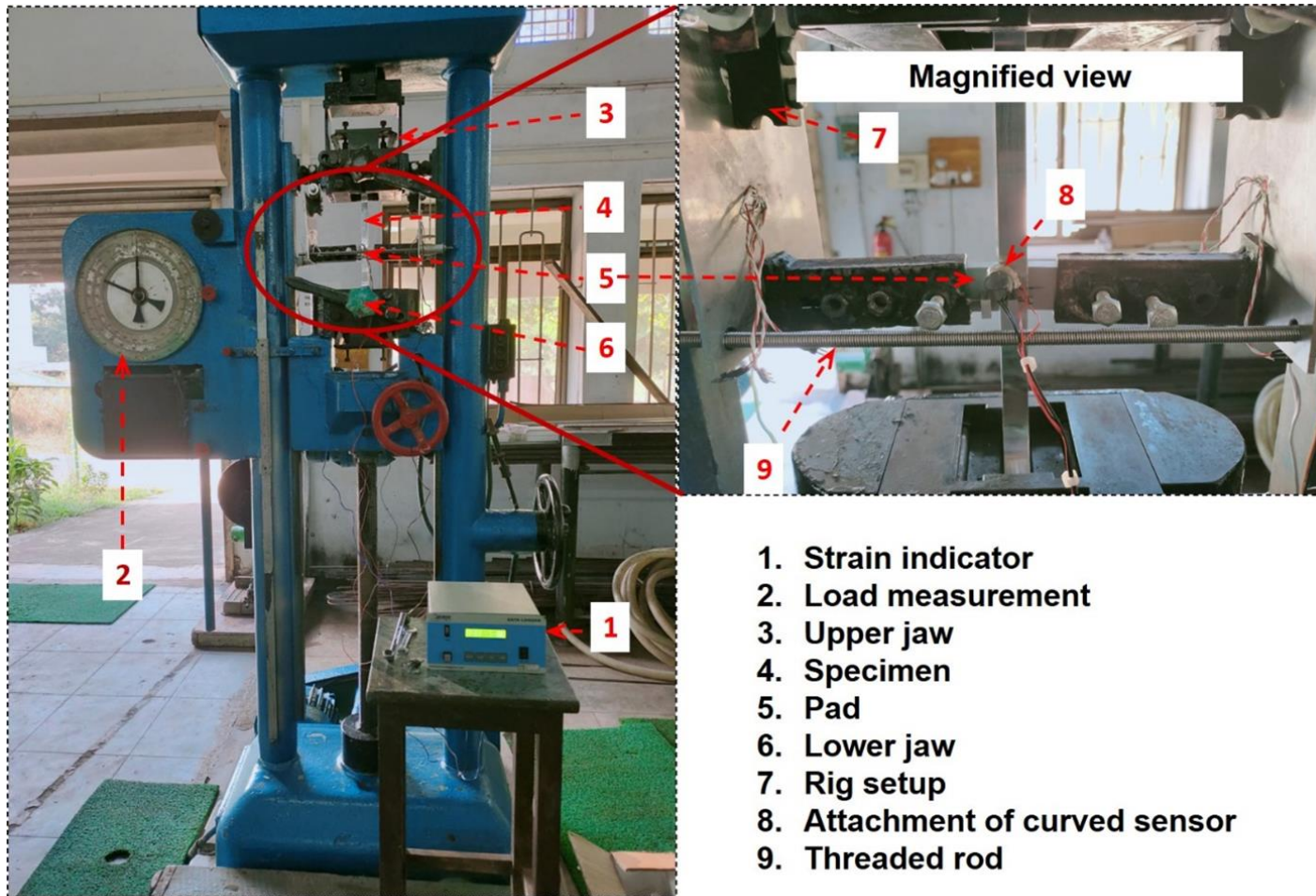


Figure 3.12: Experimental setup

CHAPTER 4

RESULTS AND DISCUSSIONS

The results obtained, from the SEA study and FEA study, for both fretting rig and thin curved strip is presented here. From these results, how the design process comes to an end and the suitable design model for fabrication have been chosen. Then, the complications involved in the fabrication and the modifications with the inclusions of those difficulties on both fretting rig and thin displacement sensor are explained followed by the experimental details regards with fabricated fretting rig and fabricated thin displacement sensor are presented. Finally, the details of fretting experiments that are conducted using both fabricated fretting rig and thin displacement sensor are reported.

4.1 FRETTING RIG RESULTS AND DISCUSSIONS

One Dimensional finite element analysis of the eleven cases considered resulted in load transfer ratios in the range of 91.92 % to 56.70 % as presented in Table 4.1. The wide range of LTR is attributed to change in length of the vertical beam (Element 6) and horizontal beam 2 (Element 7). LTR value decreased with a reduction in the length of the vertical beam. LTR value increased with an increase in the length of the horizontal beam. The highest LTR value was observed in the model with single vertical column support and without vertical beam. The lowest LTR value was observed in the model with three vertical supports and without a vertical beam.

According to the 1-D E analysis results (Table 4.1), the model represented by case-2, which has three supports and is without a vertical beam, gives the minimum LTR value of 56.70 %. However, the emphasis has been given to the machine constraints and accommodation space for the fretting rig, the considered case-2 model is not suitable for fabrication. So, after the procurement of reciprocating wear testing machine suitable alternative design and analysis of fretting rig has been made with the consideration of machine bed dimensions, accessible height for the specimen, height and width dimensions of the specimen and its details are presented in Table 4.1.

Table 4.1. LTR values of different cases

Types	Cases	Length of jth element (L_j) in mm	LTR in percentage
Type-1	Case-1	L6 = 0; L7 = 155	91.92
	Case-2	L6 = 0; L7 = 70	56.70
Type-2	Case-3	L6 = 400; L7 = 70	76.97
	Case-4	L6 = 350; L7 = 70	75.44
	Case-5	L6 = 300; L7 = 70	71.16
	Case-6	L6 = 250; L7 = 70	68.63
	Case-7	L6 = 200; L7 = 70	66.04
	Case-8	L6 = 150; L7 = 70	62.71
	Case-9	L6 = 100; L7 = 110	69.08
	Case-10	L6 = 50; L7 = 110	64.88
	Case-11	L6 = 50; L7 = 70	72.99

To select a suitable fretting rig with the inclusion of machine constraints (dimensions of the machine bed, specimen and pad etc..) and rig accommodation space in the machine, the 1-D FE analysis has been done again for different rig models mentioned as earlier cases and its schematic representation is depicted in Figure 4.1. The dimensions of this new fretting rig in the analysis are geared towards getting suitable LTR values for fretting experiments and it is based on the earlier analysis results.

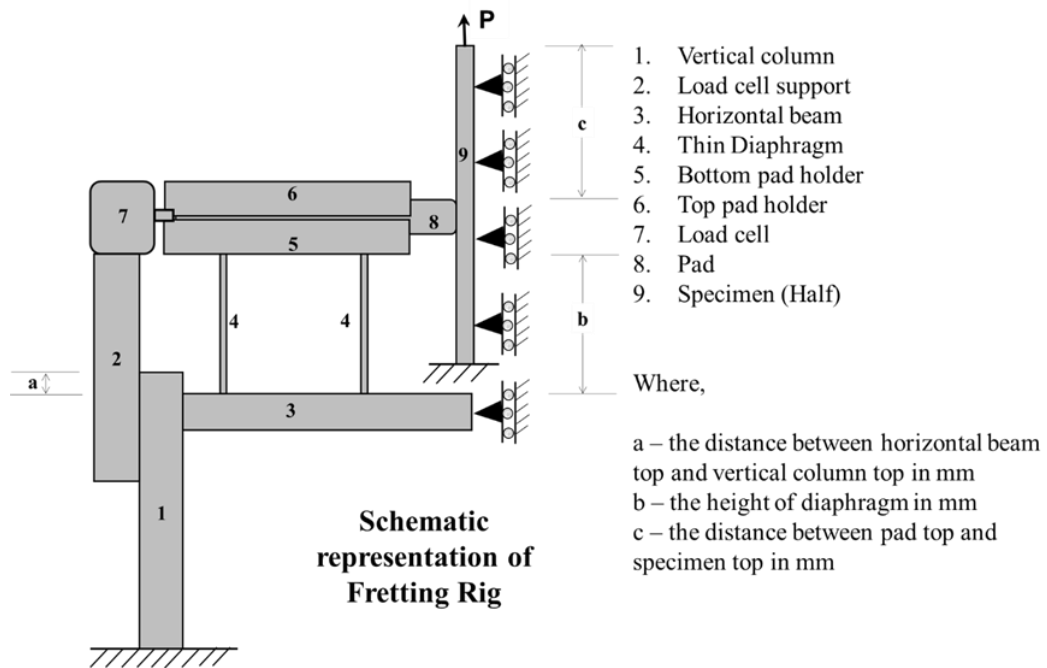


Figure 4.1: Schematic fretting rig model used for 1-D FEA after considering machine bed dimensions

The design process of the fretting rig has involved the choice of either two or three diaphragms due to the constraint in the dimensions of the machine bed. So the FEA has been performed on the fretting rig with two diaphragms and its LTR value results will be compared with the fretting rig with three diaphragms. This analysis also includes the changes in dimensional values of a, b and c which are depicted in Figure 4.1. The 1-D FEA rig model of these considered cases is shown in Figure 4.2 and the results of these FEA are given in Table 4.2.

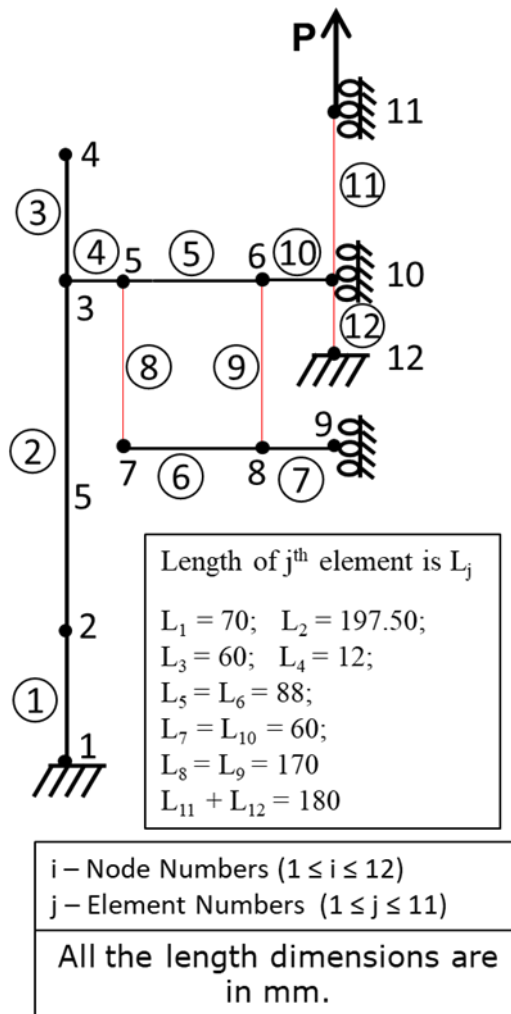


Figure 4.2: 1-D model of actual fretting rig

The results of this 1-D FEA indicates that the fretting rig with two diaphragms is giving considerably the same LTR values. However, the accommodation of two diaphragms in the fretting rig is easier than keeping three diaphragms in the fretting rig. Moreover placing three diaphragms in the fretting rig might be caused restrictions to the applied normal load. So, the design and analysis of the fretting rig started with two diaphragms only and these details are given hereafter.

Since the overall length of the Dog-Bone specimen is limited to 320 mm, a specimen gauge length has to be considered as 180 mm. Considering the changes made in length between the contact point of the pad on the specimen and the top of the specimen four different cases have been formed and their LTR values are given in Table 4.3. The

alterations made to the length of element number 3 in the analysis have not produced notable changes in the observed LTR values. From the results of the second part of the 1-D FE analysis given in Table 4.3, increasing the length of element number 12 from 60 mm to 120 mm resulted in decreasing LTR values from 59.40 % to 53.05 % have been observed. The LTR value is decreasing because the pad is applying more tangential force on the specimen when it is placed near the loading grip. From the 1-D FE analysis results, the rig model of case-15 is selected for fabrication after performing a Three-Dimensional (3-D) FE analysis.

Table 4.2. Load transfer ratios were obtained for different rig dimensions.

Name		Distance in mm			LTR in %
		a	b	c	
FRA1	A1	20	100	60	77.772
	B1				77.967
FRA1	A2	20	90	70	79.190
	B2				79.385
FRA1	A3	20	80	80	79.970
	B3				80.150
FRA1	A4	20	70	90	82.378
	B4				82.553
FRA1	A5	40	100	60	77.930
	B5				78.033
FRA1	A6	40	110	60	78.016
	B6				78.105
FRA1	A7	40	120	60	78.066
	B7				78.191
FRA1	A8	70	150	60	77.864
	B8				78.005

FRA1-A is the analysis where three diaphragms are considered.

FRA1-B is the analysis where two diaphragms are considered.

3-D FE analysis was performed using the ANSYS Workbench package and it gave the LTR value of 58.22 %. 3-D model and corresponding mesh diagram of the selected fretting rig are given in Figure 4.3:a and 4.3:b respectively. It can be referred to as an actual fretting rig.

Table 4.3. LTR values for four different cases of fretting rig 1-D FEA

S. No.	Cases	(L ₁₁ , L ₁₂)	LTR (%)
1	Case-12	(120,60)	59.40
2	Case-13	(100,80)	57.48
3	Case-14	(80,100)	55.38
4	Case-15	(60,120)	53.05

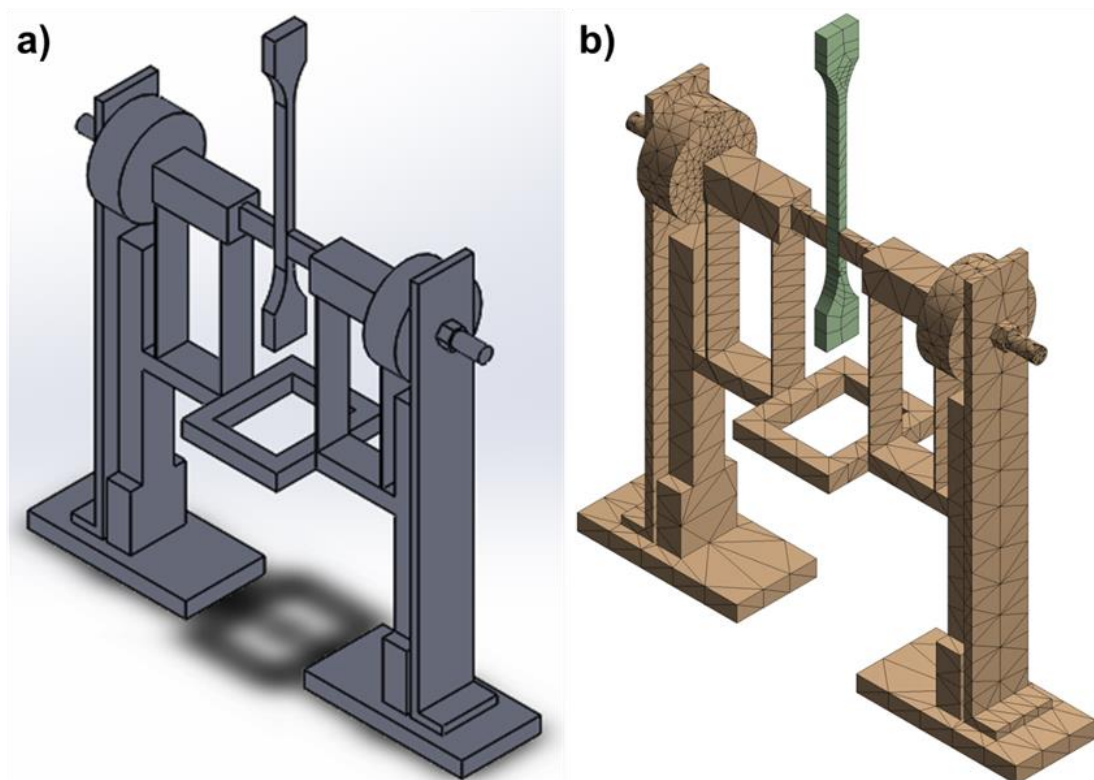


Figure 4.3: a) 3-D model and b) meshed model of actual fretting rig

4.1.1 Experimental study of the fretting rig

The fretting rig was fabricated on account of the dimensions used for 1-D and 3-D FE analysis. The fabricated fretting rig has two vertical rig column support. The load washers, used to measure normal loads, were connected on both sides of load cell support which is connected to the vertical column support. Horizontal beam support was attached to the vertical column support and it acts as a base for thin diaphragms, pad holder and pads. Two vertical thin diaphragms of thickness 2 mm were attached between horizontal beam support and pad holders with the help of screws. These

diaphragms are helpful to transfer the normal load to the specimen via pads to the maximum extent since it offers little resistance to the applied normal load in the transverse direction. However it is connected on both pad holders and horizontal beam support using small screws, the transfer of normal load is not disturbed much. There is a space in the middle of horizontal beam support which aids the specimen to pass through.

Usually, two main complications have occurred in the fretting experiments. One is to keep the normal load constant throughout the experiments and the second is to make proper contact between the pad and the specimen.

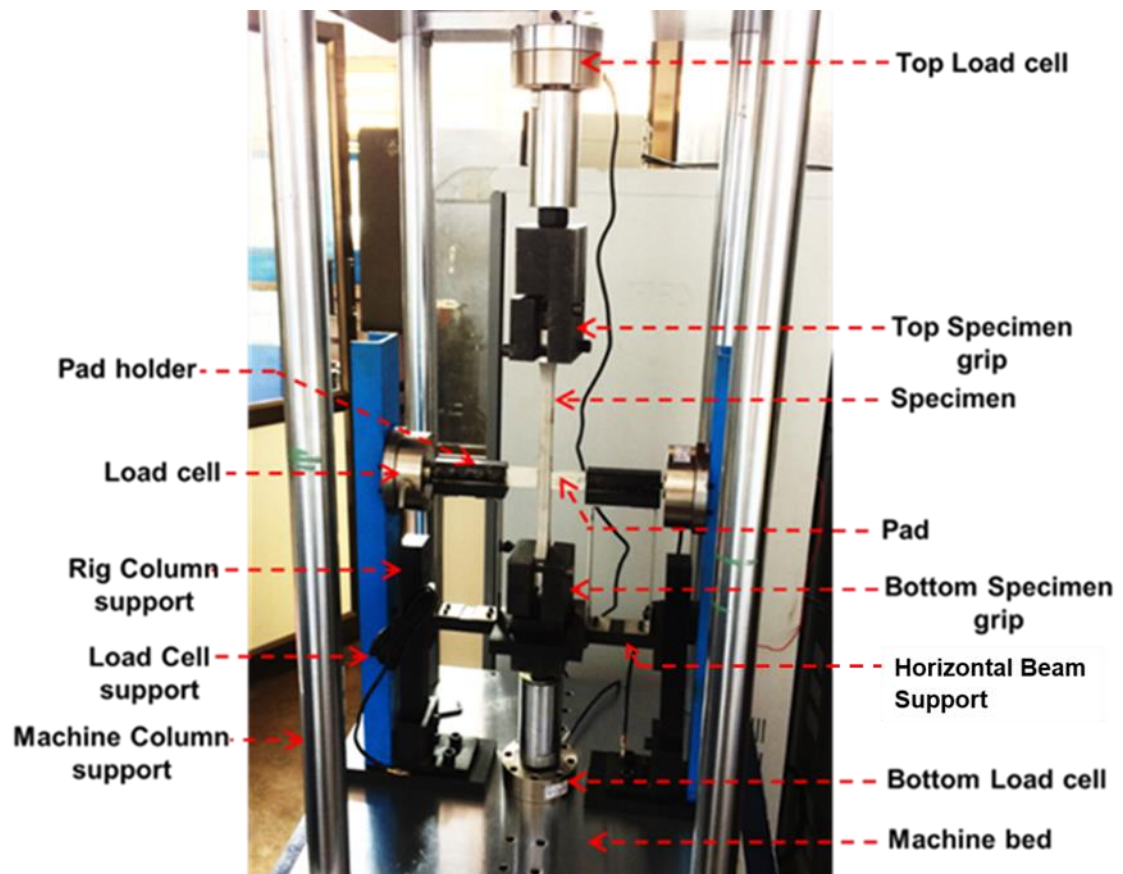


Figure 4.4: Fabricated fretting rig

While doing experiments (Figure 4.4) with the fabricated fretting rig, the problem had been encountered in the process of maintaining a constant normal load. The constant normal loads were given, by two screwed bolts which are having an attachment with the pad, on both the side of the specimen throughout the experiment. The load from the

screwed bolt is, transferred through pads onto the specimen, measured using two load cells which is capable of measuring 1 tonne. Since the given normal load on one side creates reaction force on the other side of the specimen and it affects the process of maintaining a constant normal load on the specimen. The fretting experiments could not be accomplished without maintaining the constant normal load. Moreover, the applied normal load affects the specimen too. These discrepancies can be avoided by providing some more modifications in the application of normal load using the fretting rig. So, the fretting rig with the necessary modifications in the method of applying normal load onto the specimen is depicted in Figure 4.5:a and its meshed model is shown in Figure 4.5:b.

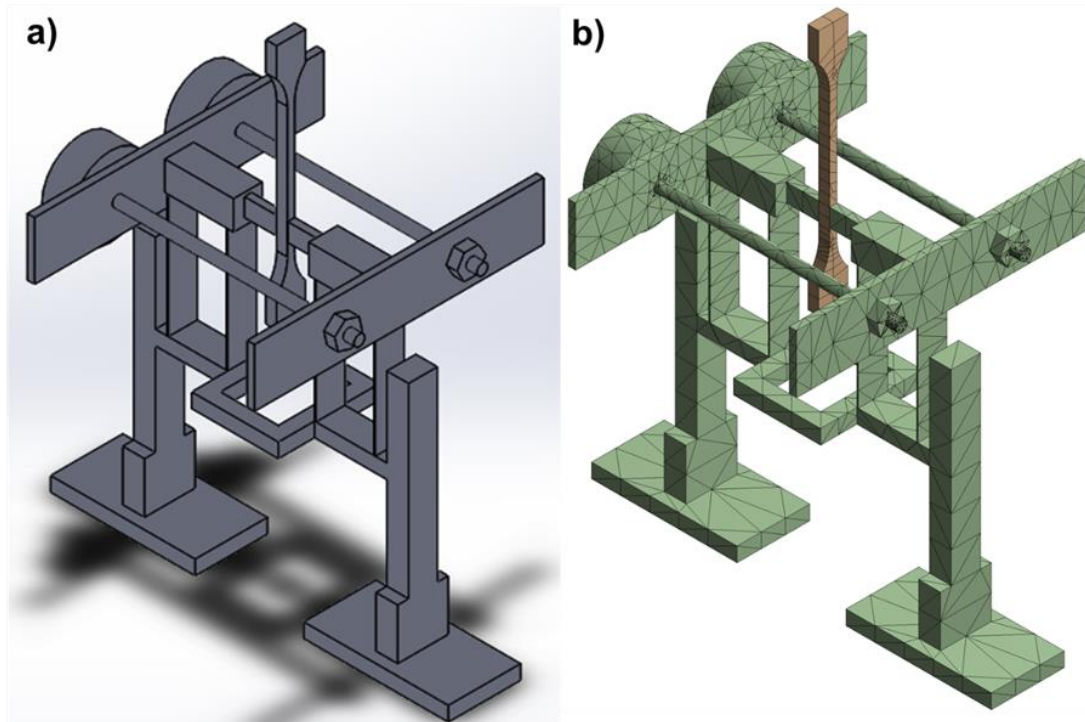


Figure 4.5: a) 3-D model and b) meshed model of modified fretting rig

In the modified fretting rig, the normal load is created by using two screwed rods which are connected with two plates and nuts on both sides of the specimen. By adjusting the nuts in the screwed rod at the same time, the normal load is transferred through the pads onto the specimen. This normal load can be measured using two load cells which are placed on either side of the specimen by which the moment problem due to the applied normal load can be nullified and it can be helpful to maintain the constant normal loads

on both sides of the specimen for the entire experiments. This arrangement is an improvement on the old fretting rig system. A similar type of applying normal load onto the specimen using two rods can be found in Murthy et al. (2003) and Murthy & Vadivuchezhian (2017). A 3-D FE analysis of the modified fretting rig model gives the LTR value of 57.14 %. While experimenting with the modified fretting rig, the constant normal load has been maintained on both sides of the specimen using two threaded rods placed sideways. The modified fretting rig is considered useful for fretting experiments which don't require any re-calibration between experiments and it is shown in Figure 4.6.

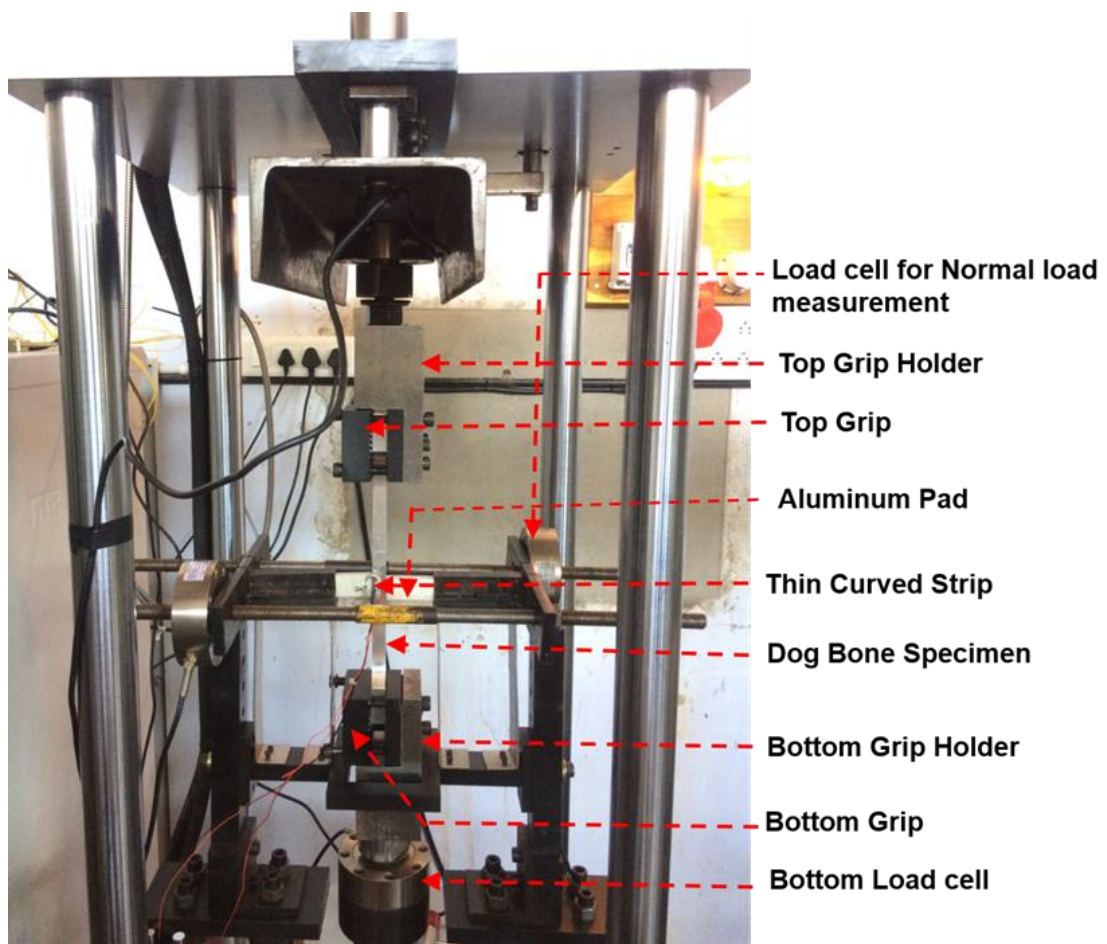


Figure 4.6. Modified fretting rig

The proper contact condition should be established between pads and specimen to ensure the complete transfer of normal load during an experiment. So, the contact condition has been ensured by keeping pressure indicating film between pad and

specimen surface. Before an experiment, all the specimen and pad surfaces were cleaned using acetone solution to make clean and smooth surfaces of pad and specimen which results to conduct experiments smoothly.

4.2 THIN DISPLACEMENT SENSOR RESULTS AND DISCUSSIONS

4.2.1. SEA Results

The curved sensor of rectangular cross-section made of spring steel was considered for analysis. The dimensions and material properties of thin curved strip material are as follows: Width (b) = 5 mm, Height (h) = 0.5 mm, Internal radius (r_i) = 7 mm, Mean radius (r) = $r_i + (h/2) = 7.25$ mm, and $I = (b \cdot h^3/12) = 0.052083$ mm⁴, $E = 200000$ MPa. Normal load (P), applied on one end of the thin strip, is 1 N and boundary condition of the other end of the curved strip has been considered as a fixed end (Figure 3.4). By using the given values, the radius of the neutral axis was calculated as 7.2471 mm and the distance between the neutral layer and the top layer (y) of the curved strip is 0.2529 mm. By considering the above values, the SEA gives the result of δ_{\max} as 0.1724 mm, δ_{mid} as 0.05747 mm and σ_{\max} as 72.97 MPa.

4.2.2 FEA Results

The FEA results of the thin strip without the slot has given δ_{\max} as 0.1687 mm, δ_{mid} as 0.05691 mm and σ_{\max} as 73.832 MPa. The FEA results of the thin curved strip without slot aren't deviating more than 5 % with the SEA results. It reveals that the FE method is a viable alternative to the cumbersome analytical techniques even for the curved member analysis. Owing to the complications involved in the calculation of both moment of inertia and displacement using SEA for the slotted curved strip, the FE approach only has been considered to select a suitable slotted thin curved strip. So, the different thin curved slotted strips have been modelled and analyzed using FEA. The hole in the curved strip results more deformation while applying the load and these cut outs merely produced severe stress gradient in the analysis of thin curved strip with holes. So, the stress gradient result of thin curved strip plays a vital role along with displacement result in the selection of suitable strip for fabrication. Therefore, the displacement and stress gradient results, obtained from FEA using ANSYS software,

were used to select an optimized design of thin curved strip to measure contact displacement in the fretting experiments. Various investigators (Viswanathan et. al (2021), Kumaran et. al 2022) studied the mesh convergences for different models similar way a convergence study was undertaken to select the element size and no. of elements has illustrated in Figure 4.7.

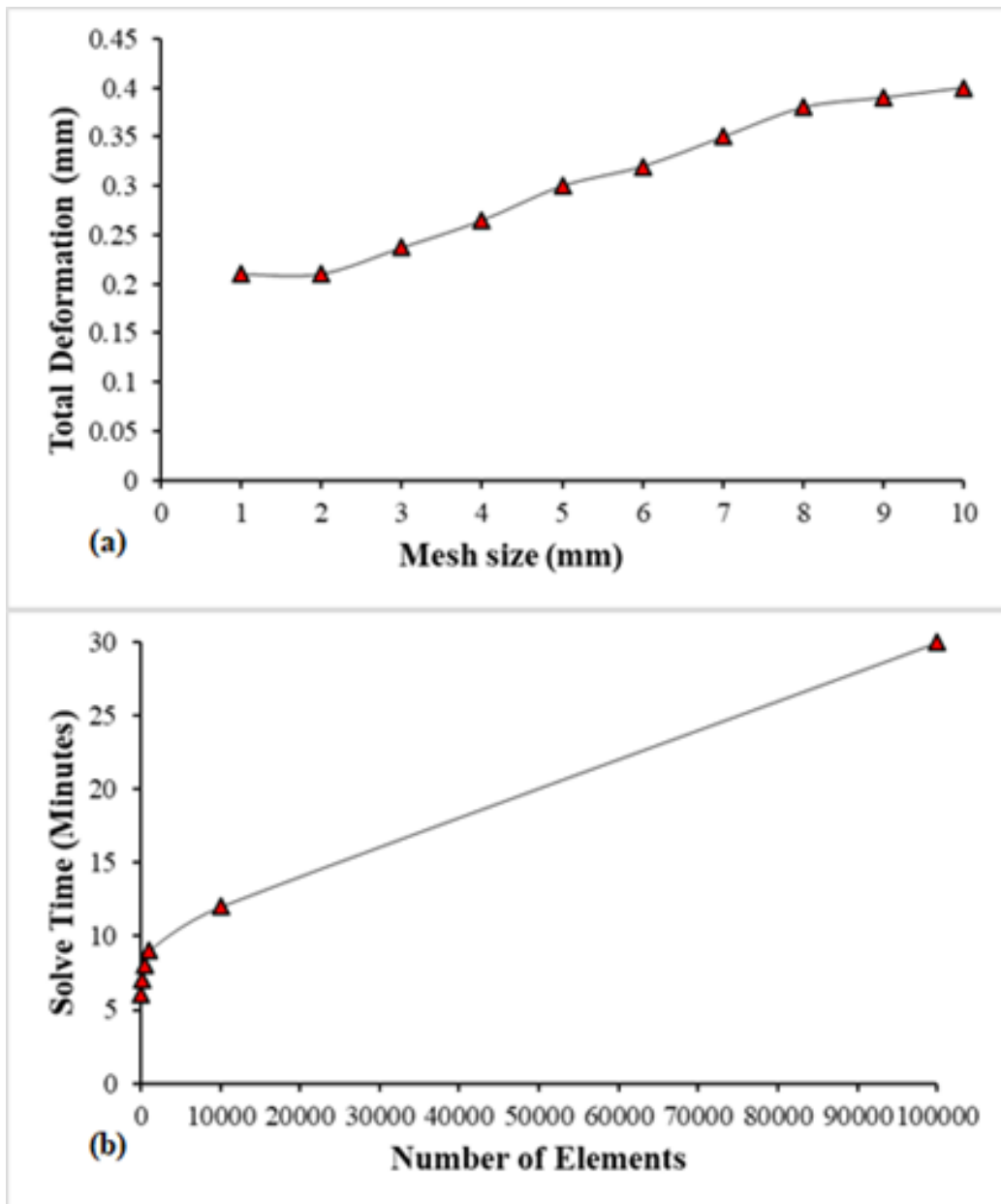


Figure 4.7 Mesh Convergence study undertaken to select the element size and no of elements

Table 4.4: Finite Element Analysis results of the thin strip with slots

S.No.	Name	von Mises Stress in MPa	Deformation at middle of the strip along loading direction in mm	Total Deformation in mm
1	Strip_2_Rec_45deg_1_0.25	110.01	0.07018	0.2105
2	Strip_2_Rec_45deg_1_0.5	107.94	0.07015	0.2104
3	Strip_2_Rec_45deg_2_0.25	153.28	0.07577	0.2273
4	Strip_2_Rec_45deg_2_0.5	148.14	0.07567	0.2270
5	Strip_4_Rec_2_2_0.25	180.37	0.06958	0.2087
6	Strip_4_Rec_4_2_0.25	187.23	0.07060	0.2118
7	Strip_6_Rec_2_2_0.25	180.04	0.07030	0.2109
8	Strip_6_Rec_4_2_0.25	183.65	0.07205	0.2161
9	Strip_4_Circ_1	123.91	0.06846	0.2054
10	Strip_4_Circ_3	213.86	0.07128	0.2138
11	Strip_6_Circ_1	130.6	0.06856	0.2057
12	Strip_6_Circ_3	214.03	0.07331	0.2199
13	Strip_4_Ellip_2_1	113.84	0.06855	0.2056
14	Strip_4_Ellip_4_1	92.864	0.06873	0.2062
15	Strip_4_Ellip_2_3	245.91	0.07059	0.2118
16	Strip_4_Ellip_4_3	197.34	0.07209	0.2163
17	Strip_6_Ellip_2_1	112.81	0.06869	0.2061
18	Strip_6_Ellip_4_1	93.983	0.06896	0.2069
19	Strip_6_Ellip_2_3	249.39	0.07203	0.2161
20	Strip_6_Ellip_4_3	195.84	0.07495	0.2248

Since the strip has a unit thickness and there is not much variation in the results of deformation and stress values while considering both SOLID185 and SHELL181 elements for FE analysis. Analysis with SHELL181 element produced results faster than analysis with SOLID185 elements. So, the strip had been modelled and analyzed

using only SHELL181 element in FE analysis. For a thin curved strip with slots, the FE analysis results are shown in Table 4.4.

The strain gauge should be pasted on the outer side of the thin curved strip at the middle position of the strip to capture the strains at that position. So, there should not be any strain and stress gradients in the middle of the strip. The von Mises stress results of all models, considered for this study, of the thin curved strips have been shown from Figure 4.8 to Figure 4.27. By considering the von Mises stress results of all twenty strip models, the edges of each slot causes stress concentration effect on the strip which also affects the stress/strain gradient at middle of each strip. The Strip_2_Rec_45deg_2_0.25 (Figure 4.10) has shown some stress gradient at middle portion of the strip than the Strip_6_Circ_3 (Figure 4.19). So, the Strip_6_Circ_3 has been selected to measure contact displacement during experiments instead of the Strip_2_Rec_45deg_2_0.25. The same process is applied to all the types of thin strips to select suitable design of thin curved strip for fabrication.

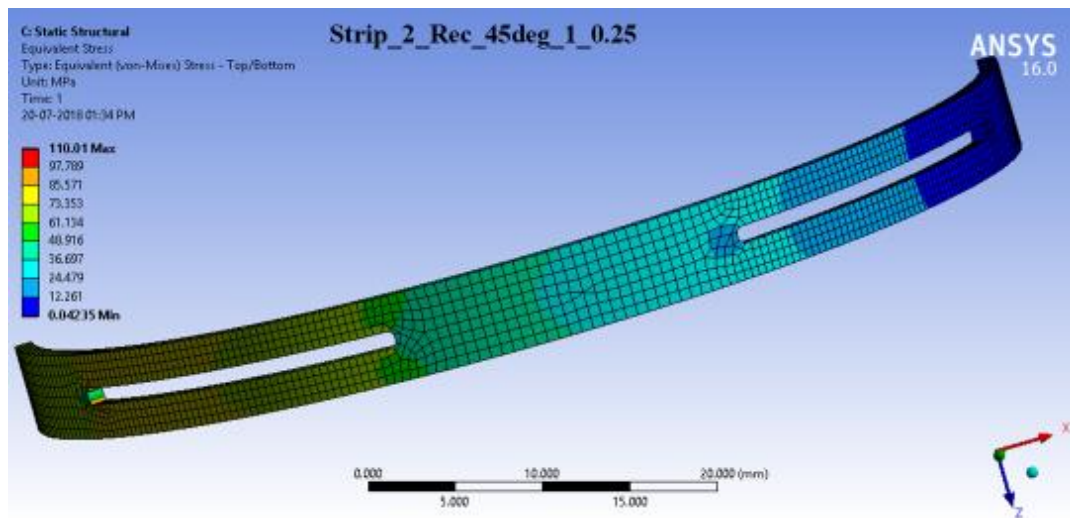


Figure 4.8: von Mises stress results of Strip_2_Rec_45deg_1_0.25 model

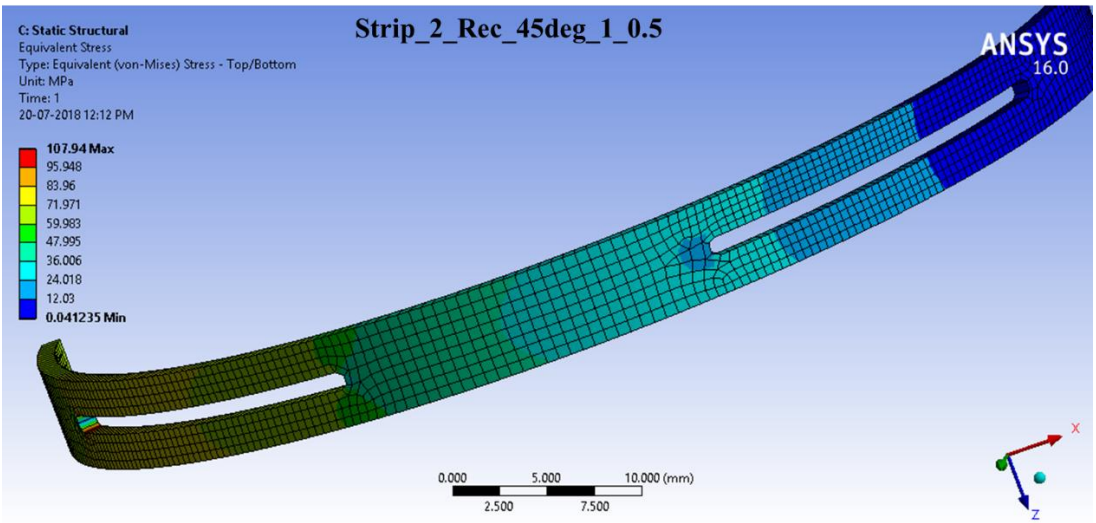


Figure 4.9: von Mises stress results of Strip_2_Rec_45deg_1_0.5 model

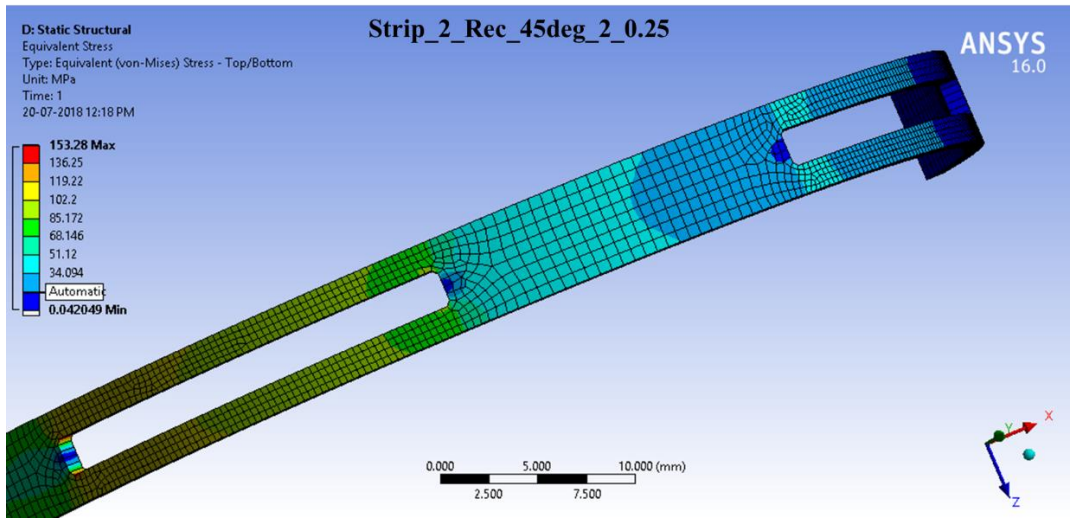


Figure 4.10: von Mises stress results of Strip_2_Rec_45deg_2_0.25 model

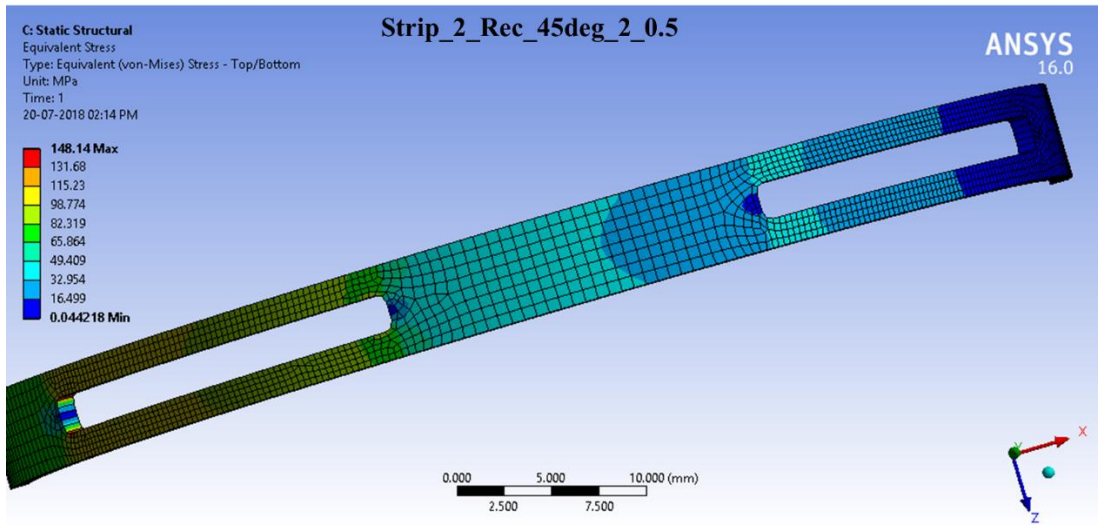


Figure 4.11: von Mises stress results of Strip_2_Rec_45deg_2_0.5 model

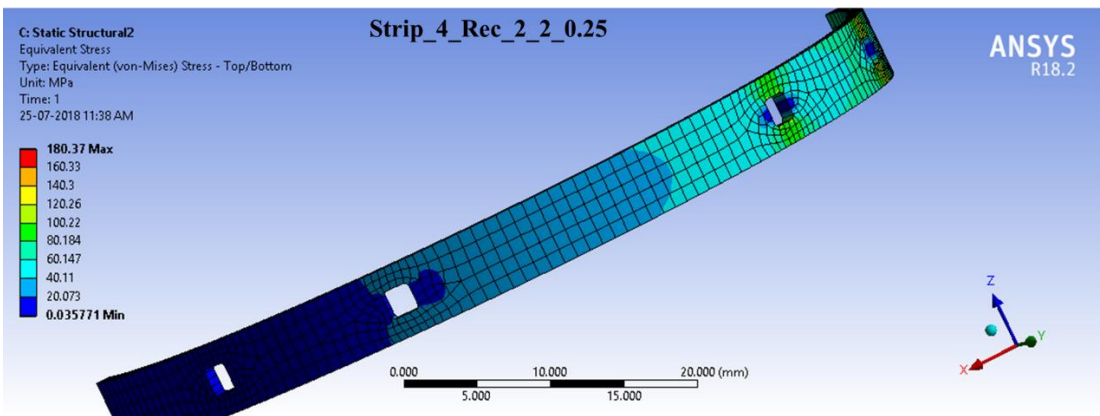


Figure 4.12: von Mises stress results of Strip_4_Rec_45deg_2_0.25 model

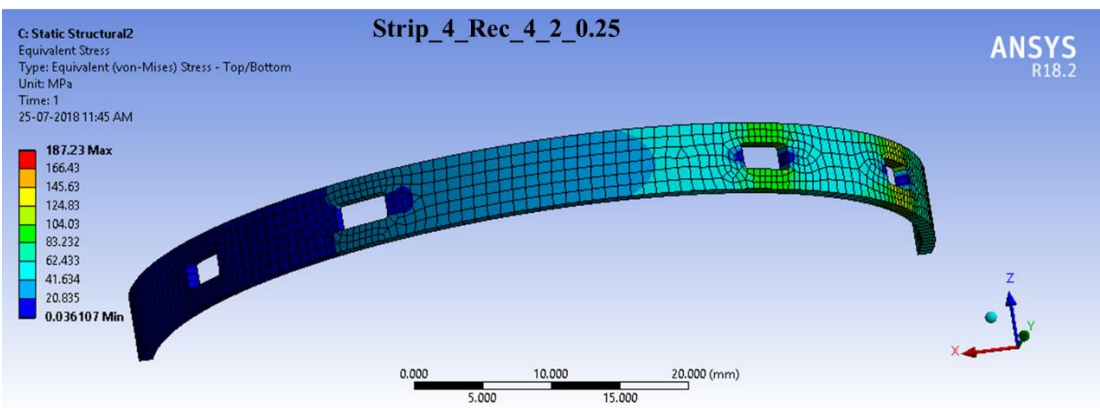


Figure 4.13: von Mises stress results of Strip_4_Rec_4_2_0.25 model

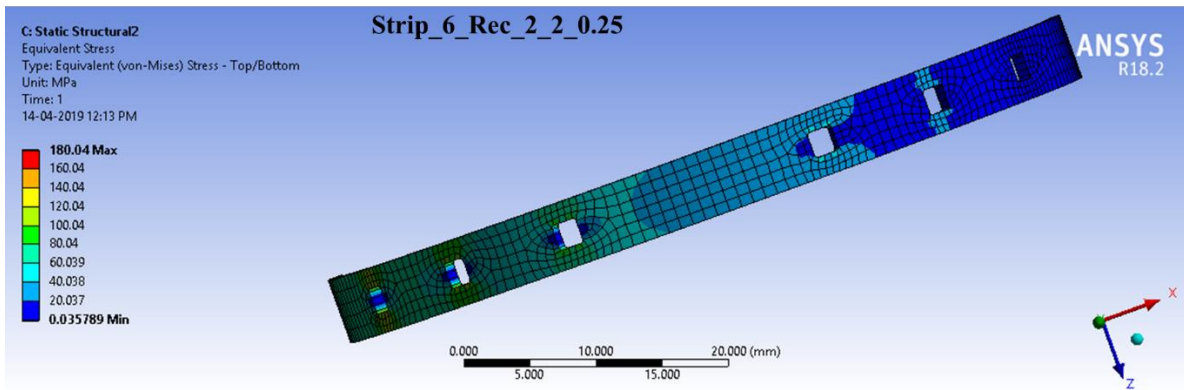


Figure 4.14: von Mises stress results of Strip_6_Rec_2_2_0.25 model

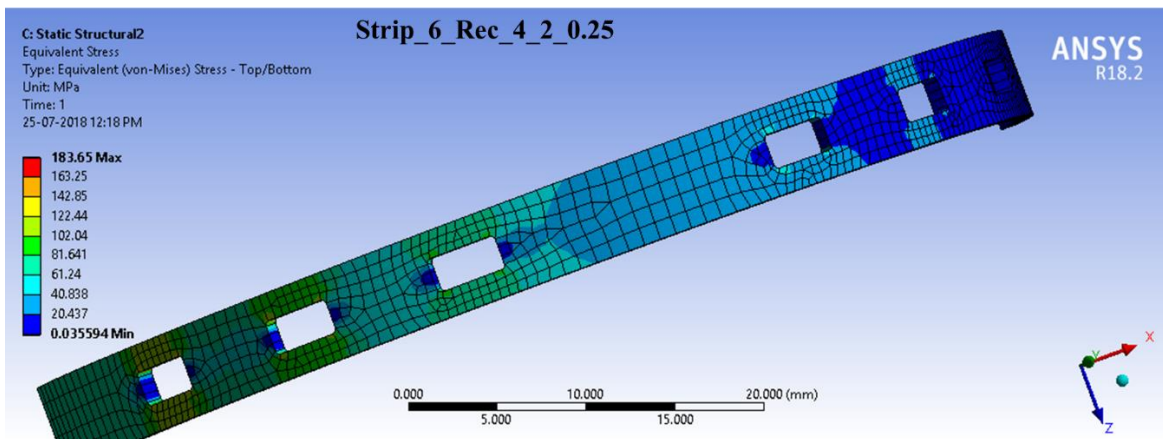


Figure 4.15: von Mises stress results of Strip_6_Rec_4_2_0.25 model

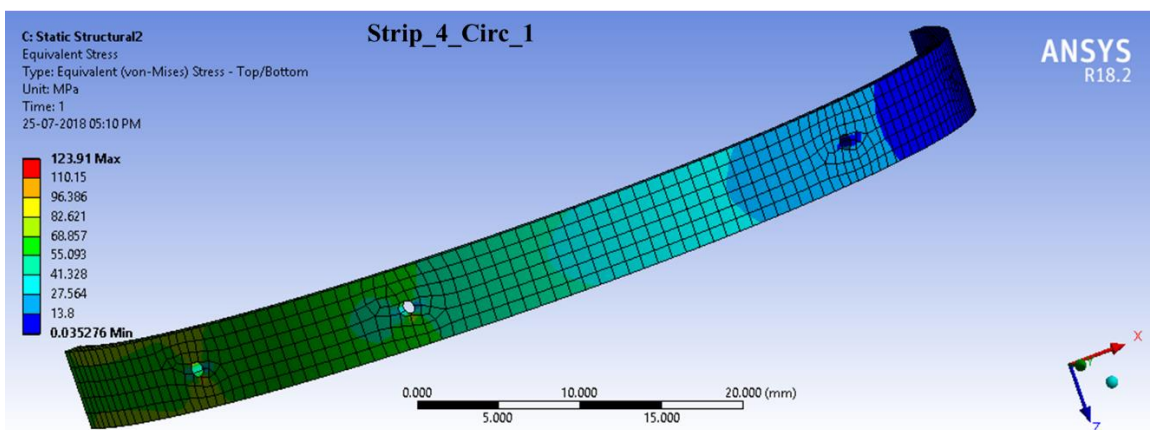


Figure 4.16: von Mises stress results of Strip_4_Circ_1 model

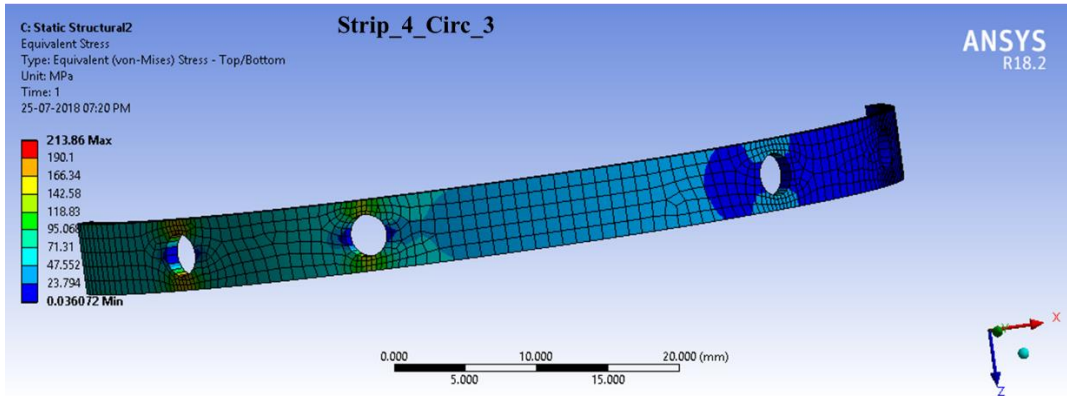


Figure 4.17: von Mises stress results of Strip_4_Circ_3 model

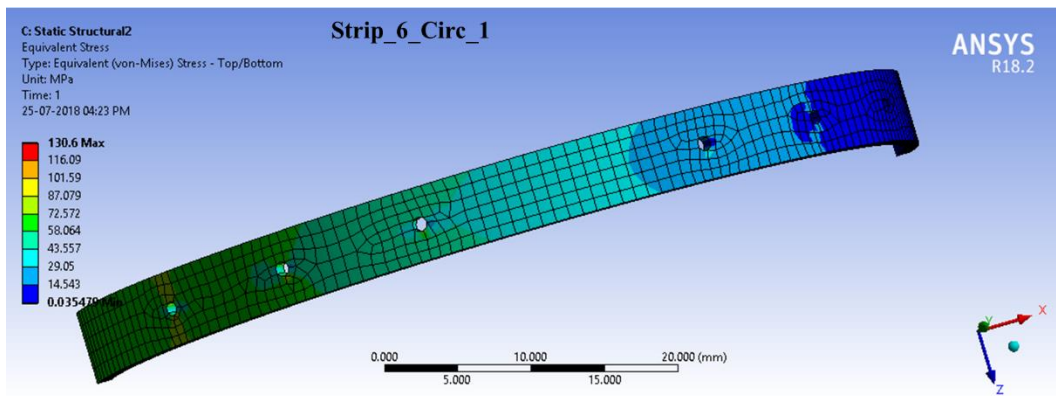


Figure 4.18: von Mises stress results of Strip_6_Circ_1 model

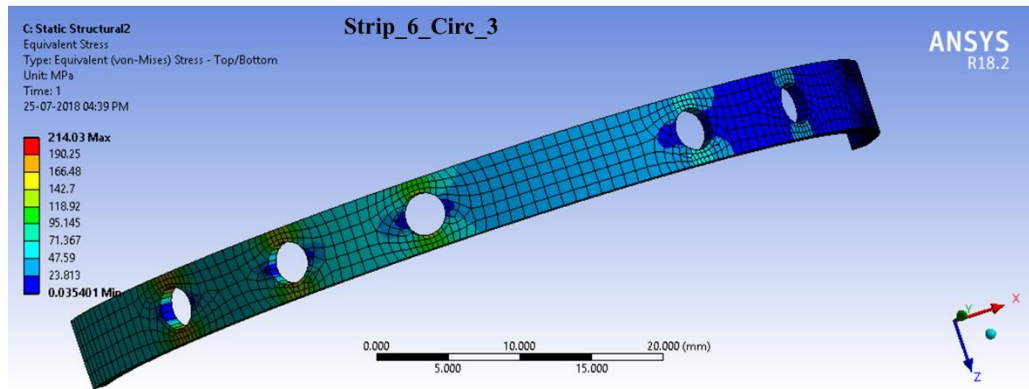


Figure 4.19: von Mises stress results of Strip_6_Circ_3 model

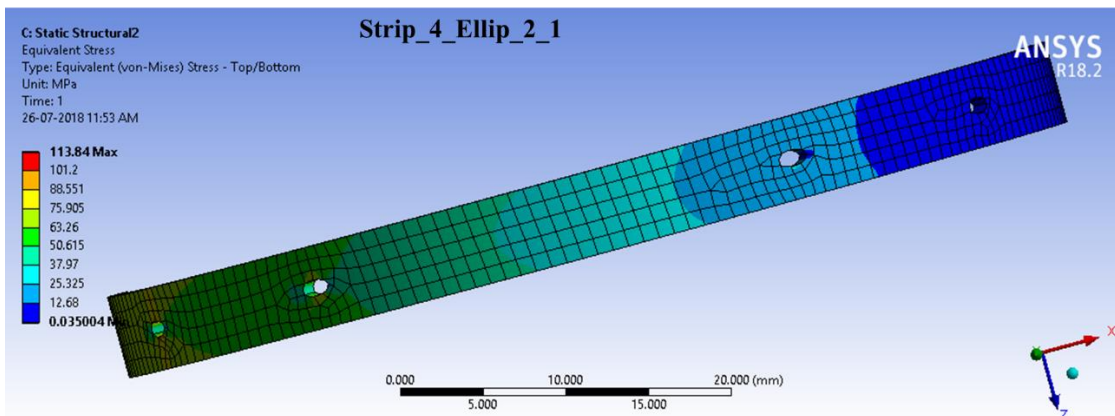


Figure 4.20: von Mises stress results of Strip_4_Ellip_2_1 model

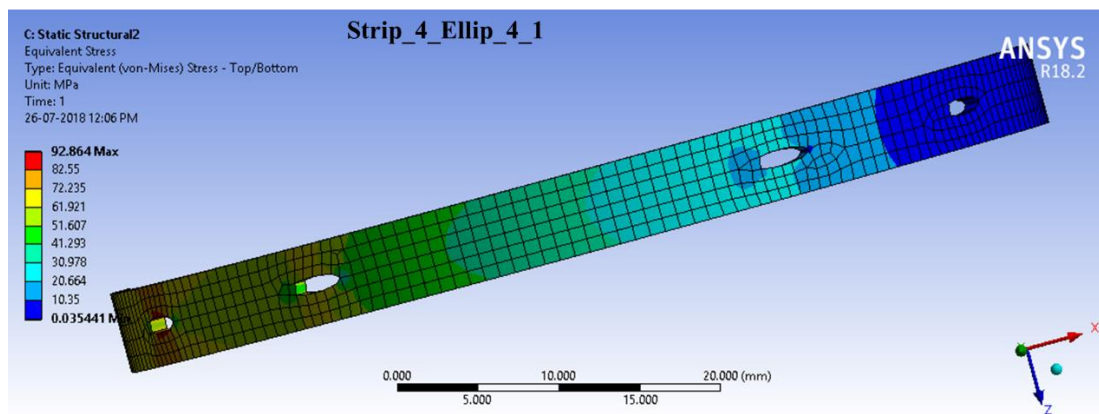


Figure 4.21: von Mises stress results of Strip_4_Ellip_4_1 model

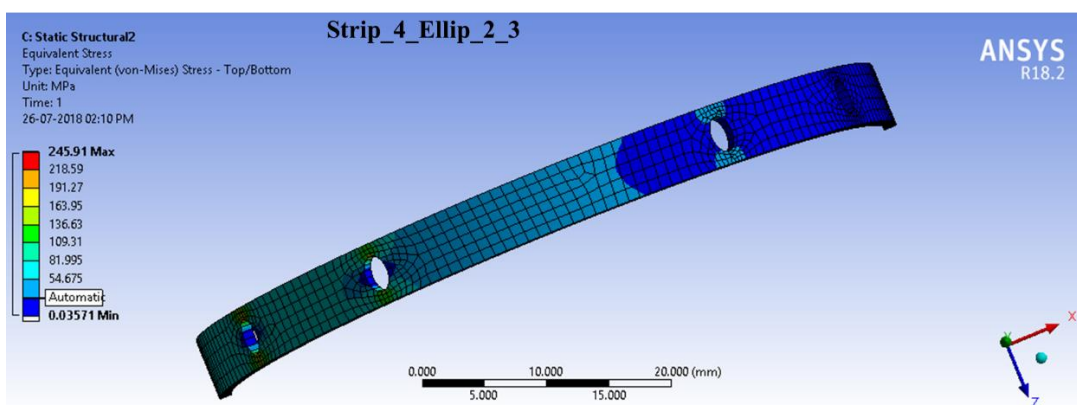


Figure 4.22: von Mises stress results of Strip_4_Ellip_2_3 model

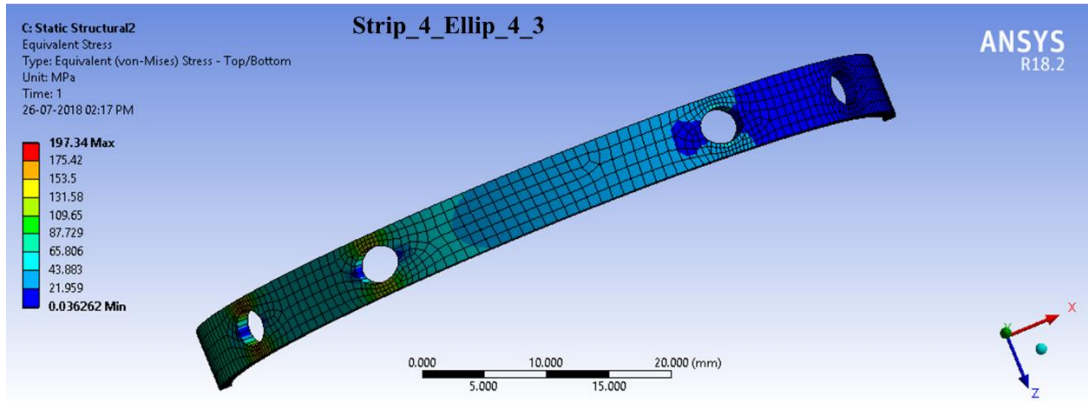


Figure 4.23: von Mises stress results of Strip_4_Ellip_4_3 model

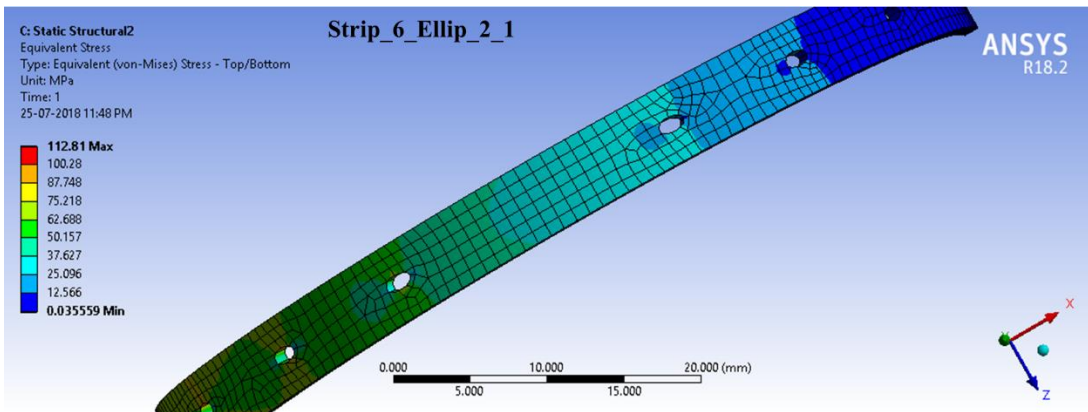


Figure 4.24: von Mises stress results of Strip_6_Ellip_2_1 model

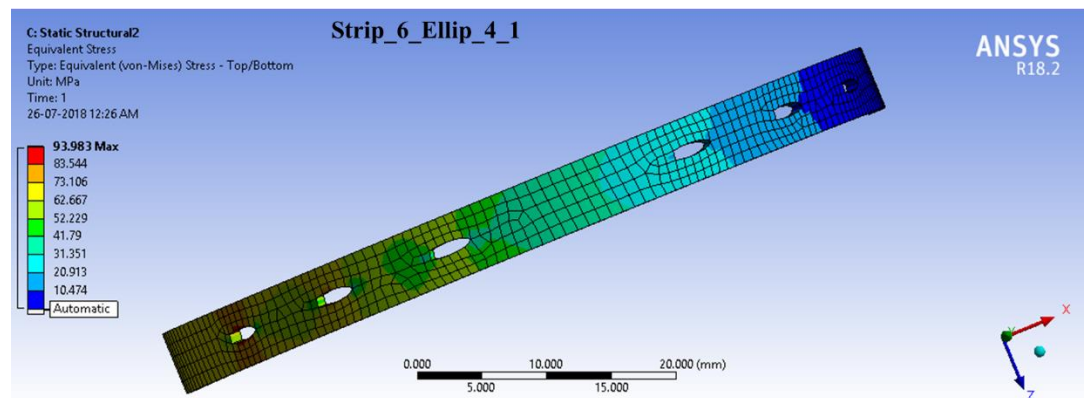


Figure 4.25: von Mises stress results of Strip_6_Ellip_4_1 model

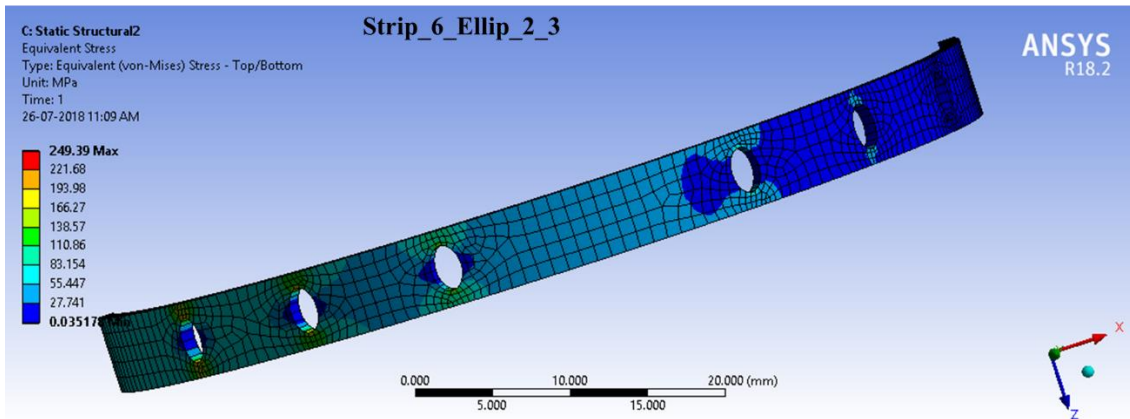


Figure 4.26: von Mises stress results of Strip_6_Ellip_2_3 model

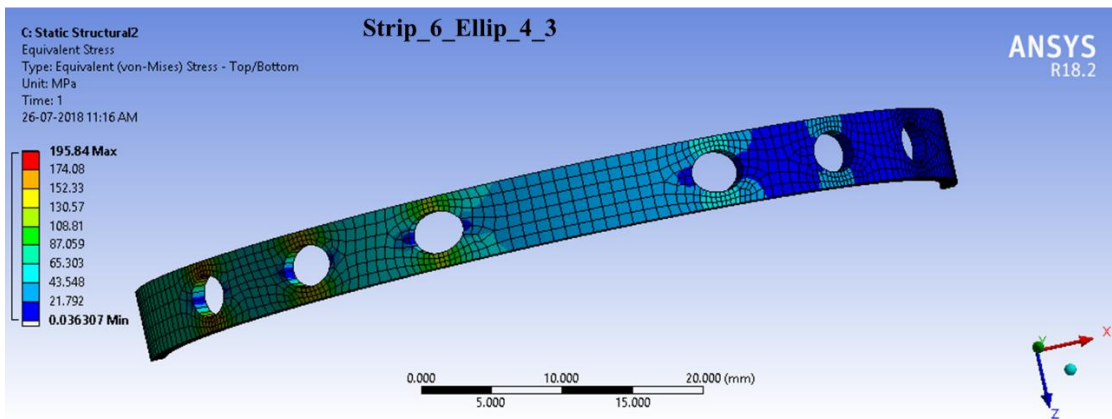


Figure 4.27: von Mises stress results of Strip_6_Ellip_4_3 model

Of the twenty configurations considered (Table 4.4), configurations numbered 7, 10, 12, 16, 19 and 20 showed zero stress gradient at the middle of the thin curved strip. In the above six selected configurations, the configurations numbered 12, 16, 19 and 20 were found to be suitable for fabrication and conducting fretting experiments.

The FE analysis results shown in Table 4.4 reveals that the increasing number and size of holes presented in the curved strip indicate that the increased in displacement and von-Mises stress values which offers the higher flexibility to the strip. The analysis confirms that there is not much significant change occurred in the results of von-Mises stress and displacement values between four- and six-holes curved strip. The reduction in area and minimum thickness of the curved strip could be the reason for the decrease in the stiffness of the curved strip. The filleted corners of the rectangular holes and the

smooth surfaces of the both cylindrical and elliptical holes of the strip have limited the stress concentration effects on the thin strip.

4.2.3 Experimental Validation

After performing preliminary FEA, its results shown that the thickness of the thin strip has the more influence on the stiffness value. Since, the vast availability of 0.5 mm thick material in market, it has been chosen for the fabrication. Keeping the view in the complications involved in making the cut-outs in thin strip and the ability to produce lower displacement values when it is made with small thickness, the thin strip without slots was adopted to conduct experiments.

During fretting experiments, tensile load applied varied from 0 to 108 kg and tensile load was applied at the free end of the dog bone specimen using load actuator. Relative Displacement at the contact interface for every increment of load was measured using curved strip pasted (attached) to pad and dog bone specimen. The strain gauge was pasted to the curved strip and strain gauge was connected to data logger and data acquisition system. The values of displacement and strain obtained by conducting fretting experiments (static load) and the outcomes of experiments are compared with finite element modelling results. The results obtained from experiment are discussed below.

In experiments, the displacement values were observed as 0.05579 mm, which is less than SEA result of 0.05747 mm (+3.02 %) and FEA result of 0.05691 mm (+2.02 %). The small variation in the displacement value obtained from the experiments is due to the following factors; the small moment occurred during the process of applying load in the experiments, the effect of adhesive and its thickness, material nature and its properties and environmental effect. The experiments confirm that thin curved strip without slot has the ability to capture the small displacement values and the fabrication of thin strip without slot is easier when compared with thin strip with slot. Hence thin curved sensor without slot can be used for fretting experiments. However, the thin strip with slots can be utilized in partial slip fretting experiments (where the measurement of displacement value is even lesser) despite the complication towards in its fabrication.

4.3 FRETTING EXPERIMENTS USING FABRICATED FRETTING RIG AND THIN DISPLACEMENT SENSOR

Fretting experiments have been conducted using fabricated fretting rig and fabricated thin curved sensor without slot in fatigue testing machine. The modified fretting rig has been attached to the machine bed. Thin curved sensor without slot is attached to the specimen and pad using separate holders and then these holders are pasted on the pad and specimen with the help of Araldite paste. Thickness of the glue is around 1 mm and it has been cured for one day for the strong adhesion. Before pasting, all the surfaces were cleaned with acetone solution. The strain gauges pasted on the outer and inner mid-surface of the thin strip are helpful to measure the strain values on the outer and inner surfaces of thin strip when load is applied. So, both the strain gauges values have to be calibrated to zero and it has done before each experiment.

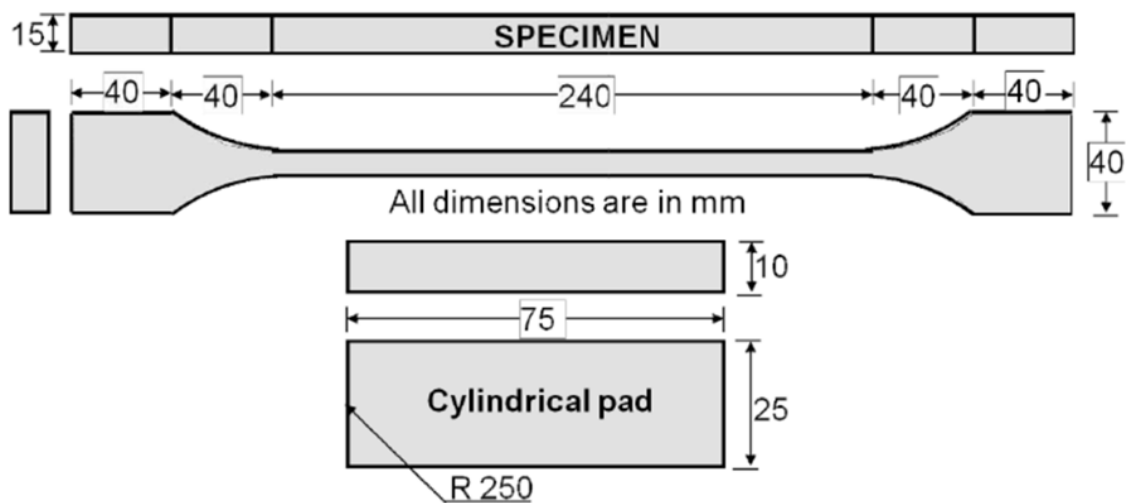


Figure 4.28: Schematic of specimen and cylindrical pad

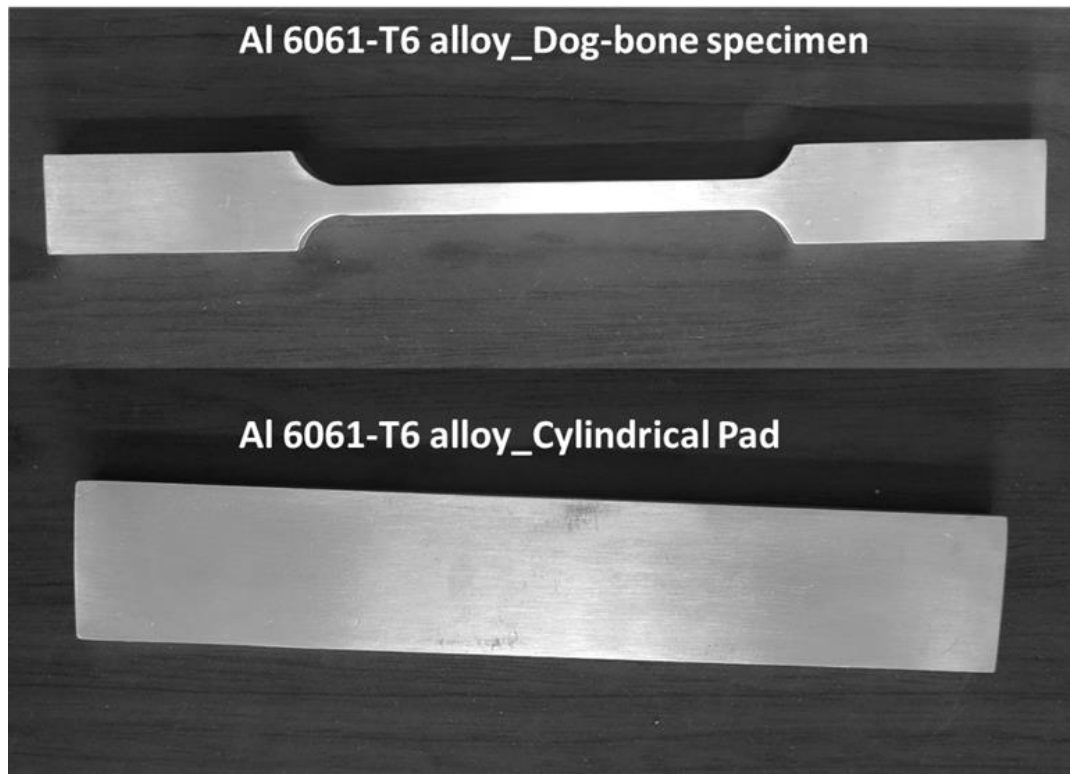


Figure 4.29: Fabricated Dog-bone specimen and cylindrical pad

The fretting experiments were conducted with single clamped configuration as mentioned in ASTM test standard E2789-10. The tentative specimen (flat dog bone specimen) and cylindrical pad (with curvature of 250 mm at contact point) dimensions are given in Figure 4.28. Aluminium alloy Al 6061-T6 have been used to fabricate flat dog bone specimen and cylindrical pad specimens. The fabricated specimen and pad are shown in Figure 4.29. The chemical composition of Al 6061-T6 alloy in weight percentage is presented in Table 4.5.

Table 4.5: Chemical composition of Al 6061-T6 alloy (%)

Chemical Composition	Cu	Mg	Si	Fe	Mn	Zn	Ti	Cr	Al
Al 6061-T6 alloy	0.185	0.741	0.585	0.423	0.12	0.058	0.024	0.087	Bal.

Table 4.6: Fretting experiment results

No. of cycles	Q/P Ratio
0	0.1
50	0.12
100	0.18
150	0.25
200	0.29
250	0.33
300	0.42
350	0.48
400	0.53
450	0.59
500	0.63

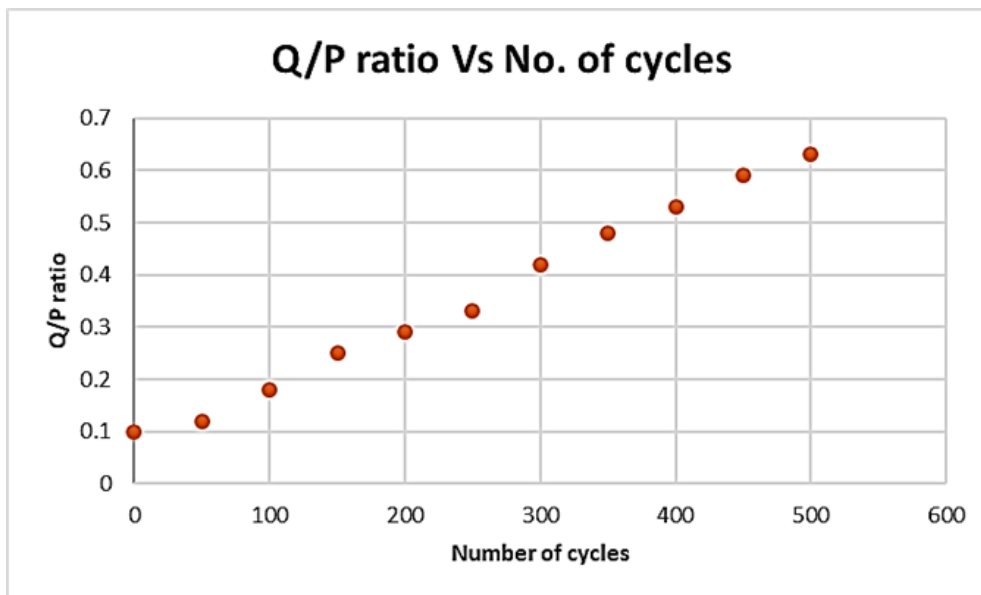


Figure 4.29: Fretting experiment result- Q/P ratio vs No. of cycles

A fretting experimental setup with cylinder on flat configuration has been developed to identify the changes in tangential force between pad and specimen surfaces by which the changes occurred in the ratio between tangential force and normal force (Q/P ratio) concerned with numbers of cycle. During the experiments, the tangential load and

coefficient of friction values for each 50 cycles have been noted and with the help of these values and normal load value the graph was plotted. The oscillatory motion on the specimen was controlled by the hydraulic actuator. The normal load was applied on the pads using threaded rod and nut arrangement which helps us to keep the constant normal load as constant throughout the experiments without any recalibration.

The testing parameters for the fretting experiments are, the normal load value of 3 kN, the experiments were last long for 500 cycles and operating frequency value of 1 Hz. The output obtained from the experiment is Q/P ratio as a function of Number of cycles and it is tabulated in Table 4.6 and depicted in Figure 4.30. These results were verified with the results obtained from fretting experiments conducted by Vadivuchezhian (2013). These results provides considerable insight into the usage of fretting rig and thin curved sensor in fretting experiments and share a number of similarities with Vadivuchezhian (2013) findings.

CHAPTER 5

CONCLUSIONS

In summary, this study involves the design and analysis of fretting rig and thin displacement contact sensor which results the fabrication of both and it also dealt with the difficulties faced during fabrication process as well as fretting experiments. From the study, the following conclusions were drawn:

5.1 CONCLUSIONS FROM FRETTING RIG DESIGN

- By considering the changes in the length of the horizontal beam and vertical support, eleven cases of design in the fretting rig were formed and its finite element study has been performed with suitable boundary conditions by using ANSYS software.
- The analysis results showed that the increase in the length of the vertical column leads to increase in the Load Transfer Ratio (LTR) values. Of the eleven cases considered, the finite element model presented in case-2 (without vertical column) was found to have the optimum Load Transfer Ratio (LTR) of 50.83 %.
- The 1-D FE analysis has been done again for four different fretting rig cases with the consideration of machine constraints (dimensions of the machine bed, accessible height for fretting rig and accommodation space for a specimen in the machine frame).
- The minimum LTR value was getting for fretting rig case number 15 and this case has been verified with three-dimensional finite element analysis results.
- Following this, the selected fretting rig was fabricated and tested. These tests revealed that the fabricated fretting rig failed to maintain constant normal load during fretting experiments. So, the necessary modifications have been made in the fabricated fretting rig to conduct fretting experiments by applying constant normal load on the specimen. The fretting rig thus designed would be used for conducting fretting experiments.

5.2 CONCLUSIONS FROM THIN DISPLACEMENT SENSOR DESIGN

- In a curved sensor, the more number of slots and increases in slot dimension could increase the ability to capture the micro-level displacement values and it enables them to hold higher flexibility.
- Twenty-one configurations were considered with different shapes and sizes of the slots and six configurations show zero stress gradient at the middle of the thin curved strip.
- Among these six configurations, four configurations with circular slots and elliptical slots were found suitable for the fabrication of thin curved strip and for measuring contact displacement during fretting experiments.
- Thin strip with rectangular slots was not suitable due to the high-stress gradient at the middle of the strip.
- Small variation between the displacement value obtained from experiments and that from analytical approach and numerical approach is less than 4 % and it can be reduced by focusing on factors such as the process of applying the load, selection of adhesive and its thickness, selection of material and environmental conditions.
- Use of thin strip without slot has been verified when displacement value observed experimentally was compared with that of SEA result and FEA result. This validates the use of the thin strip without slot for conducting fretting experiments.
- Even though thin curved strip without slot ensures its use in fretting experiments, thin curved strip with slots can be considered to be very useful in fretting experiments despite the complications involved in its fabrication.

5.3 CONCLUSIONS FROM FRETTING EXPERIMENTS

- Fretting experiments have been conducted using fabricated fretting rig and fabricated thin curved sensor without slot in fatigue testing machine.

- The output obtained from the experiment is Q/P ratio as a function of Number of cycles and it is correlated with the results obtained from fretting experiments conducted by Vadivuchezhian (2013).
- These results provides considerable insight into the usage of fretting rig and thin curved sensor in fretting experiments and share a number of similarities with Vadivuchezhian (2013) findings.

5.4 LIMITATIONS OF THE STUDY

- The results obtained from the experiments that have conducted on fretting rig, on thin displacement sensor and fretting experiments with the help of fabricated fretting rig and fabricated thin displacement sensor under normal environmental temperature ($T_{env} = 32 \text{ }^{\circ}\text{C}$) and high humid conditions (Humidity = 76 %).
- The effect of environmental conditions on fretting experiments is not considered in this study.
- Since the number of cycles by which the experiments have operated is within 500 cycles, the microstructural analysis on specimen and pad have not been taken.

5.5 SCOPE FOR FUTURE WORK

Further experimental studies are needed to identify the effects of parameters which influences the fretting rates and mechanisms. An additional insights on this study withdraws the more fretting results and it would be useful to the better understanding of tightly clamped component stress analysis. There is scope for improving the friction, fretting fatigue and fretting wear characteristics of Al 6061-T6 alloy by considering it as a metal matrix to build new composite components. The experimental results obtained from this study can be helpful to find tangential force profile in fretting contacts.

REFERENCES

- A.A. Walvekar et al. (2014). “An experimental study and fatigue damage model for fretting fatigue.” *Tribology International*, 79, 183–196.
- A. Ramalho, Celis, J. (2003). “Fretting Laboratory Tests: Analysis of the Mechanical Response of Test Rigs.” *Tribology Letters*, 14, 187–196. <https://doi.org/10.1023/A:1022368414455>.
- Ahn, Y.J. & Barber, J.R. (2008). “Response of frictional receding contact problems to cyclic loading.” *International Journal of Mechanical Sciences*, 50, 1519-1525.
- Alic, J.A. and Kantimathi, A. (1979). “Fretting fatigue, with reference to aircraft structures.” *SAE paper No. 790612*.
- Arora, P.R., Jacob, M.S.D., Salit, M.S., Ahmed, E.M., Saleem, M. and Edi, P. (2007). “Experimental evaluation of fretting fatigue test apparatus.” *International Journal of Fatigue*, 29(5), 941 – 952.
- Asai, K., Kudo, T. & Yoda, H. (2013). “Experimental Validation of Fretting Fatigue Strength and Fretting Wear Rate at Contact Surface of Turbine-Blade-Shroud Cover.” *Journal of Engineering for Gas Turbines and Power*, 136(4), 042101-042107.
- Bhushan, B. (2013). “Principles and Applications of Tribology.” 2nd ed, New York, John Wiley & Sons.
- Bramhall, R. (1973). “Studies in fretting fatigue.” *D.Phil. thesis*, University of Oxford.
- Carlos Navarro, Sergio Muñoz, Jaime Domínguez. (2008). “On the use of multiaxial fatigue criteria for fretting fatigue life assessment.” *International Journal of Fatigue*. 30(1). 32-44.
- Cattaneo, C. (1938). “Sul contatto di due corpi elastici. Atti Accad. naz.” *Lincei Rc*, 27, 342-348, 434-436, 474-478.

- Ciavarella, M. (1998). “The generalized Cattaneo partial slip plane contact problem. i - theory.” *International Journal of Solids and Structures*, 35(18), 2349-2362.
- Ciavarella, M. & Macina, G. (2003). “New results for the fretting-induced stress concentration on Hertzian and at rounded contacts.” *International Journal of Mechanical Sciences*, 45, 449-467.
- Ciavarella, M., Hills, D.A. & Monno, G. (1998). “The influence of rounded edges on indentation by a flat punch.” *Proceedings of the Institution of Mechanical Engineers Part-C, Journal of Mechanical Engineering Science*, 212, 319-327.
- Conner, B.P. and Nicholas, T. (2006). “Using a dovetail fixture to study fretting fatigue and fretting palliatives.” *Journal of engineering materials and technology*, 128, 133-141.
- D. Nowell and D.A. Hills. (1990). “Crack initiation criteria in fretting fatigue.” *Wear*, 136, 329-343.
- D. Nowell, D. Dini, and D.A. Hills. (2006). “Recent developments in the understanding of fretting fatigue.” *Engineering Fracture Mechanics*, 73(2), 207-222.
- Hills, D.A., & Nowell, D. (1994). “Mechanics of Fretting Fatigue.” Dordrecht, Kluwer Academic Publishers.
- De Pauw J, De Waele W, Hojjati-Talemi R, De Baets P. (2014). “On the use of digital image correlation for slip measurement during coupon scale fretting fatigue experiments.” *Int J Solids Struct*, 51, 3058–3066.
- Degat, P.R., Zhou, Z.R. & Vincent, L. (1997). “Fretting cracking behaviour on pre-stressed aluminium alloy specimens.” *Tribology International*, 30, 215-223.
- Ding, J., Bandak, G., Leen, S.B., Williams, E.J. & Shipway, P.H. (2009). “Experimental characterisation and numerical simulation of contact

evolution effect on fretting crack nucleation for Ti–6Al–4V.” *Tribology International*, 42, 1651-1662.

- Dobrominski JM. (1992). “Variables of Fretting Process: Are There 50 of Them? In: Attia MH, Waterhouse RB, editors. Stand. Frett. Fatigue Test Methods Equipment, ASTM STP 1159”. Philadelphia: American Society for Testing and Materials, p. 60–66.
- Eden, E.M., Rose, W.N. and Cunningham, F.L. (1911). “The endurance of metals.” *Proceedings of the Institute of Mechanical Engineers*, 4, 68-76.
- Endo, K. and Goto, H. (1976). “Initiation and propagation of fretting fatigue cracks.” *Wear*, 38, 311-324.
- Farris, T. N., H. Murthy, and J. F. Matlik,. (2003a). “Fretting fatigue. In R. O. Ritchie and Y. Murakami (eds.), *Comprehensive structural integrity: Fracture of materials from macro to nano*, volume 4: Cyclic Loading.” Elsevier, Amsterdam, 281 – 326.
- Farris, T. N., Murthy, H. and Matlik, J. F. (2003b). "Fretting fatigue," *Comprehensive structural integrity: Fracture of materials from macro to nano.* Elsevier Publications. <https://doi.org/10.1016/B0-08-043749-4/04080-5>.
- Feng, I-Ming and Rightmire, B.G. (1952). “The mechanism of fretting.” *Mass. Inst. of Tech.*, Cambridge, Mass., AD 4463.
- Feng, I-Ming and Rightmire, B.G. (1953). “The mechanism of fretting.” *Lubrication Engineering*, 9, 134-136 and 158-161.
- Feng, I-Ming (1955). “Fundamental study of the mechanism of fretting.” *MIT Lubrication Lab*, Cambridge, Mass., Final Report AD59089.
- Feng, I-Ming and Rightmire, B.G. (1956). “An experimental study of fretting.” *Proc. Inst. Mech. Engrs.*, London, 170, 1055-1060.

- Flamant, A. (1892). “Sur la répartition des pressions dans un solide rectangulaire chargé transversalement. *Compte. Rendu.*” *Acad. Sci. Paris*, 114, 1465.
- Fouvry, S., Duó, P. & Perruchaut, P. (2004). “A quantitative approach of Ti–6Al–4V fretting damage: friction, wear and crack nucleation.” *Wear*, 257, 916-929.
- Godfrey, D. (1950). “Investigation of fretting corrosion by microscopic observation.” *NACA Technical Note*. 2039.
- Godfrey, D. and Bailey, J.M. (1953). “Coefficient of friction and damage to contact area during the early stages of fretting-I. Glass, copper or steel against copper.” *NACA Technical Note* 3011.
- Godfrey, D. and Bailey, J.M. (1954). “Early stages of fretting of copper, iron and steel.” *Lubrication Engineering*, 10, 155-159.
- Godfrey, D. (1956). “A study of fretting wear in mineral oil.” *Lubrication Engineering*, 12, 37-42.
- Golden, P.J., Hutson, A.L., Bartha, B.B. and Nicholas, T. (2008). “Fatigue loading and life prediction in three fretting fatigue fixtures.” *Experimental Mechanics*, 48(3), 253 – 263.
- Goto, H. and Ashida, M. (1999). “The influence of oxygen and water vapour on the friction and wear of an aluminium alloy under fretting conditions.” *Wear*, 116, 141–155.
- H.H. Farrahi, and G. Maeder (1992). “An experimental study of fretting by means of X-Ray diffraction.” *Fat Frac Eng Mat Struct*, 15(1), 91–102.
- Halliday, J.S. & Hirst, W. (1956). “The fretting corrosion of mild steel.” *Proc. R. Soc, A* 236, 411.
- Hills, D. and Nowell, D. (1994). “Mechanics of fretting fatigue.” Kluwer, Dordrecht, The Netherlands.

- Hills, D.A. & Dini, D. (2004). “What level of friction guarantees adhesion in a complete contact?.” *Journal of Strain Analysis*, 39(5), 549-551.
- Hills, D.A., Ramesh, R., Fleury, R.M.N. & Parel, K. (2017). “A unified approach for representing fretting and damage at the edges of incomplete and receding contacts.” *Tribology International*, 108, 16-22.
- Hirsch, M.R. & Neu, R.W. (2011). “Fretting damage in thin sheets: Analysis of an experimental configuration.” *Tribology International*, 44, 1503-1510.
- Hoepfner, D.W. and Goss, G.L. (1974). “A fretting fatigue damage threshold concept.” *Wear*, 27, 61-70.
- Hutchings, I.M. (1992). “Tribology: Friction and Wear of Engineering Materials.” 1st ed., London, Edward Arnold.
- J.F Ferrero, E Yettou, J.J Barrau, S Rivallant. (2004). “Analysis of a dry friction problem under small displacements: application to a bolted joint.” *Wear*, 256:1135–1143.
- J. Juoksukangas et al. (2015). “Applying the digital image correlation method to fretting contact for slip measurement.” *Journal of Engineering Tribology*, 231, 509-519.
- J. Juoksukangas et al., (2016). “A comparison of relative displacement fields between numerical predictions and experimental results in fretting contact.” *Proceedings of the Institution of Mechanical Engineers, Part J: Journal of Engineering Tribology*, 230(10), 1273-1287. doi:10.1177/1350650116633573.
- J. Meriaux, M. Boinet, S. Fouvry, J.C. Lenain. (2010). “Identification of fretting fatigue crack propagation mechanisms using acoustic emission.” *Tribology International*. 43(11). 2166-2174.
- J. Meriaux, S. Fouvry, K.J. Kubiak, S. Deyber. (2010). “Characterization of crack nucleation in TA6V under fretting–fatigue loading using the potential drop technique.” *International Journal of Fatigue*. 32(10). 1658-1668.

- J.A. Araújo, D. Nowell. (2009). “Mixed high low fretting fatigue of Ti 6/4: tests and modelling.” *Tribology International*, 42, 1276-1285..
- Jäger, J. (1998). “A new principle in contact mechanics.” *ASME Journal of Tribology*, 120(4), 677-684.
- K. Vadivuchezhian, S. Sundar and H.Murthy. (2011). “Effect of variable friction coefficient on contact tractions.” *Tribology International*, 44, 1433–1442.
- Kubiak, K.J., Liskiewicz, T.W. & Mathia, T.G. (2011). “Surface morphology in engineering applications: Influence of roughness on sliding and wear in dry fretting.” *Tribology International*, 44, 1427-1432.
- Kuno, M., Waterhouse, R.B., Nowell, D. and Hills, D.A. (1989). “Initiation and growth of fretting fatigue cracks in the partial slip regime.” *Fatigue & Fracture of Engineering Materials & Structures*. 12. 387-398. <https://doi.org/10.1111/j.1460-2695.1989.tb00547.x>
- L. Favrow, et al. (2000). "Fretting Fatigue Testing Methodology Incorporating Independent Slip and Fatigue Stress Control," in *Fretting Fatigue: Current Technology and Practices*, ed. D. Hoepfner, V. Chandrasekaran, and C. Elliott (West Conshohocken, PA: ASTM International), 391-403. <https://doi.org/10.1520/STP14743S>.
- Lavella, M. & Botto, D. (2011). “Fretting wear characterization by point contact of nickel superalloy interfaces.” *Wear*, 271, 1543-1551.
- Lee, H. Mall, S. Sanders, J.H. Sharma, S.K. Magaziner, R.S. (2007). “Characterization of fretting wear behavior of Cu–Al coating on Ti–6Al–4V substrate.” *Tribology International*, 40, 1301–1310.
- Lee, H. Mall, S. and Murray, K.N. (2007). “Fretting wear behaviour of Cu–Al coating on Ti-6Al-4V substrate under dry and wet (lubricated) contact condition.” *Tribology Letters*, 28, 19-25.

- Leidich, E., Maiwald, A. & Vidner, J. (2013). “A proposal for a fretting wear criterion for coated systems with complete contact based on accumulated friction energy density.” *Wear*, 297, 903-910.
- Leonard, Benjamin D.; Ghosh, Arnab; Sadeghi, Farshid; Shinde, Sachin; Mittelbach, Marc (2014). “Third body modeling in fretting using the combined finite-discrete element method.” *International Journal of Solids and Structures*. 51(6), 1375–1389. doi:10.1016/j.ijsolstr.2013.12.036.
- M.H. Zhu and Z.R. Zhou. (2011). “On the mechanisms of various fretting wear modes.” *Tribology international*. 44(11), 1378-1388.
- Mang T., Bobzin K. & Bartels T. (2011). *Industrial Tribology: Tribosystems. Wear and Surface Engineering, Lubrication*, Wiley-VCH.
- McDowell, J.R. (1953). “Fretting corrosion tendencies and several combinations of materials.” *Symposium on Fretting Corrosion, STP 144, ASTM*, Philadelphia, 24-39.
- McVeigh, P. A., and Farris, T. N. (1997). "Finite Element Analysis of Fretting Stresses." *ASME. J. Tribol.*, 119(4). 797–801. <https://doi.org/10.1115/1.2833887>.
- Merhej, R. & Fouvry, S. (2009). “Contact size effect on fretting wear behaviour: application to an AISI 52100/AISI 52100 interface.” *Lubrication Science*. 21. 83-102.
- Mindlin, R.D. (1949). “Compliance of elastic bodies in contact.” *ASME Journal of Applied Mechanics*, 16, 249-268.
- Mohrbacher, H., Blanpain, B., Celis, J.P., Roos, J.R., Stals, L. & Van Stappen, M. (1995). “Oxidational wear of TiN coatings on tool steel and nitrided tool steel in unlubricated fretting.” *Wear*, 188, 130-137.
- Mohrbacher, H., Blanpain, B., Celis, J. & Roos, J.R. (1995). “The influence of humidity on the fretting behaviour of PVD TiN coatings.” *Wear*, 180, 43-52.

- Mulvihill, D.M., Kartal, M.E., Olver, A.V., Nowell, D. & Hills, D.A. (2011). “Investigation of non-Coulomb friction behaviour in reciprocating sliding.” *Wear*, 271, 802-816.
- Murthy, H., Gao, G. and Farris, T.N. (2006). “Fretting fatigue of single crystal nickel at 600 °C.” *Tribology international*, 39(10), 1227–1240.
- H. Murthy and K. Vadivuchezhian. (2017). “Estimation of friction distribution in partial-slip contacts from reciprocating full-sliding tests.” *Tribology international*. 108, 164-173.
- Naidu, N.K.R. & Raman, S.G.S. (2005). “Effect of contact pressure on fretting fatigue behaviour of Al–Mg–Si alloy AA6061.” *International Journal of Fatigue*, 27(3), 283-291.
- Nishioka, K., Nishimura, S. and Hirakawa, K. (1968). “Fundamental investigations of fretting fatigue–Part 1, On the relative slip amplitude of press-fitted axle assemblies.” *Bulletin of JSME*, 11, 45, 437-445.
- Nishioka, K. and Hirakawa, K. (1969a). “Fundamental investigations of fretting fatigue– Part 2, Fretting fatigue testing machine and some test results.” *Bulletin of JSME*, 12, 50, 180-187.
- Nishioka, K. and Hirakawa, K. (1969b). “Fundamental investigations of fretting fatigue– Part 3, Some phenomena and mechanisms of surface cracks.” *Bulletin of JSME*, 12, 51, 397-407.
- Nishioka, K. and Hirakawa, K. (1969c). “Fundamental investigations of fretting fatigue– Part 4, The effect of mean stress.” *Bulletin of JSME*, 12, 51, 408-414.
- Nishioka, K. and Hirakawa, K. (1969d). “Fundamental investigations of fretting fatigue– Part 5, The effect of relative slip amplitude.” *Bulletin of JSME*, 12, 52, 692-697.

- Nishioka, K. and Hirakawa, K. (1972). “Fundamental investigations of fretting fatigue–Part 6, Effects of contact pressure and hardness of materials.” *Bulletin of JSME*, 15, 80, 135-144.
- Murthy, H and Vadivuchezhian, K. (2017). “Estimation of friction distribution in partial-slip contacts from reciprocating full-sliding tests.” *Tribology International*, 108, 164–173.
- Nowell, D. (1988). “An analysis of fretting fatigue.” *D.Phil. thesis*, University of Oxford.
- Nowell, D. & Hills, D.A. (1987). “Mechanics of fretting fatigue tests.” *International Journal of Mechanical Sciences*, 29(5), 335-365.
- Ouyang, Z.X., Pan, S.C., Li, Y.P. and Quyang, Y.P. (1993). “Friction coefficient in fretting between titanium and stainless steel alloy.” *Journal of Strain Analysis*, 28, 63-66.
- Pape, J.A. and Neu, R.W. (1999). “Influence of contact configuration in fretting fatigue testing.” *Wear*, 225 – 229, 1205 – 1214.
- Pape, J.A. & Neu, R.W. (2007). “A comparative study of the fretting fatigue behavior of 4340 steel and PH 13-8Mo stainless steel.” *International Journal of Fatigue*, 29, 2219-2229.
- Pearson, S.R., Shipway, P.H., Abere, J.O. & Hewitt, R.A.A. (2013). “The effect of temperature on wear and friction of a high strength steel in fretting.” *Wear*, 303, 622-631.
- R. Ramesh. (2018). “An Analysis of Incomplete Contacts in Partial Slip.” *D.Phil. thesis*, University of Oxford.
- Ruiz C, Boddington PHB., Chen KC. (1984). “An investigation of fatigue and fretting in a dovetail joint.” *Exp Mech.*, 24(3), 208–217.

- Rybiak, R., Fouvry, S. & Bonnet, B. (2010). “Fretting wear of stainless steels under variable temperature conditions: Introduction of a ‘composite’ wear law.” *Wear*, 268, 413-423.
- Siegfried Fouvry, Philippe Kapsa, Leo Vincent. (1996). “Quantification of fretting damage.” *Wear*, 200, 186-205.
- S. Fouvry, Ph. Kapsa, L. Vincent, K. Dang Van. (1996). “Theoretical analysis of fatigue cracking under dry friction for fretting loading conditions.” *Wear*, 195, 21-34.
- Schijve J. (2009). “Fatigue of Structures and Materials.” 2nd ed. Springer Netherlands.
- Sinclair, G. B., Cormier, N. G., Griffin, J. H., and Meda, G. (2002). "Contact Stresses in Dovetail Attachments: Finite Element Modeling." *ASME. J. Eng. Gas Turbines Power*, 124(1), 182–189. <https://doi.org/10.1115/1.1391429>.
- Sneddon, I. N. (1951). “Fourier Transforms.” McGraw-Hill, New York.
- Socie DF, Marquis GB.(1999). “Multiaxial Fatigue.” Warrendale: Society of Automotive Engineers.
- Spink GM. (1990). “Fretting fatigue of a 2.5%NiCrMoV low pressure turbine shaft steel: The effect of different contact pad materials and of variable slip amplitude.” *Wear*, 136, 281–297.
- Suresh S. (1998). “Fatigue of Materials.” 2nd ed. Cambridge: Cambridge University Press.
- Swalla, D. R. and Neu, R. W. (2001). “Influence of coefficient of friction on fretting fatigue crack nucleation prediction.” *Tribology international*, 34(7), 493 – 503.
- Szolwinski, M. P., Harish, G., Farris, T. N., & Sakagami, T. (1998). “In-situ measurement of near-surface fretting contact temperatures in an aluminum alloy.” *American Society of Mechanical Engineers (Paper)*, (98 -TRIB-1-61), 1-9.

- Terres, M.A., Laalai, N. & Sidhom, H. (2012). “Effect of nitriding and shot-peening on the fatigue behavior of 42CrMo4 steel: Experimental analysis and predictive approach.” *Mater Des*, 35, 741–748.
- Timoshenko, S. P. (1955). “Strength of materials. Part I: Elementary theory and problems (3rd ed.).” Princeton. N. J.: Van Nostrand.
- Tomlinson, G.A. (1927). “The rusting of steel surfaces in contact.” *Proc. Roy. Soc. Lond. Ser. A.*, 115A, 472-483.
- Tomlinson, G.A., Thorpe, P.L. and Gough, H.J. (1939). “An investigation of the fretting corrosion of closely fitted surfaces.” *Proc. Inst. Mech.Engs.*, 141, 223-249.
- Vázquez, J.V., Navarro, C. & Domínguez, J. (2013). “Analytical solution for a cylindrical contact with reverse slip.” *Journal of Strain Analysis*, 48(3), 189-197.
- Vingsbo O, Söderberg S. (1988). “On fretting maps.” *Wear*, 126(2), 131–147.
- Warlow-Davies, E.J. (1941). “Fretting corrosion and fatigue strength: brief results of preliminary experiments.” *Proc. I. Mech. E.*, 146, 33-38.
- Waterhouse, R.B. (1955). “Fretting corrosion.” *Proc. Inst. Mech. Engrs.*, 169, 1159-1172.
- Waterhouse, R.B. (1972). “Fretting corrosion.” Pergamon Press, Oxford, England.
- Wharton, M. H. and Waterhouse, R. B. (1980). “Environmental effects in the fretting fatigue of Ti-6Al-4V.” *Wear*, 62(2), 287 – 297.
- Wittowsky, B.U., Birch, P.R., Dominguez, J. and Suresh, S. (1999). “An apparatus for quantitative fretting fatigue testing.” *Fatigue Fracture Engineering Material Structure*, 22, 307 – 320.

- Wright, K.H.R. (1952a). “An investigation of fretting corrosion.” *Proc. Inst. Mech. Engrs.*, 1B, 556-571.
- Wright, K.H.R. (1952b). “Discussion and communication on an investigation of fretting.” *Corrosion. Proc. Inst. Mech. Engrs.*, 1B, 571-574.
- X. Zhang, D. Liu, G. Liu, Z. Wang, B. Tang. (2011). “Improvement of the fretting damage resistance of Ti-811 alloy by Cu/Ni multilayer films.” *Tribology International*, 44, 1488-1494.
- Zalnezhad, E., Sarhan, A.A., & Jahanshahi, P. (2014). “A new fretting fatigue testing machine design, utilizing rotating–bending principle approach.” *The International Journal of Advanced Manufacturing Technology*, 70, 2211-2219.

PUBLICATIONS BASED ON PRESENT RESEARCH WORK

International Journals

1. **Raja Pandi R.,** Vadivuchezhian Kaliveeran, (2020). “Finite element analysis of rig used for fretting experiments.” *Materials Today: Proceedings*, 27, 2349-2354. <https://doi.org/10.1016/j.matpr.2019.09.126>
2. **Raja Pandi R.,** Vadivuchezhian Kaliveeran, (2022). “Design of Thin Curved Sensor to Measure Contact Slip in Fretting Experiments.” *Journal of Naval Architecture and Marine Engineering*, 19, 46-56. <https://doi.org/10.3329/jname.v19i1.52171>

International Conferences

1. **Raja Pandi R.,** Vadivuchezhian Kaliveeran, Gowtham S., Ramesh M.R., (2017) “Effect of normal load on coefficient of friction for stainless steel alloys (SS 304L and SS 316) under dry sliding condition.”, ICRAMC.
2. **Raja Pandi R.,** Vadivuchezhian Kaliveeran., “Design of low frequency fretting rig”, 7th International Engineering Symposium - IES 2018, March 7-9, 2018, Kumamoto University, Japan.
3. **Raja Pandi R.,** Vadivuchezhian Kaliveeran, “Numerical Study of New Displacement Sensor for Fretting Experiments” *Materials and Manufacturing Methods - 2019*, July 5-7, 2019, NIT Tiruchirappalli.
4. **Raja Pandi R.,** Vadivuchezhian Kaliveeran, “Finite element analysis of rig used for fretting experiments” *Materials and Manufacturing Methods - 2019*, July 5-7, 2019, NIT Tiruchirappalli.

CURRICULUM VITAE



Name : RAJA PANDI R.

Permanent Address:

3-1-146, Ram Nagar, Opp. to Union office, T. Kallupatti. Madurai District, Tamil Nadu. PIN:-625702.

Contact No. : +91-9597017173.

Email ID : pandi.raja145@gmail.com

Experience:

Assistant Professor (2013-2015)

College : Rajalakshmi Engineering College, Chennai.

Education:

Master of Engineering (2011-2013)

Discipline : Engineering Design.

College : College of Engineering, Guindy, Chennai.

Bachelor of Engineering (2006-2010)

Discipline : Mechanical Engineering

College : K.L.N. College of Engineering, Madurai.